USING TERRESTRIAL LASER SCANNING TO ESTIMATE CANOPY STRUCTURE IN PEATLAND CONIFERS UNDER A CLIMATE MANIPULATION

by

Angela D. Seibert

A thesis

submitted in partial fulfillment

of the requirements for the degree of

Master of Science in Geoscience

Boise State University

August 2023

© 2023

Angela D. Seibert

ALL RIGHTS RESERVED

BOISE STATE UNIVERSITY GRADUATE COLLEGE

DEFENSE COMMITTEE AND FINAL READING APPROVALS

of the thesis submitted by

Angela Deborah Seibert

Thesis Title: Using Terrestrial Laser Scanning to Estimate Canopy Structure in Peatland Conifers Under a Climate Manipulation

Date of Final Oral Examination: 05 April 2023

The following individuals read and discussed the thesis submitted by student Angela Deborah Seibert, and they evaluated the student's presentation and response to questions during the final oral examination. They found that the student passed the final oral examination.

Nancy F. Glenn, Ph.D.	Chair, Supervisory Committee
Anna Bergstrom, Ph.D.	Member, Supervisory Committee
Jeffrey Warren, Ph.D.	Member, Supervisory Committee

The final reading approval of the thesis was granted by Nancy F. Glenn, Ph.D., Chair of the Supervisory Committee. The thesis was approved by the Graduate College.

DEDICATION

To my loving and supportive parents.

ACKNOWLEDGMENTS

I would like to express my gratitude for my advisor and lab manager, Dr. Nancy Glenn and Josh Enterkine. Thank you, both, for your support, empathy, and patience during this time. Thank you, Nancy, for your faith in me and the opportunity to be part of the SPRUCE project. Thank you, Josh, for teaching me the ins and outs of TLS and being a funny and kind friend. I am grateful to have had the opportunity to learn so much about a new field from both of you.

Thank you to my committee members, Anna Bergstrom and Jeffrey Warren, for their patience, advice, and support through the duration of my project. Each meeting I had with both of you was always very grounding.

Thank you to the funding sources that made this work possible from the U.S. Department of Energy, Office of Science, Office of Biological and Environmental Research and Oak Ridge National Laboratory (#4000145196). Additionally, thank you to the Boise State University Department of Geosciences for their excellent administrative support and additional funding.

Finally, thank you to my family, partner, and friends for their unconditional love and support over the last two years. I could not have done this without you.

ABSTRACT

Northern peatlands are major terrestrial carbon sinks, storing 415 ± 150 Gt of carbon. The composition of peatland vegetation affects this carbon storage capacity, and thus quantifying the vegetation helps to constrain uncertainty in peatland carbon storage estimates. Ground layer vegetation, such as *Sphagnum sp.* moss contributes greatly to carbon storage capacity. In forested or treed peatlands, the tree canopy structure directly influences peatland solar insolation, soil temperature, and water table levels. Each of these factors impacts the ground layer vegetation. Currently, there is uncertainty about how the peatland tree canopy structure is influenced by elevated levels of carbon dioxide (CO_2) and temperature. Providing canopy structural metrics in a nondestructive, spatially comprehensive way across different temperature and CO_2 treatments is challenging for traditional methods such as destructive harvesting, Digital Hemispherical Photography (DHP), and allometric regressions. Terrestrial Laser Scanning (TLS) is well-suited to provide non-destructive detailed horizontal and vertical canopy structural information.

As part of the Spruce and Peatland Responses Under Changing Environments (SPRUCE) study located in northern Minnesota, USA, we use TLS to evaluate leaf area index (LAI), leaf area density, and leaf inclination angle over time (2015 - 2022) and space of two conifer species, *Picea mariana* (black spruce) and *Larix laricina* (eastern larch). The SPRUCE site is in a treed peatland bog under elevated CO_2 and temperature conditions. The research questions in this study are 1) How accurately can we predict the LAI of the spruce and larch trees using TLS data? 2) How are the spruce and larch tree

canopy structures within 12 SPRUCE plots changing from 2015 - 2022? We expected 1) A volumetric pixel-based model (VCP) will predict LAI with an accuracy of 90% as validated by destructively harvested and DHP LAI estimates 2) Under elevated CO_2 and temperature, LAI will increase, leaf area density will decrease in lower canopies, and leaf inclination angles will become more vertical. At the species level, we expected the spruce and larch trees to respond with opposing trends for each metric under the same treatment. Using TLS data, we developed a modified VCP model that uses measures of point contact frequency to estimate LAI, leaf inclination angles, and leaf area density. The results indicate that the model predicts LAI with a coefficient of determination of 0.89 ($R^2 = 0.89$), an RMSE of 0.98, and a normalized RMSE = 0.17. We also found that the model maintains moderate accuracy across voxel size input parameters, suggesting it may maintain accuracy in different treatment conditions where tree structural relationships can change. Our canopy structural results supported the hypothesis that LAI increases more significantly over time under warmer conditions when compared to control plots. Lower canopy leaf area density trends did not support the hypothesis as they showed no statistically significant trends across time. Leaf inclination angle trends through time did not support the hypothesis as they tended to decrease. As temperatures increased across the temperature gradient, though, leaf angles became more vertical in upper canopies under elevated CO_2, leading to inconclusive support for or against the hypothesis. Species data did not support the hypothesis that spruce and larch canopy structures would differ significantly under the same treatments. The larch LAI, however, did not increase as significantly through time as the spruce under elevated CO_2 conditions. Additionally, we

identified anomalous fluctuations in time series data and proposed potential temperature thresholds where LAI differed the most under ambient or elevated CO_2 conditions.

The findings from this study suggest that accurately quantifying canopy structure through time may be possible in different environmental conditions and species using TLS. We add support to previous findings that LAI increases more significantly through time under warming conditions compared to control conditions. These results demonstrate TLS's utility for making species-level canopy structural estimates across horizontal and vertical profiles. Incorporating vertical canopy profile metrics such as leaf area density with LAI data can assist in better explaining how LAI is changing across time and temperature gradients.

TABLE OF CONTENTS

LIST OF TABLES

LIST OF FIGURES

LIST OF ABBREVIATIONS

aCO_2	Ambient carbon dioxide
ALS	Airborne Laser Scanning
CANUPO	Dimensionality method for classifying point clouds
CW	Canopy width
DHP	Digital Hemispherical Photography
DOE	Department of Energy
E3SM	Energy Exascale Earth System Model
eCO_2	Elevated carbon dioxide
eLAI	Effective Leaf Area Index
ELM-SPRUCE	Earth Land Model – Spruce and Peatland Responses Under Changing Environments
flnr	Fraction of leaf nitrogen in Ribulose-1,5-bisphosphate carboxylase/oxygenase
Ladensity	leaf area density
LAI	Leaf Area Index
LAI_i	Leaf Area Index of an individual tree
LM	Leaf mass
NDVI	Normalized Difference Vegetation Index
NIR	Near Infrared
nRMSE	Normalized Root Mean Square Error

RiSCAN Pro	Riegl's lidar scan registration software
RMSE	Root Mean Square Error
S1	The name of the boreal bog at the study site
SGA	Sampled Ground Area
SLA	Specific Leaf Area
SPRUCE	Spruce and Peatland Responses Under Changing Environments
TLS	Terrestrial Laser Scanning
VCP	Volumetric Pixel (Voxel) – Based Model
Voxel	Volumetric Pixel

CHAPTER ONE: INTRODUCTION

Peatlands are wetlands that are present in every climatic zone and continent, covering about 4 million km^2 of land globally, most of them occurring in northern (boreal) and temperate regions. They form when waterlogged substrate accumulates, leading to a low oxygen environment. Depending on the type of peatland, substrate accumulation depth varies from 10 cm to 100 cm before a wetland is classified as a peatland (Xu et al., 2018). The peatland's anoxic environment slows microbial decomposition and results in higher net rates of organic matter production. Large stores of partially decomposed organic matter can then accumulate for thousands of years, forming the abundances of peat that make up the ecosystem. There are two main types of peatlands, fens and bogs. Each type is classified based on its hydrology, morphology, and dominant vegetation. Fens are fed by groundwater (geogenous) and they are located in land depressions. They are characterized by a neutral pH and their dominant vegetation includes grasses, sedges, and rushes. Bogs are acidic, precipitation fed (ombrogenous) and raised above the groundwater. Boreal bogs are characterized by *Sphagnum spp.* moss and woody vegetation (Joosten & Clarke, 2002) such as *Picea mariana* and *Larix laricina*.

Picea mariana (black spruce) and *Larix laricina* (eastern larch) are the dominant tree species characterizing the boreal peatlands across the northeastern United States. Spruce trees are evergreen conifers that are shade tolerant and are typically more dominant than larch trees. They are often found in low drainage peatlands and their

abundance is sensitive to elevated water temperature (Evans et al., 2016). They are not usually found in the wetter regions of peatlands as they incur needle damage with excess water intake (Islam et al., 2003). The larch trees are a deciduous conifer and can be found within the same ranges as the black spruce. They are less shade tolerant and have exhibited increased abundance in more open and wetter regions of peatlands (Montague & Givnish, 1996). Under drying conditions, they have shown increases in fine root growth (Malhotra et al., 2020). Previous studies have found that the *Larix* genus has more symmetric leaf area estimates than the *Picea* genus (Sterba et al., 2019). Spruce and larch biomass and aboveground net primary production are significant pathways for carbon to enter boreal peatlands (Hanson et al., 2020).

Spruce and larch tree presence impacts peatland understories and carbon storage capacity. In forested peatlands, the canopy cover directly influences insolation and water-holding capacity (Strack et al., 2019). Tree and vegetation presence affects the rate of carbon flux in peatlands through vascular transport controls, such as evapotranspiration, on the water table and temperature (Kettridge et al., 2013). Changes in tree architecture including leaf area index (LAI), leaf area density, and leaf inclination angles each impact the hydrologic and atmospheric dynamics of peatlands. Vertical leaf angles shifting to flatter angles can result in increased light interception, leaf temperature, and lower rates of carbon dioxide fixation (L.-X. Liu et al., 2003). Changes in the density of leaves in the canopy affects soil moisture and temperature, impacting water availability in the understory. von Arx et al. (2013) found that LAI below 4 created environments not suitable for seedling establishment in both conifer and broadleaf forests. Leaf area density differences throughout the vertical canopy profile impacts leaf respiration and

carbon budgets as higher canopy leaves have higher rates of dark and light respiration (Souza et al., 2021). Quantifying changes in the overstory canopy of peatlands may add insight to how peatland carbon budgets can change temporally and spatially.

Recently, with average warming temperatures and rising carbon dioxide (CO_2) levels peatlands are at risk of drying out and shifting from carbon sink to carbon source. As peatlands dry out due to warmer temperatures, water tables drop, causing greater levels of oxygen to make stable carbon labile, increasing emissions. Boreal regions, the region of the globe with the highest density of peatlands, are currently warming at twice the rate of the global terrestrial ecosystem average (Holmgren et al., 2015). This underscores the importance of estimating temperature thresholds where boreal peatland carbon emissions may change. Recent studies have found that warming resulted in peatlands shifting from carbon sinks to carbon sources (Hanson et al., 2020; J. Liu et al., 2022). The estimated emissions projections for boreal peatlands will benefit from being further constrained by boreal conifer canopy structure empirical data, granting further confidence in future peatland carbon emission estimates.

The Spruce and Peatland Under Changing Environments project (SPRUCE; https://mnspruce.ornl.gov/) is an *in-situ* whole ecosystem study in a boreal forested peatland bog located in the Marcell Experimental Forest in northern Minnesota, USA (N47°30′19″, W93°27′18″). Here, researchers are using warming and elevated CO_2 treatments to measure how the bog responds to a changing environment. The bog is elevated at 418 m above mean sea level. It is an ombrotrophic 8.1 ha acidic bog with a pore water pH of approximately 3 to 4. Peat depths are on average 2.27 m and have a basal age of 5,100 - 11,100 cal BP based on the deepest centimeter of peat (McFarlane et

al., 2018; Sebestyen & Griffiths, 2016). SPRUCE researchers have placed 12.8 m diameter, 7 m tall open-top octagonal chambers around 10 plot sections of the bog. Two plots are under control conditions and have no chamber. Each plot comprises a total area of 114.8 m^2. The warming treatments are +0°C, +2.25°C, +4.5°C, +6.75°C, and +9°C. These treatments began in June 2014 and are achieved via blowing heated air 1 m above the plot surface and with deep peat heating approximately 3 m below the surface. One set of 5 chambered plots are undergoing the warming treatments and are injected with +500 ppm CO_2 while another group of 5 plots undergoes warming but are not injected with CO_2 (Hanson et al., 2016). The CO_2 treatments began in August 2015.

SPRUCE researchers have been actively collecting empirical data to develop a modified version of the land surface component (ELM) of the Energy Exascale Earth System Model (E3SM), known as ELM-SPRUCE. They have incorporated microtopography, isotope, microbial processes, phenological processes, and root biomass data among many other empirical datasets (Carrell et al., 2022; Graham et al., 2022; Malhotra et al., 2020; Schädel et al., 2020). ELM-SPRUCE uses a model-experimental coupling framework to incorporate these data and make predictions about carbon emissions. SPRUCE researchers have found increased labile carbon outputs and methane emissions with elevated temperature conditions (R. M. Wilson et al., 2021). Currently the model incorporates canopy structural data such as tree volume, tree height, and LAI. LAI is currently estimated using specific leaf area, fraction of leaf N in RuBisCO (flnr), leaf carbon to nitrogen ratio, stem to leaf ratio, and fine root to leaf ratio (Shi et al., 2020b). An empirical dataset of canopy structure would help to constrain the uncertainty associated with these estimates.

Terrestrial laser scanning (TLS) is an active, ground-based lidar remote sensing technique. Lidar works by emitting a laser pulse at an object of interest and uses the timing of the return pulse, the speed of light, and the refractive index of the atmosphere to determine the distance from the scanner to the object. The TLS sensor provides other information about the nature of the return pulse including the intensity of reflectance, the number of return pulses, and the vector that the pulse travels. This information adds applicable elements for characterizing areas or objects of interest. Using mirrors, the instrument emits large numbers of laser pulses each second, generating dense three-dimensional datasets called point clouds. Researchers use multiple TLS scan positions surrounding the area of interest to avoid potential data gaps, or occlusion. In forests, the number of necessary scan positions is determined based on tree density and spatial patterns (L. Li et al., 2021). The subsequent point clouds provide detailed x, y, z coordinate information about scanned objects like vegetation.

TLS point clouds can provide detailed geometric data about both the vertical and horizontal profile of the black spruce and eastern larch at the SPRUCE site. The site presents some unique challenges that make collecting accurate LAI measurements challenging. Three well-established methods for measuring LAI are: destructive harvesting, allometric-based regressions, and digital hemispherical photography (DHP). Destructive harvesting involves cutting trees down and measuring leaves with scanners. It is considered the most accurate means of LAI estimation, but it cannot be consistently used as it disrupts the bog's functionality. Previously, spruce researchers used destructive biophysical linear regressions to derive allometric relationships for estimating LAI, but these were pre-treatment and do not account for changes in canopy structure or LAI due

to warming and CO_2 treatments (Griffiths et al., 2017). DHP is a challenging method to apply at the SPRUCE site because the chamber walls obscure photos. TLS is a useful alternative to these methods as it is nondestructive and unaffected by the chamber walls. However, like the allometric method, TLS requires validation data that can impede its predictive capacity if the validation data does not cover all vegetation that is under each condition of interest. Parameters can be highly sensitive to model validation, which highlights the need for a model that can consistently predict LAI with moderate accuracy across different input parameters.

The need to quantify LAI independently of allometric relationships is based on the observation that many of the plots in the warmest chambers are losing their understory leaves, but the LAI alone does not quantify the understory volume of leaves. A volumetric-based model using J. W. Wilson, (1960)'s contact frequency method offers a unique workflow for quantifying both the vertical and horizontal canopy profile (Almeida et al., 2019; Hosoi & Omasa, 2006; S. Li et al., 2017). With this model, quantification of LAI, leaf area density, and leaf inclination angle is possible, enabling us to analyze the upper portion to the lowest portion of the canopy across time and treatments.

Thesis Organization

This thesis contains two chapters that use TLS, destructive harvesting, and DHP methods to investigate the canopy structure of trees at the SPRUCE site. TLS point clouds are the primary means of quantifying canopy structure throughout each study. In the first study, we developed and validated a volumetric pixel (voxel)-based model that uses the contact frequency principle to quantify the LAI, leaf area density, and the leaf

inclination angle of the dominant boreal trees at the SPRUCE site. After validating the model against eight destructively harvested individual tree LAI estimates and two DHP LAI estimates we found that the model maintained moderately consistent accuracy across different input parameters. This result provided evidence that the model would be applicable to estimate canopy metrics in the treatment plots. In the second study, we applied the validated model to the SPRUCE plots to quantify canopy structural traits across time and temperature gradients under elevated and ambient CO_2. Additionally, we compared these plots to the unchambered control plots. Our main finding indicated that the LAI in the plots under warming was significantly increasing over time and ambient CO_2 plot LAI was significantly decreasing as temperatures increased, but LAI under elevated CO_2 did not significantly change with increasing temperature. This thesis provided a method for LAI estimation that maintains accuracy across input parameters and extended current studies about how tree canopies change over time under different levels of CO_2 and temperature.

CHAPTER TWO: VALIDATING A TERRESTRIAL LASER SCANNING & VOXEL-BASED METHOD TO MEASURE CONIFER CANOPY STRUCTURE

Introduction

Developing accurate methods and models to quantify canopy structural metrics is integral for monitoring vegetation and its impacts on processes such as photosynthesis, evapotranspiration, and respiration (Gonzalez-Meler et al., 2004). Canopy structural metrics can be challenging to accurately estimate across large spatial and temporal ranges. Many previous studies have found that terrestrial laser scanning (TLS) can effectively be used to measure canopy structural metrics, across broad spatial and temporal scales (Calders et al., 2018; Disney, 2019, p. 20; L. Li et al., 2021; Olsoy et al., 2014). Despite the evidence supporting TLS as an effective means of canopy metric quantification, models still require validation against manually made structural measurements, which are sometimes not representative of trees under different environmental conditions. This inconsistency can make allometric-based models less effective (Sterba et al., 2019). Creating a model for canopy structural estimation that maintains moderate accuracy across input parameters is needed to estimate canopies under conditions other than the original validation canopy conditions.

Canopy Metrics Significance

Leaf area index (LAI), the total projected leaf area per unit ground area (m^2/m^2), represents the plant surface available for sunlight and carbon dioxide (CO_2) intake. It is a necessary component for assessing and scaling photosynthesis and evapotranspiration within an ecosystem. It is therefore an essential ecosystem model input that mechanistically describes ecosystem structure and function and simulates responses

under changing conditions (Wang & Fang, 2020). LAI is influenced by climate, soil fertility, tree density, species, and water availability (Bond-Lamberty et al., 2002). Overstory LAI affects understory resource availability which subsequently impacts regeneration, succession dynamics, and species competition (Yazaki et al., 2016).

Including LAI in ecosystem models has improved model predictive outcomes in a variety of ecosystems. Incorporating an LAI parameter to the Penman-Monteith equation improved estimates of evapotranspiration by 14% in North American grasslands, wet tundra, temperate coniferous forests, temperate deciduous forests, xeric shrublands, and boreal forest (Qu & Zhuang, 2018). Climate models applied across China and Canada revealed that LAI estimates improved gross primary production, evapotranspiration, and water use efficiency predictions (Asaadi et al., 2018; Y. Li et al., 2018; & Qu & Zhuang, 2020). Improving LAI predictions supports more representative terrestrial ecosystem models.

Methods of LAI Estimation

LAI can be estimated directly and indirectly. One main direct method is destructive harvesting where tree leaves are manually collected (Norby et al., 2003). Leaf surface area, or specific leaf area (SLA) can be estimated from the collected samples using a scanner and finding the leaf area per unit of dry leaf mass. LAI is calculated by multiplying the SLA and the total dry mass of each foliage age class (Fang et al., 2019). Direct measurements can be spatially restricted due to their labor-intensive nature, but they are considered the most accurate estimate of LAI. Indirect methods include digital hemispherical photography (DHP) and satellite, airborne, and terrestrial remote sensing. DHP is a well-accepted, indirect ground truth method for estimating LAI (Alexandridis et

al., 2013; Gilardelli et al., 2018). It involves using a fisheye lens to calculate the gap fraction from the inversion of the Beer-Lambert law, which represents the ratio of sky pixels to total pixels in the image (**Equation 2.1**) (Chianucci, 2019).

$$P(\theta) = exp\left[\frac{-G(\theta)\Omega(\theta)L}{cos\theta}\right] \quad (2.1)$$

$P(\theta)$ is the gap fraction, θ is the zenith view angle, $G(\theta)$ is the mean projection of a unit leaf area projected on a plane normal to the zenith direction, $\Omega(\theta)$ is the clumping factor, and L is the effective leaf area index. From the Beer-Lambert law, LAI using hemispherical photography is estimated using equation 2.2 (Chianucci, 2019).

$$LAI = \int_0^{\frac{\pi}{2}} \frac{1}{n}\left[-\sum_{i=1}^{n} ln\ P_i(\theta)\right] cos\theta sin\theta d\theta \quad (2.2)$$

Where n is the number of hemispherical measurements.

Terrestrial remote sensing is an indirect method that uses gap- and contact frequency-based or biophysical regression-based models to estimate LAI. Biophysical regressions rely on relationships between vegetation structural traits, such as height and diameter at breast height (DBH), and ground truth LAI values to develop models that estimate unknown LAIs based on other tree traits (Olsoy et al., 2016). Methods relying on different tree attributes to predict LAI can be prone to error when trees experience varying environmental conditions (Chianucci & Cutini, 2013). For example, trees of the same species and height may not have the same LAI if one tree is under conditions that cause it to lose more leaves than the other tree. Gap- and contact frequency-based models are advantageous in situations where environmental conditions can alter allometric relationships as they estimate LAI using ratios of leaf occupied space to leaf unoccupied

space (Cifuentes et al., 2014; Hosoi & Omasa, 2006; S. Li et al., 2017; Seidel et al., 2012). These ratio-based estimations are made independently for each canopy of interest.

TLS-based LAI estimates are generally performed at finer scales and higher point densities than Airborne Laser Scanning (ALS) methods, better enabling TLS data-based LAI estimates to effectively correct for sources of error. TLS point cloud densities can be over 100,000 points/m^2 (Cerreta et al., 2020) and footprints range from 0.1 cm to 3 cm (Yin et al., 2020). The TLS's dense point cloud enables the separation of photosynthetic, or leaf material, from non-photosynthetic material, or wood material, for the estimation of LAI. It is also commonly used to estimate the clumping indices, leaf angle distributions, leaf area density profiles, and projection coefficients. ALS's coarser spatial resolution makes it more challenging to distinguish between leaf and wood material, making many airborne-based LAI estimations effective LAI (eLAI) measurements (Alonzo et al., 2015; Lin & West, 2016; Tang et al., 2014; Zhu et al., 2018, 2020). An eLAI is an estimation of LAI where wood material is included, or clumping is not corrected for. The high-density data derived from TLS enables the geometric analysis of features down to a single leaf or branch scale, where ALS data can result in coarser, sometimes less-accurate LAI estimates.

Forms of Error Impacting Lidar-Based LAI Estimation

Woody material is a major source of error in TLS and ALS LAI estimation. Wood components can contribute to an average LAI overestimation of 17% across conifer, broadleaf, and mixed trees (Zhu et al., 2018). The amount of wood that makes up vegetation can be estimated by subtracting leaf-off return pulses from leaf-on return pulses, but this requires the vegetation to be deciduous or have a leaf-off stage (Barclay et

al., 2000; Clawges et al., 2007). Radiometric and geometric information derived from TLS data is a more widely applicable approach to separate leaf and wood points (Atik et al., 2021; Krishna Moorthy et al., 2020; Sun et al., 2021; Vicari et al., 2019; Zhao et al., 2020; Zhu et al., 2018). Many researchers have found that geometric features are highly effective for distinguishing between leaves and wood, having accuracies ranging from 76% to 91.5% (Krishna Moorthy et al., 2020; Vicari et al., 2019; Yun et al., 2016; Zhu et al., 2018). However, features of reflectance may be more applicable for distinguishing between leaf and wood features in conifers where needle geometries are more complex at a finer scale than broadleaved trees.

Leaf inclination angle variation impacts the interception of light in the canopy and can affect lidar beam leaf contacts and therefore is a source of error for estimation of canopy traits like LAI, NDVI, and the fraction of absorbed photosynthetically active radiation (Huemmrich, 2013). The leaf angle distribution represents the distribution of the leaf inclination angles throughout the canopy at different viewing angles. It is calculated as the angle between the leaf normal and the zenith (Y. Li et al., 2017). The distribution of leaves through canopies can vary depending on canopy height, seasonality, species type, and resource availability (Raabe et al., 2015). Goel (1988), Lemeur & Blad, (1975), & Wit (1965) described six leaf angle distribution functions derived from leaf normal distributions observed from empirical data. The main functions are spherical, uniform, planophile, erectophile, plagiophile, and extremophile (**Table 2.1**) (Hu et al., 2018). Each angle can alter the probability estimation that light enters the tree canopy, making it a common source of LAI error. For more information about each function's orientation see Hu et al., (2018). The leaf angle distribution function is typically assumed

to be spherical (Chianucci & Cutini, 2013) this assumption can only be made if imagery is captured at a zenith angle of 57.5 degrees where the LAI estimation is independent of the leaf inclination angle or if the leaf angles are estimated as such (J. Zou et al., 2021). TLS and ALS data are often captured at multiple view angles so the leaf angle distribution should be quantified when estimating LAI. Previous studies have found that not correcting for the leaf inclination angle from TLS data led to a 20% - 65% error in LAI and leaf area density estimates (Hosoi & Omasa, 2006; Woodgate et al., 2017).

The leaf projection coefficient, $G(\theta)$, is a function of the leaf angle distribution and it is necessary for accurately accounting for how variation in leaf angle through the canopy affects LAI and leaf area density estimates. The coefficient represents the unit of foliage projected onto the plane normal to the direction of the laser beam (Hosoi & Omasa, 2006; Wang & Fang, 2020). Oftentimes, researchers estimating LAI will make the assumption that leaves are distributed in a spherical manner ($G(\theta) = 0.5$) (Hu et al., 2014; Ryu et al., 2012). Making this assumption at zenith view angles other than 57.5° (X. Zou et al., 2014) rather than characterizing the leaf angle distribution function and estimating $G(\theta)$ can generate LAI estimation errors (Pisek et al., 2013). The mean projection coefficient is estimated by integrating the leaf inclination angle distribution function over the leaf inclination angle. Yan et al., (2021) estimated LAI using TLS for conifers and found that assuming a spherical distribution function across zenith angles generated errors up to 53% if scanning from a nadir view.

Table 2.1. Leaf inclination angle distribution functions

Leaf Inclination Angle Distribution Function Name	Leaf Inclination Angle Distribution Function	Average Leaf Inclination Angle (θ_l)
Spherical	$g(\theta_l) = \sin(\theta_l)$	57.3
Uniform	$g(\theta_l) = 2/\pi$	45.00
Planophile	$g(\theta_l) = 2 \cdot (1 + \cos 2\theta_l)/\pi$	26.76
Erectophile	$g(\theta_l) = 2 \cdot (1 - \cos 2\theta_l)/\pi$	63.24
Plagiophile	$g(\theta_l) = 2 \cdot (1 - \cos 4\theta_l)/\pi$	45.00
Extremophile	$g(\theta_l) = 2 \cdot (1 + \cos 4\theta_l)/\pi$	45.00

Another commonly addressed form of error is the clumping effect, which alters the probability of detecting or not detecting a leaf due to overlap. A canopy has more clumped leaves as the clumping index approaches 0. As it approaches 1 the canopy has a random distribution of foliage, and when the index is greater than 1 the canopy is considered uniform. Clumping can occur at the between-crown and within-crown spatial scale, making it spatially complex. Using the Beer-Lambert law to estimate the gap fraction requires the assumption that the leaves of the trees are randomly distributed. Tree leaves are typically not randomly distributed leading to leaf clumping. There are several clumping estimation methods available using gap fraction and gap size distributions. Researchers have combined the two methods for estimating clumping at within- and between- canopy scales (Chianucci, 2019; Leblanc, 2002) (**Equation 2.3**).

$$\Omega(\theta) = \frac{ln[F_m(0,\theta)]}{ln[F_{mr}(0,\theta)]} \cdot \frac{[F_m(0,\theta) - F_{mr}(0,\theta)]}{[1 - F_m(0,\theta)]} \tag{2.3}$$

Where Ω is the clumping index, θ is the zenith angle, F_m is the total gap fraction, and F_{mr} is the gap fraction after removing large gaps. Clumping can also be corrected for using voxelization techniques that standardize the point cloud and reduce point overlap (Hosoi & Omasa, 2006). Previous studies have found that clumping causes an average LAI underestimation of 14.2% and that clumping indices were lower on average in coniferous forests than in broadleaf forests (Zhu et al., 2018).

Study Site and Research Objectives

In this study, we evaluated conifer structure using TLS as part of the Department of Energy's project, Spruce and Peatland Responses Under Changing Environments (SPRUCE) study which examines the influences of elevated temperature and CO_2 conditions over time (2015 - 2022) in a boreal peatland ecosystem. SPRUCE researchers have previously used destructive biophysical linear regressions to derive allometric relationships for estimating LAI, but these were pre-treatment and do not account for changes in canopy structure or LAI due to warming and CO_2 treatments. This problem requires a canopy structure estimation with modifiable parameters that maintain moderate accuracy against validation. We developed a modified version of the VCP model and corrected for wood components, leaf inclination angle, leaf projection coefficient, and clumping. This study combines methods from: Almeida et al. (2019); Hosoi & Omasa (2006); S. Li et al. (2017); & Yan et al. (2021). SPRUCE is an ideal study location to develop, modify, and validate a contact-frequency voxel-based LAI model.

The research goal in this study was to determine how accurately a VCP-based TLS method can estimate the LAI of the two main conifer species at the SPRUCE site, *Picea mariana* (black spruce) and *Larix laricina* (eastern larch). We expected that this

method would maintain an accuracy of at least 90% across input parameters as validated by eight individual tree destructively harvested measurements and two plot based hemispherical photography measurements. The VCP method addresses four of the major challenges associated with predicting LAI using TLS. These challenges are leaf and wood separation, clumping, leaf angle distribution, and the leaf projection coefficient. The model estimates leaf area density and inclination angle across the canopy vertical profile and LAI across the canopy horizontal profile. We present these measurements and their relationships through the vertical canopy profile and with each other.

Methods

Study Site Description

The SPRUCE (https://mnspruce.ornl.gov/) whole-ecosystem climate experiment is located in the S1 bog of the Marcell Experimental Forest in northern Minnesota, USA (N47°30′19″, W93°27′18″) (**Figure 2.1A**). The bog is an 8.1-hectare acidic ombrotrophic bog with an average peat depth of 2.27 m. Ombrotrophic bogs have perched water tables (418 m above sea level) and are maintained predominantly through precipitation. Annual precipitation is approximately 768 mm and average air temperature from 1961 to 2005 was 3.3°C. The soils are a low drainage Greenwood series, a Typic Haplohemist (http://websoilsurvey.nrcs.usda.gov) with a deep peat age of 5,100 - 11,100 cal BP composed of materials deposited by glacial lakes (Sebestyen & Griffiths, 2016). The peatland understory is characterized by varieties of ericaceous shrubs, mosses, and lichens (Lynch et al., 2002). The primary SPRUCE vegetation of interest in this study are the two dominant conifer species, *Picea mariana* (Mill.) B.S.P. (black spruce) and *Larix laricina* (Du Roi) K. Koch (eastern larch or tamarack). The site is considered highly

vulnerable to climate change due to its location near the southern boundary of the boreal region. Previous SPRUCE study results have found that the site is a carbon sink, but more recent findings reveal that, with warming, it will likely shift to a carbon source (Hanson et al., 2020). In this study, we created and validated a model to predict canopy structure metrics across 12 plots (**Figure 2.1B**) at the SPRUCE site.

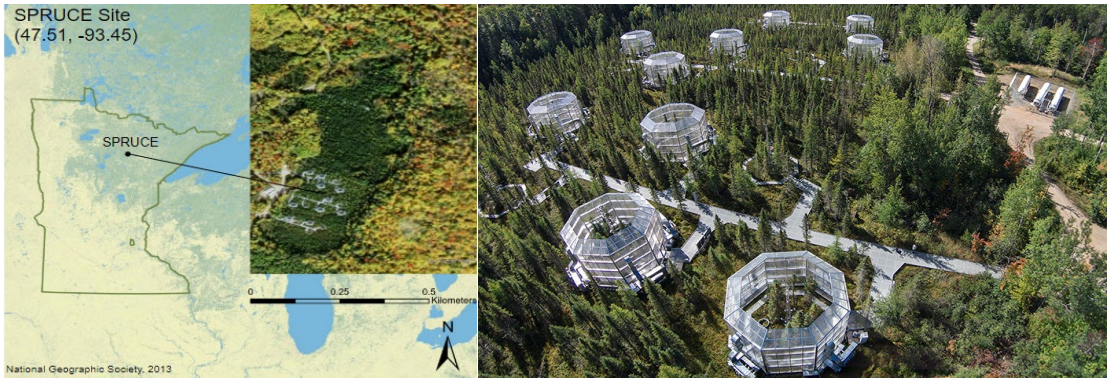

Figure 2.1A. The SPRUCE study site is in a boreal peatland bog located in northern Minnesota, USA. B. Sections of the peatland are partitioned into 12 m diameter, open top chambers. The chambers generate different levels of temperature and CO_2 manipulation.

The spruce and larch trees underwent disturbance events in 1976 that led to 46 years of regrowth in the S1 bog. The trees were strip cut to study regeneration in the spruce trees. Seedlings larger than 1 cm in diameter at 1.3 m above the *Sphagnum spp.* surface are included as trees in this study. Both tree species are often found in low nutrient, anoxic, acidic conditions such as the S1 bog. However, the black spruce can be found in a variety of soil moisture regimes and elevations. The SPRUCE site has a raised water table, but black spruce has also been found in dry substrate of drained peatlands (Lynch et al., 2002). The larch tree is most found in peatlands, along a similar geographic range to the black spruce. *L. laricina* grows best in well-drained loamy soils along fresh bodies of water, but the tree is scarcely found in areas with these soils because of its

intolerance to shade and the tendency to be outcompeted by other trees (Uchytil, 1991). Both the larch and spruce tree's growth season begins in early to late spring, early May, and ends in late autumn, early November.

Sections of the peatland are under elevated carbon dioxide and temperature conditions to generate aboveground and belowground warming effects. The warming effects take place using 12.8 m diameter and open-top chambers (**Figure 2.1B**), with a total area of 114.8 m^2 per chamber (Hanson et al., 2016). Air warming via blowing heated air 1 m above the bog surface and peat warming via heating elements inserted 3 m into the peat layer, occur at a range of temperatures: +0°C, +2.25°C, +4.5°C, +6.75°C, and +9°C. Peat warming began in June 2014 and air warming began in August 2015 (Hanson et al., 2016). Throughout chambers, there are two of each temperature treatment. One temperature treatment undergoes elevated carbon dioxide by injecting CO_2 to a concentration of +500 ppm above ambient. The injections began in June 2016 (Hanson et al., 2016). Additionally, the study includes two unchambered control plots.

TLS Data Collection and VCP LAI Estimation Model

TLS scans of the plots were collected using a Riegl VZ-1000 which has a 1550 nm laser and an angular resolution of 0.04 degrees. Data collection took place biyearly, during spring, the beginning of the growth period, and summer, the maximum growth period. Only summer scans were used in this study. From 2015 - 2019, the scans were first taken from four points symmetrically placed around plot perimeters (Graham, 2020). Following the extensive growth of the trees, from 2020 - 2022 five to eight scan positions were placed symmetrically around the plot to reduce occlusion effects (**Figure 2.2**).

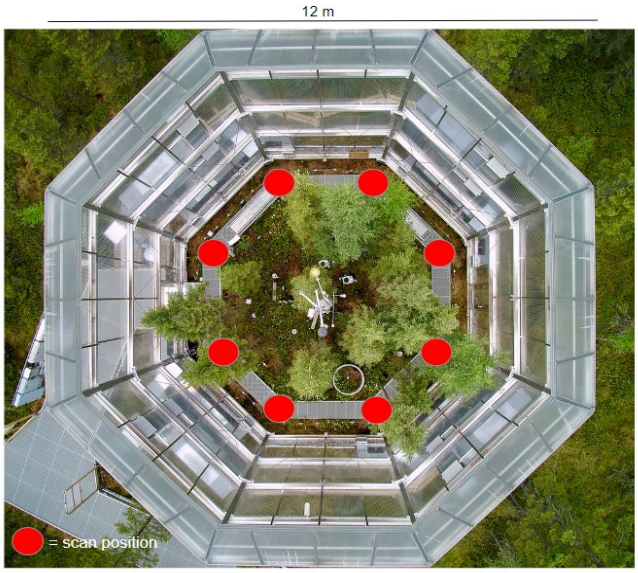

Figure 2.2. Nadir view of a chambered plot at the SPRUCE site. Red circles indicate TLS scan position locations.

We estimated the LAI from the plot point clouds using the VCP method initially developed by Hosoi & Omasa (2006). Point clouds were preprocessed using a point deviation filter and correcting the intensity by the range to obtain reflectance values of the points. We used CloudCompare's Cloth Simulation Filter tool (Zhang et al., 2016) to extract the ground points of each point cloud. We removed any remaining non-tree points manually. We manually collected 66,456 wood points and 65,964 leaf points to build a random forest based on the number of return and intensity value features to separate the leaf and wood components of each tree point cloud (**Figure 2.3A & B**). Its parameters included 100 decision trees and no max node depth. We tested the model fit using a ten-fold cross validation where 90% of the training data was used to classify 10% of the remaining data in ten different partitions. The random forest and VCP algorithm work with multiple conifer trees and individual conifer trees as validated by destructive and DHP-based estimates of LAI.

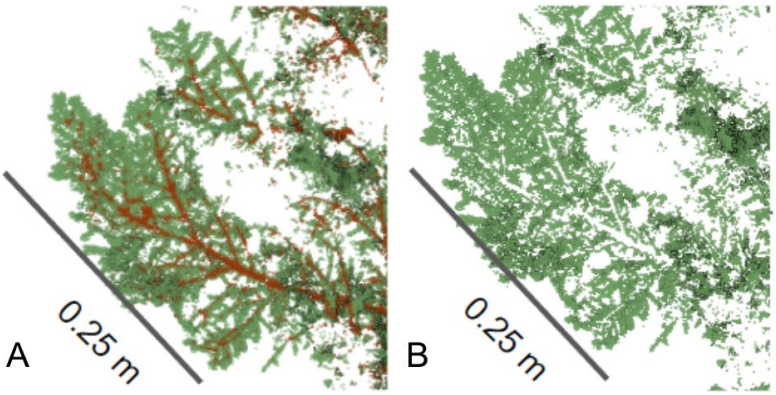

Figure 2.3A. Spruce conifer branch before wood component removal. B. Spruce conifer branch after wood component removal using the random forest model based on reflectance and number of returns features.

We used the Python package Open3D v0.16.1 (Zhou et al., 2018) to voxelize and estimate the point cloud's normal vectors. We visualized the point clouds using Open3D and CompuTree (Computree Core Team, 2017). Using 3.25 cm voxels (grid cell volume = 0.00003433 m^3), we voxelized the tree to normalize the raw point cloud data and generate volumetric and area-based data (**Figure 2.4A & B**).

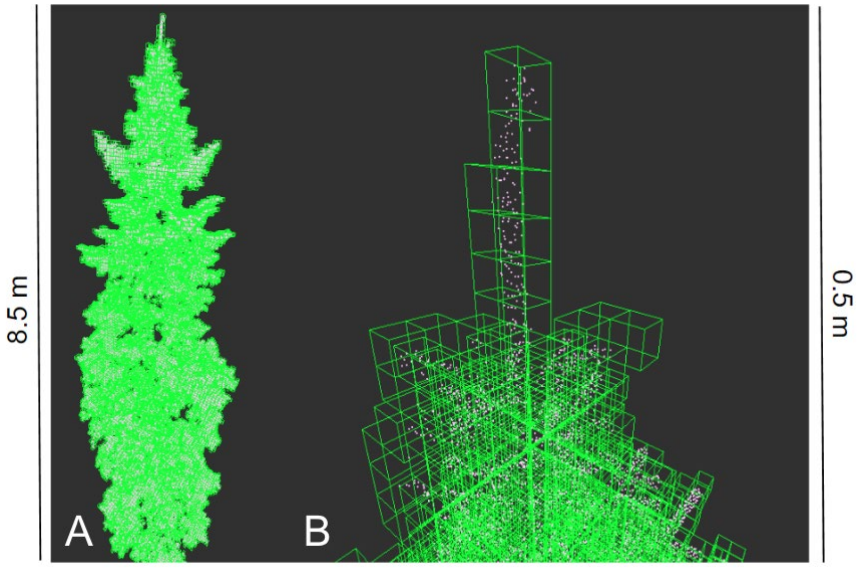

Figure 2.4A. Full spruce tree voxelized using 3.25 cm voxels. B. Top 0.5 m of a spruce tree voxelized using 3.25 cm voxels. ***Data visualized using CompuTree, 2022.***

We generated canopy profiles by slicing the voxelized tree point cloud into 0.5 m cross sections through the vertical canopy (**Figure 2.5).**

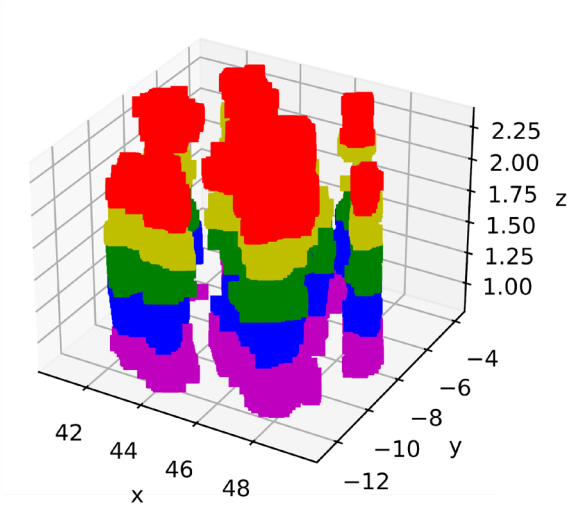

Figure 2.5. SPRUCE plot horizontally sliced to generate 0.5 m width vertical canopy profiles. Color is representative of an individual 0.5 m slice.

At each half meter slice, we calculated a distribution of leaf inclination angles. Using the Open3D algorithm, we estimated the leaf normal vectors through principal axis calculation of the adjacent points and the use of a covariance analysis (**Figure 2.6**), which we used to estimate the leaf inclination angles (**Equation 2.4**) (Yan et al., 2021).

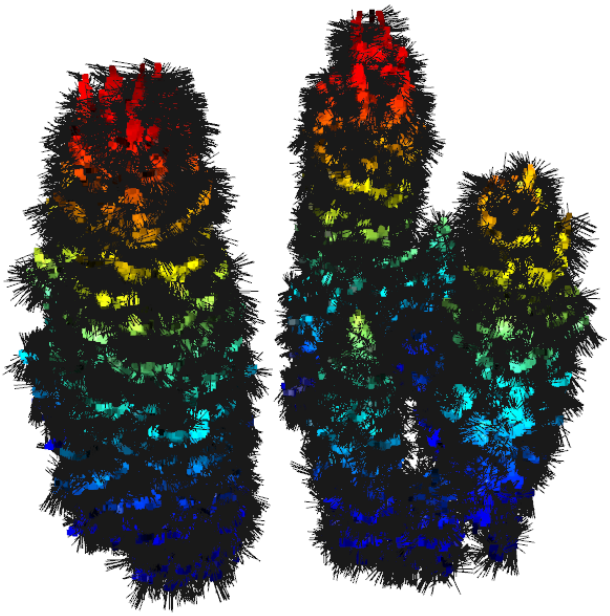

Figure 2.6. SPRUCE trees with estimated leaf normal vectors using a principal axis and covariance analysis. Colors represent 0.5 m change in tree height.

$$\theta_l = \begin{cases} arccos \dfrac{n \cdot v}{||n||\,||v||} & n \cdot v > 0 \\ 180^\circ - arccos \dfrac{n \cdot v}{||n||\,||v||} & n \cdot v \leq 0 \end{cases} \quad (2.4)$$

Where n is the normal vector to the leaf and v is the real vertical direction or the zenith laser of the TLS in this study. From the leaf angles (θ_l), we found the leaf angle distribution function $g(\theta_l)$, which is needed to estimate the leaf projection function $G(\theta)$. Both the leaf angle distribution function and the mean projection function account for how differences in the viewing angle (laser zenith angle) affect the interpretation of leaf angles impact on light transmission in the canopy. The leaf angle distribution function is the probability that a leaf normal will fall within a unit interval of an inclination angle. We calculated the leaf projection function by integrating the leaf angle distribution function over the leaf inclination angles (**Equation 2.5 & 2.6**), (Almeida et al., 2019; Hosoi & Omasa, 2006; S. Li et al., 2017; Yan et al., 2021).

$$G(\theta) = \int_0^{2\pi} g(\theta_l)\, S(\theta, \theta_l) d\theta_l \quad (2.5)$$

$$S(\theta, \theta_l) = \begin{cases} cos\theta\ cos\theta_l, & \theta \leq \frac{\pi}{2} - \theta_l \\ cos\theta\ cos\theta_l[1+\frac{2(tan\ x - x)}{\pi}], & \theta > \frac{\pi}{2} - \theta_l \end{cases} \quad (2.6)$$

$$x = cos^{-1}(cot\theta cot\theta_l)$$

$S(\theta, \theta_l)$ is the average of $|cos(\overrightarrow{n_B}, \overrightarrow{n_L})|$, which is the absolute value of the cosine of the angle between the laser unit vector and the leaf normal vector (Hosoi & Omasa, 2006; Yan et al., 2019). The resulting leaf projection function led to the correction factor calculation, $\alpha(\theta)$, ((**Equation 2.7**), Hosoi & Omasa, 2006; S. Li et al., 2017). The correction factor corrects for how the interpretation of leaf angles at different laser zenith views affect the LAI estimate.

$$\alpha(\theta) = \frac{cos\theta}{G(\theta)} \quad (2.7)$$

To determine the final contact frequency counts and estimate the leaf area density we performed a convex hull using the SciPy spatial package (SciPy v0.14.0) to calculate the volumes of voxels that the beam contacted and the voxels that the beam passed through, representing a gap. From the convex hull we calculated the number of possible voxels that would fill the plot area, 66.44 m^2, and subtracted the number of actual voxels to find the empty voxels which the beam passed through (**Figure 2.7**).

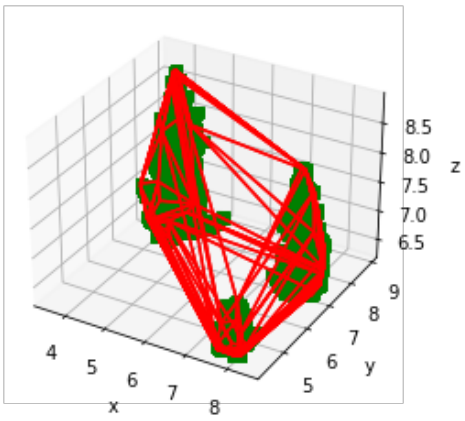

Figure 2.7. A convex hull found the volume of voxels in the canopy space where a laser beam contacted the canopy and where laser beams passed through the canopy at each 0.5 m layer (Visualized using SciPy v1.7.3).

For each canopy 0.5 m horizontal profile, we calculated a leaf area density value based on the contact frequencies using **equation 2.8** (Almeida et al., 2019; Hosoi & Omasa, 2006). LAI is then estimated from the leaf area density as the sum of the leaf area densities through the vertical profile (**Equation 2.9**).

$$LAdensity(h, \Delta H) = \alpha(\theta)\frac{1}{\Delta H} \cdot \sum_{k\,=\,m_h}^{m_h+\Delta H} \frac{n_l(k)}{n_l(k) + n_p(k)} \tag{2.8}$$

$$LAI(h) = \alpha(\theta) \cdot \sum_{k\,=\,m_h}^{m_{HT}} \frac{n_l(k)}{n_l(k) + n_p(k)} \tag{2.9}$$

Where $LAdensity$ is the leaf area density in m^2/m^3, $\alpha(\theta)$ is the leaf angle-based correction factor, m_h is a single canopy profile layer, ΔH is the thickness of each canopy profile in m, $n_l(k)$ is the number of laser beams intercepted at a voxel in a canopy layer, $n_p(k)$ is the number of laser beams passing through a voxel in a canopy layer, and m_{HT} is the treetop height.

To evaluate the degree of error that is effectively corrected for in the LAI prediction, we conducted an error analysis. We determined the degree of LAI estimate

error that would result from not correcting for wood components, leaf inclination angle distribution, assuming a spherical mean projection coefficient, or clumping by evaluating the values as corrections were removed using **equation 2.10**.

$$error = \frac{LAI_{precorr} - LAI_{corr}}{LAI_{corr}} \cdot 100 \quad (2.10)$$

Where $LAI_{precorr}$ is the LAI with one of the correction procedures removed from the model prediction. LAI_{corr} is the corrected LAI.

Destructive Harvest Collection and LAI Calculation

Destructive harvesting of larch and spruce trees took place for a set of direct measurements of LAI at only one time during the study to minimize impacts to the bog. In the summer of 2018, after new foliar cohorts were fully expanded, researchers took three to seven TLS scans of four larch trees and four spruce trees outside of designated plots, generating four point clouds (n = 8 trees). Registered point clouds were processed to remove noise or points with weak returns. Each of these trees were outside of experimental plots. The larch tree heights included 2.13 m, 2.84 m, 6.5 m, and 8.95 m. The spruce tree heights included 2.49 m, 3.62 m, 5.56 m, and 8.93 m. The destructive harvest LAI estimates provided 8 samples for the VCP model validation.

After collecting the scans of the eight trees outside of the chamber plots, SPRUCE researchers used destructive harvesting techniques to collect dry weights for bole sections, branches, and needles of the four larch trees and four black spruce trees and their fresh foliage surface area. Using the leaf metrics, we calculated the SLA, the ratio of fresh foliage surface area to dry foliage mass. The ground area for each tree (i.e., the

canopy area projected onto the ground) was calculated as shown in **equation 2.11**. LAI was quantified by multiplying the SLA and the total foliage dry mass of each tree and dividing by the sampled ground area (**Equation 2.12**).

$$SGA = \pi \times (\frac{1}{2} \times (CW))^2 \quad (2.11)$$

$$LAI_i = (SLA \times LM) \,/\, SGA \quad (2.12)$$

SGA is the sampled ground area in m^2 and CW is the canopy width in m. LAI_i is the LAI of an individual tree, SLA is the specific leaf area in leaf area per unit of dry leaf mass (m^2/g), LM is the total foliage dry mass of a tree (g).

Hemispherical Photography Collection and LAI Estimation

In August of 2022, we collected six hemispherical photographs per plot (n = 72 photos) to validate TLS estimates of LAI. Photograph positions were placed symmetrically around the perimeter of a SPRUCE plot. The camera was attached to a 1.5 m monopod with a digital inclinometer and photos were collected at both nadir and 57.5° view angles. We recorded the photographs using the Rokinon 8 mm f/2.8 UMC Fisheye II Lens for a Sony E Mount. We adjusted the camera to be 1 - 2 steps overexposed (Seidel et al., 2012). Challenges with chamber wall removal from the hemispherical photographs introduced errors to the LAI estimates. As a result, we only processed and estimated the LAI from the unchambered plots, 2 out of 12 plots. These were used as additional metrics of model validation.

We estimated the LAI of the digital hemispherical photographs using the HemispheR R package (Chianucci, 2019). After applying a circular mask to the image, we selected the blue channel for classification because it has the most contrast between sky and leaf pixels (Brusa & Bunker, 2014). A gamma value of 2.2 corrected the gray

pixels of the image (Glatthorn & Beckschäfer, 2014) before binarizing it. We used the Otsu method to binarize the image. The Otsu algorithm defines the binarization threshold by minimizing the intra-class variance, which is the weighted sum of the two classes' variances (Chianucci, 2019). From the binarized image, we calculated the gap fraction using **equation 2.1**. The gap fraction was calculated using a maximum zenith angle of 90 degrees, lower zenith angle of 0 degrees, upper zenith angle of 70 degrees, 5 zenith rings, and 8 azimuth sectors. The final LAI estimate was calculated using the inverted angular gap fraction and Miller's theorem (Miller, 1967) (**Equation 2.13**).

$$LAI = 2\int_0^{\frac{\pi}{2}}(-ln(P_0\theta cos\theta sin\theta d\theta)) \quad (2.13)$$

We estimated two different clumping indices from an ordered weighted average gap fraction and calculated the ratio between them to estimate a clumping correction factor (Chianucci, 2019) (**Equation 2.14)**

$$\Omega(\theta)L = \frac{-\int_0^{\frac{\pi}{2}} ln\left[\sum_{i=1}^{n} w'_i \; P_i \downarrow \theta\right]}{-\int_0^{\frac{\pi}{2}} ln\left[\sum_{i=1}^{n} w'_i \; P_i \uparrow \theta\right]} \quad (2.14)$$

$$w'_i = \frac{2(n+1-i)}{n(n+1)}; \; w'_i = \frac{1}{n}\sum_{j=1}^{n}\frac{1}{j} \quad (2.15)$$

where w'_i represents the two different weighted vectors (**Equation 2.15**). The workflow provided estimates of Effective Leaf Area Index (eLAI), LAI, a clumping correction factor, canopy openness estimate, and the mean leaf tilt angle.

Results

VCP Model Validation

The cross validation for the leaf and wood separation method resulted in a 95% accuracy. The number of returns explained 36.1% of the classification and the reflectance

values explained 63.9% of the classification. The model had an average overall accuracy on test data of 92% and an average F1 score of 87% based on seven manually classified trees. We compared our separation method to two other available methods. One was based on eigen-features (Krishna Moorthy et al., 2020) and the other was based on dimensionality and known as the CANUPO method in CloudCompare v2.12. The geometric-based algorithms did not produce the same accuracy for the conifers (see Appendix A for leaf and wood model separation accuracies).

We validated the VCP model using eight trees with destructively harvested-based individual LAIs (LAI_i) and two DHP-based LAI estimates at the plot scale. A simple linear regression analysis showed that the model predicted LAI of the individual trees and the tree plots with a coefficient of determination of 0.89 ($R^2 = 0.89$), an RMSE of 0.98, and an nRMSE of 0.17 (**Table 2.2, Figure 2.8**). The lowest nRMSE and highest R^2 value was found using a voxel size of 3.25 cm (**Figure 2.9**). Values of nRMSE ranged from 0.17 - 0.23, and R^2 values ranged from 0.81 - 0.89. TLS-based LAI_i measurements overestimated values for five of the eight destructively harvested trees. The remaining three tree LAI_is were underestimated. Compared to DHP LAI estimates, TLS underestimated the LAI of one of the two plots.

Table 2.2. TLS-based estimates of LAI at the individual tree and plot level, destructive harvest-based LAIi at the individual tree level, DHP-based LAI at the plot level.

Plot or Individual Tree	Species	Max Height (m)	TLS-based LAI_i or LAI	Destructive- based LAI_i or DHP-based LAI
Tree 1	spruce	2.49	2.57	1.19
Tree 2	spruce	3.62	2.92	3.65
Tree 3	spruce	6.5	6.82	7.38
Tree 4	spruce	8.93	6.93	6.38
Tree 1	larch	2.13	1.34	0.75
Tree 2	larch	2.84	2.07	0.97
Tree 3	larch	5.56	4.86	3.44
Tree 4	larch	8.95	6.98	8.58
Plot 7	all	6.72	4.87	4.87
Plot 21	all	7.73	4.55	5.26

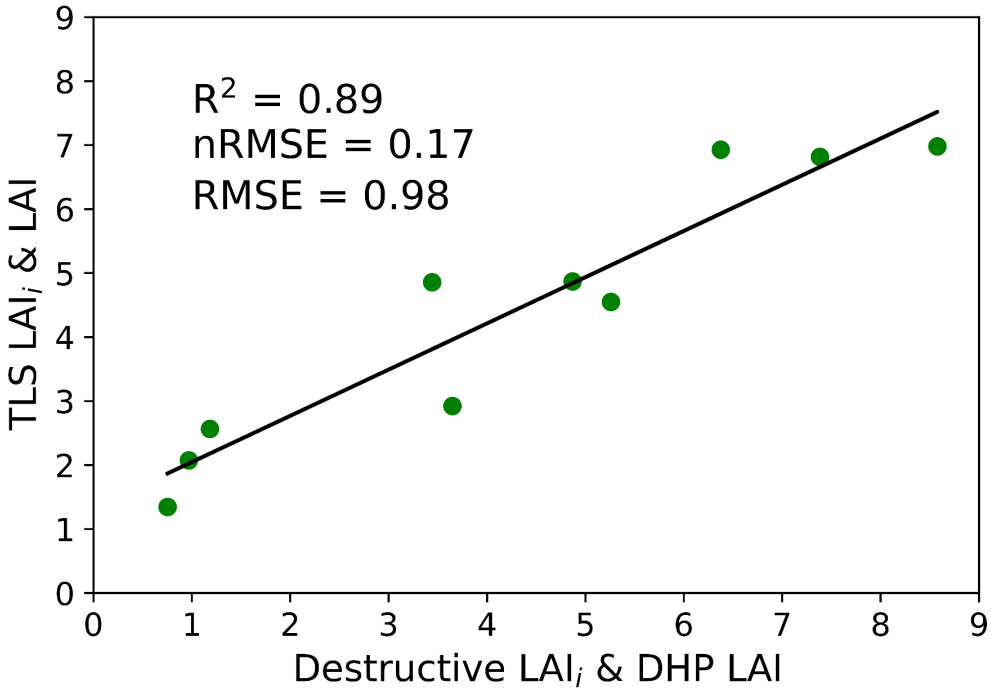

Figure 2.8. Validation of the TLS-based LAI_i and LAI against the destructively harvested LAI_i and DHP LAI (n = 10).

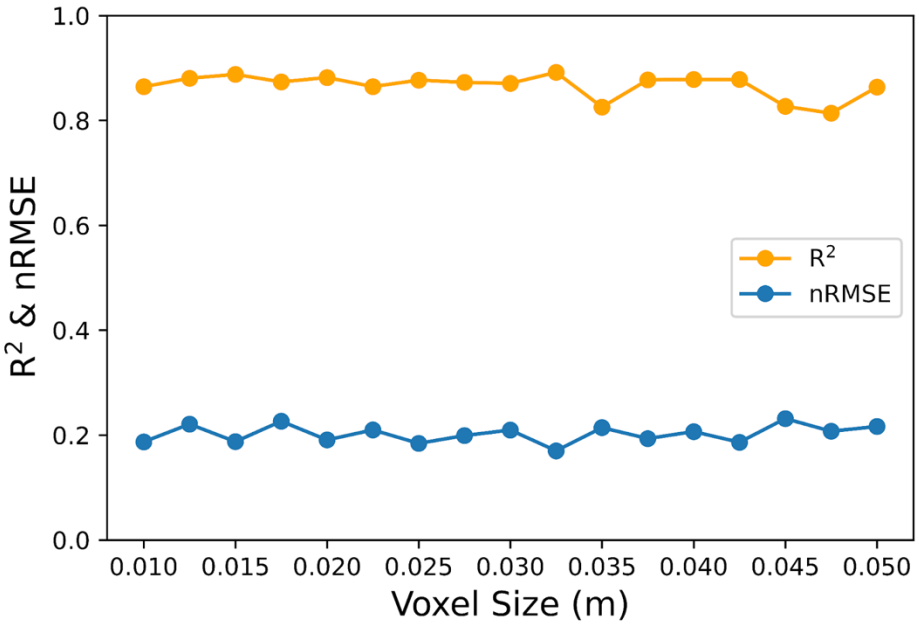

Figure 2.9. R^2 and nRMSE values of the validated LAI estimates calculated across different voxel sizes.

Destructively Harvested Leaf Area Density

We estimated leaf area densities using TLS data for each of the individual trees used for validation. Distributions of individual leaf area density through the vertical canopy increased in the center and upper portion of the canopy for the largest spruce tree. Similarly, individual tree leaf area density increased in the center of the canopy for the largest larch tree. The average leaf density of the four individual spruce trees was 0.49 m^2/m^3. The average leaf density of the four individual larch trees was 0.40 m^2/m^3 (see Appendix A for individual tree leaf area density figures).

Destructively Harvested Leaf Inclination Angles

The two main leaf angle distribution functions for the larch and spruce trees in the study were best represented by the spherical (**Equation 2.16**) and erectophile (**Equation 2.17**) functions.

$$g(\theta_l) = sin\theta_l \quad (2.16)$$

$$g(\theta_l) = 2(1 - cos2\theta_l) / \pi \quad (2.17)$$

Where $g(\theta_l)$ is the leaf distribution function and θ_l is the leaf inclination angle. Neither species of tree only represented one distribution or the other across all eight individuals. Individual spruce trees tended to have vertically distributed leaves, on average following the erectophile distribution. The larch trees had a more normal distribution of leaf angles, representing a spherical distribution, which is more symmetrical and planar. We evaluated the average leaf angle throughout the canopy height of the largest larch and spruce tree. Generally, leaf angles were more spherical in the upper canopy and more vertical in lower portions of the canopy of both trees (see Appendix A for individual tree leaf angle figures).

Leaf Angle and Leaf Area Density

To determine if there was a relationship between leaf inclination angle and leaf density, we compared the two metrics through the vertical canopy. We found that as leaf area density increased in the canopy of each of the eight trees, leaves tended to be more symmetrically distributed. When leaf area density decreased, leaves shifted to more vertical distributions (see Appendix A for individual tree leaf angle and leaf area density figures).

Leaf Area Index Correction Factor Error Analysis

We conducted a percent error analysis to determine the amount of LAI error each correction factor accounted for. Inputting point clouds with wood components into the VCP model resulted in an average 2.8% overestimation of LAI. When we removed the leaf inclination angle distribution function estimation, the LAI was overestimated on average by 66.2%. Assuming a spherical distribution and setting the projection coefficient value to 0.5 ($G(\theta) = 0.5$), generated an average 14.2% LAI overestimation. Removing the needle clumping correction workflow resulted in an average 6.5% LAI underestimation.

Table 2.3. Correction factor error analysis.

Correction Factor Removed	Wood Component Separation	Leaf Inclination Angle	Projection Coefficient Calculation	Clumping
Mean Error	2.8%	66.2%	14.2%	-6.5%

Discussion

In this study, we asked, how accurately can we predict the LAI of the spruce and larch trees using TLS data. We expected to achieve a 90% accuracy using a contact frequency-based method and corrections for wood components, leaf inclination angle distribution, leaf projection coefficient calculation, and clumping. The use of the modified VCP model method, initially proposed by Hosoi & Omasa (2006) enabled us to predict the LAI of 8 peatland conifers and 2 peatland conifer plots. Using Yan et al., (2021)'s leaf inclination angle estimation method for conifers allowed for the correction of the projection coefficient and provided additional vertical information about the larch and spruce canopies. The model predicted LAI at the individual tree and conifer plot scale with a $R^2 = 0.89$, RMSE = 0.98, and nRMSE = 0.17 as validated by destructively harvested and DHP estimates. The model maintained moderate prediction accuracy ($R^2 > 0.80$) across different voxel sizes. Our error analysis showed that leaf inclination angle distribution affected the LAI correction the most, generating a 66.2% LAI overestimation when removed from the model. We found that separation of the wood component only corrected for 2.8% of the LAI estimation in comparison. Previous studies found that wood components accounted for 17.1% of overestimation error, but this included broadleaf trees which tend to have a higher woody area than conifer trees (Zhu et al., 2018). Taken together, results suggest that woody components contribute to less error in conifers. Other types of error that affect remote sensing derived LAI estimates such as but not limited to, voxel size, occlusion, saturation, and topography can be found in (L. Tian et al., 2021; Wang & Fang, 2020; Yan et al., 2019).

Recent studies estimating LAI using TLS and a version of the voxel contact frequency model have found the model to be highly reliable for predicting individual magnolia tree LAI with accuracies being 99.9% and 90.7% on two different magnolia species (S. Li et al., 2017). Oshio et al. (2015) estimated leaf area density of broadleaf trees using voxel contact frequency methods with an accuracy of 95%. Each of these studies and others (Béland et al., 2014; Grau et al., 2017) found LAI, PAI, and clumping prediction accuracy was highly dependent on the specified voxel size and voxel processing. Our results showed that in the larch and spruce trees, with all correction factors applied, moderate LAI prediction accuracy can be achieved using a wide range of voxel sizes. Nguyen et al. (2022) found voxel effects on plant area density accuracy measurements were dependent upon the size of the wood and foliage present. Conifer trees with smaller branches and foliage were less susceptible to voxel size discrepancies. The wide range of applicable voxel sizes provides confidence that the LAI of the SPRUCE conifer trees can be estimated well across trees under treatment conditions. Based on previous studies, the chosen voxel size and its relationship to the estimation metric can vary across study systems (Béland & Kobayashi, 2021). Therefore, it is essential to perform one's own voxel tests. Additional options include using information about leaf size (Béland et al., 2014) or the range and scan resolution (S. Li et al., 2017) to make a voxel size selection.

To our knowledge, the full workflow of the modified VCP method in this study has not been tested on the eastern larch and black spruce species at the individual and plot level scale. Researchers have tested versions of this method on broadleaf species (Béland & Kobayashi, 2021; Hosoi et al., 2013; Itakura & Hosoi, 2019; Y. Li et al., 2017;

Oshio et al., 2015; Rouzbeh Kargar et al., 2019; Su et al., 2018), individual conifers (Lin & West, 2016), to estimate eLAI (Flynn et al., 2022), ALS data (Almeida et al., 2019), or as applied single workflow sections to conifers (S. Li et al., 2017). Here, we provided evidence that our version of the full workflow of the VCP method is applicable to conifer trees at the plot and individual tree spatial scale.

Our results support previous black spruce LAI and leaf area density research. Researchers have previously found that black spruce LAI ranges from 0.178 - 8.97 and an average of 3.9 based on 71 studies in the Global LAI Database from the Oak Ridge National Laboratory (ORNL) (IIO & ITO, 2014) and Angstmann et al., (2012). Based on 10 studies from the ORNL LAI database, eastern larch LAI ranged from 0.68 - 3.29, with an average of 1.9. Our LAI estimates are within the presented ranges for previous black spruce studies. There are no current studies that measure leaf area density in the black spruce or the eastern larch, but Sterba et al. (2019) measured leaf area density in 74 *Picea abies* (Norway spruce) and 120 *Larix decidua* (European larch) and found that their leaf area densities ranged from 0 m^2/m^3 - 1.4 m^2/m^3 and 0 m^2/m^3 - 1.3 m^2/m^3 respectively. Our leaf area density estimate ranges for spruce were similar ranging from 0.06 m^2/m^3 - 1.5 m^2/m^3.

We extend previously recorded eastern larch canopy datasets that have been developed based on trees in different environments, using different species of larch, and with time-consuming manual methods. Eastern larch LAI studies are more limited than black spruce studies, resulting in less estimations of eastern larches as large as the ones in the current study. The current eastern larch LAI database is based on eastern larch trees found mainly in fen habitats (IIO & ITO, 2014), which differ from the SPRUCE bog

environment. Leaf area density estimates also differed for larch trees in our study, 0.11 m^2/m^3 - 0.67 m^2/m^3. Larch trees were considered a dominant species in some mixed plots in Sterba et al. (2019) while in our study the black spruce is exceedingly dominant, potentially leading to lower leaf area densities than theirs. We also examined a different species which affects leaf area density values. Yan et al. (2021) estimated leaf inclination angle distributions of unspecified species from the larch and spruce genera. They found that 3 spruce trees had a range of 33.7° - 47.56° and 4 larch trees had a range of 31.4° - 45.6°. The researchers were only able to measure portions of the tree's needles due to using manual measurements and comparing them with subsequent 3D models. In our validation study we attempted to estimate each individual leaf angle throughout 8 trees and 2 plots of trees. The differing needle analysis coverage and unknown species could lead to this inclination angle discrepancy. However, their findings support our findings that spruce and larch trees tend to, generally, have similar leaf inclination angle distributions. Additionally, it is well documented that leaf inclination angle is affected by location (S. Li et al., 2023), further explaining the discrepancy between our findings.

Our main finding indicates that the version of the VCP we presented has modifiable parameters that are robust to validation metrics and can predict canopy structural parameters with moderate accuracy at different spatial scales. This canopy structure evaluation method is highly suitable for analyzing canopy changes over time under different environmental conditions, such as elevated CO_2 and elevated temperature levels since it holds moderate prediction accuracy across different input parameters. The VCP model can provide measures of both 3D vertical and 2D horizontal canopy parameters, which are useful for constraining carbon emission predictions from climate

models such as the SPRUCE site's modified version of the Energy Exascale Earth System Model's land component (ELM). Peatlands are underrepresented in many land surface models, generating uncertainty in global climate predictions (H. Tian et al., 2015). The SPRUCE site's version, ELM_SPRUCE, was developed to improve peatland representation in ELM.

Although our data indicates that the model consistently predicts LAI with moderate accuracy there are limitations in this study that should be addressed. The small validation sample size (n = 10) is a limiting factor in this study. However, the range of validation sample sizes across LAI models is broad. S. Li et al. (2017)'s model validation study consists of only 2 magnolia trees, each a different species. Yan et al. (2021)'s leaf angle validation study consisted of four larch and three spruce trees. While other studies have used around 30 measurements for validation (Indirabai et al., 2020). In a future study, we propose updating the current VCP model with at least four more larch and four more spruce destructively harvested trees to build a validation dataset. We aimed to limit destruction to the bog as much as possible, leading to more emphasis on the nondestructive method. Leaf inclination angles and leaf density values were also not validated using manual methods, but they are each directly related to the LAI estimation, which was validated. Making broad conclusions about spruce and larch canopy structure at this point is not possible due to the sample size of the dataset, but the dataset is useful in that it offers a broad larch and spruce size dataset. The general contact-frequency method has been applicable to other environments, but this specific modified model is not necessarily applicable to other species of trees. However, the code is available at github.com/angelaseibert/CanopyStructureBCAL and the dataset is available upon

request. We propose that the model could be tested on different study sites. Future studies using the TLS VCP method should be applied to larger scale sample sites monitoring the effects of elevated temperature and CO_2 conditions on foliage over time. Additionally, we propose using the VCP method to quantitatively assess the effects of fungal diseases that cause foliage damage over time, such as Anthracnose.

Conclusion

As average temperatures and CO_2 levels rise, we must validate methods to monitor the vegetation that affects the terrestrial carbon sink storage capacity of ecosystems like peatland bogs. Using TLS and a voxel-based contact frequency model, this study established that we can indirectly and accurately estimate LAI across a series of modified parameters and, importantly, maintain that accuracy. However, it should be noted that the validation sample size in this study is small, but it is of diversely sized trees and applies two different methods of LAI estimation, destructive harvest and DHP. If future studies were to use this model, they would require an additional canopy structure validation dataset. We propose future studies involving broader model testing, integrating novel clumping methods available to further constrain the model, and manually measuring leaf area densities for further validation.

CHAPTER THREE: USING TERRESTRIAL LASER SCANNING TO MONITOR VERTICAL AND HORIZONTAL PEATLAND CONIFER CANOPY PROFILES ACROSS TIME UNDER A CLIMATE MANIPULATION

Introduction

Temporal changes in vegetation structure impact ecosystem function by altering processes including evapotranspiration (Giuliani et al., 2013), photosynthesis (Laine et al., 2016), soil and vegetation respiration (Gonzalez-Meler et al., 2004), and decomposition rates (de Godoy Fernandes et al., 2021). Each of these processes have subsequent impacts on carbon storage capacity (Dusenge et al., 2019; Scott et al., 2006). Canopy structure specifically has been shown to alter carbon sequestration through its relationship with these processes (Dechant et al., 2020; Hickey et al., 2022; Ringgaard et al., 2014; Wallace et al., 2018). Canopy structure datasets from different ecosystems are often integrated into larger climate models to constrain uncertainties about potential carbon emissions as the Earth's average temperature rises and carbon dioxide (CO_2) levels increase (Norby et al., 2022). Evaluating canopy structure changes in forested northern peatland ecosystems, a major terrestrial carbon sink, under controlled elevated temperature and CO_2 conditions may help resolve what elements of the canopy change over time under these treatments.

Northern Peatlands and Temporal Dynamics

Northern peatlands, a terrestrial carbon sink storing an estimated 415 ± 150 Gt of carbon Beaulne et al. (2021), are underrepresented in climate models (H. Tian et al., 2015) even though they are warming at twice the rate as the global terrestrial ecosystem average (Holmgren et al., 2015). With average rising temperatures, northern peatlands are

currently at risk of shifting from carbon sinks to carbon sources based on projected warming levels (Hugelius et al., 2020). However, since northern peatlands are underrepresented in climate models there are still uncertainties about their current carbon storage capacity and the potential degree of emissions. Many researchers are working to improve representations of boreal peatlands by providing refined empirical datasets of permafrost processes (Hugelius et al., 2020), microforms (Graham et al., 2022), microbial processes (Carrell et al., 2022), and root biomass (Malhotra et al., 2020). Canopy structure datasets are also important for better quantifying peatland carbon flux (Wedeux & Coomes, 2015). Datasets should be generated for individual peatlands to appropriately minimize uncertainties at the global scale. Forested peatlands are highly affected by canopy structure, making a thorough analysis of canopy structure in boreal forested peatlands necessary for constraining uncertainties in carbon sequestration.

Leaf Area Index Temporal Dynamics

Globally, increased LAI, the total projected leaf area per unit ground area (m^2/m^2), has contributed to a 12.4% increase in the cumulative global terrestrial carbon sink since 1981 (Chen et al., 2019). It is necessary, however, to evaluate LAI at an ecosystem level to refine these estimates and account for species-level environmental response differences. Temporal and spatial changes in tree LAI have been found in some ecosystems under elevated CO_2 and temperature conditions but are undetectable in others. A catchment level study in Iran revealed that MODIS-derived tree LAI (500 m spatial resolution) is projected to increase by 2.2 - 3.1% under warmer temperatures. This study was limited because they could not evaluate what species within the catchment would be most impacted and there is a high degree of uncertainty associated with MODIS

LAI estimates (Ramezani et al., 2020). At the species level, previous research found a monoculture of sweetgum trees under elevated CO_2 conditions demonstrated little change in LAI (Norby et al., 2022). They proposed investigating whether similar results would arise in a more heterogeneous system. Global model projections of LAI from the most recently developed earth system models vary greatly, further underscoring the necessity of broadening LAI datasets with fine scale measurements (Mahowald et al., 2016).

Leaf Area Density Temporal Dynamics

Leaf area density is a vertically comprehensive canopy metric that characterizes radiation balance with the atmosphere and the canopy layers (Lalic & Mihailovic, 2004). It is defined as the total one-sided leaf area per unit canopy layer volume (Hosoi & Omasa, n.d.). Oftentimes, canopy structure is measured only using the two-dimensional metric, LAI. Limiting canopy structural analyses to LAI estimations does not account for the distribution of leaves throughout the vertical canopy. Monitoring leaf area density over time can help better evaluate physiological processes like respiration and radiative transfer. Time series analyses of leaf area density have enabled researchers to effectively monitor the effects of storms and pruning practices on agricultural trees (D. Wu et al., 2018). Leppä et al. (2020) showed the utility of leaf area density as a monitoring metric for peatland fens pre and post tree harvest, but there are no current studies where elevated CO_2 and temperature effects on leaf area density are evaluated over time and space for groups of peatland trees. It is well-documented that elevated CO_2 levels tend to increase leaf thickness and decrease leaf stomatal density (Luomala et al., 2005), but understanding where in the canopy leaf distribution is changing would provide a novel connection between tree structure and function.

Leaf Inclination Angles Temporal Dynamics

An additional metric that enhances comprehensive understanding of vertical profile tree canopy structure is the leaf inclination angle. The leaf inclination angle is calculated as the angle between the leaf normal and the zenith angle (Y. Li et al., 2018; Yan et al., 2021). Leaf inclination angles affect rainfall interception (Holder et al., 2020), light distribution in the canopy (Itakura & Hosoi, 2019), and photosynthetic efficiency (Mantilla-Perez & Salas Fernandez, 2017). Determining how leaf angles change over time and through the canopy can elucidate information about canopy understory effects, tree species niche dynamics, and responses to variable environmental conditions. Shade-tolerant conifers, such as those in the *Picea* genus, a tree genus commonly found in peatlands, have higher leaf and branch plasticity, relative to other conifer species, in response to changing environmental conditions (Niinemets, 2010). They may be more apt to shifting their leaf angles under altered environmental conditions to maximize or reduce carbon gain based on current resource conditions (Burgess et al., 2017; Long et al., 2006). Conifers are some of the most abundant trees in boreal ecosystems. Boreal peatland ecosystems are warming faster than peatlands in other regions of the planet (Ruiz-Pérez & Vico, 2020), emphasizing the need to evaluate conifer needle trait changes over time and through the vertical canopy profile.

Tree Characteristics and Dynamics

Generating datasets of descriptive canopy structure metrics for conifers commonly found in boreal peatlands will support better boreal peatland dynamic's understanding. *Picea mariana* (black spruce) and *Larix laricina* (eastern larch), trees well-adapted to grow in the low nutrient, acidic boreal peatland bog environments, each

have defined characteristics and some known temporal dynamics that suggest their differing niches may result in contrasting responses to changing environmental conditions. Peatland spruce and larch tree dominant overstory is generally associated with *Sphagnum spp.*, sparse understories, and peatland areas with lower drainage. Previous studies have found that black spruce abundance decreases in peatland regions with higher water temperatures and flooding and eastern larch abundance decreases in regions with greater canopy closure (Evans et al., 2016; Islam et al., 2003), which emphasizes differing niches between species. The trees have also exhibited differing responses to seasonal changes and drying. The larch typically has a longer period of maximum gross photosynthetic rate toward the end of the growing season, and they have greater fine root growth under drying conditions (Jensen et al., 2019; Malhotra et al., 2020). Although the spruce and larch trees have similar geographic ranges, they have previously demonstrated differing responses to environmental conditions, which suggests the trees may have different LAI, leaf area density, and leaf angle responses to warming and elevated CO_2.

Spruce and Peatland Responses Under Changing Environments & ELM-SPRUCE

Larger climate model parameters can constrain uncertainty from the use of fine-scale temporal empirical analyses. Researchers working on the Spruce and Peatland Responses Under Changing Environments study (SPRUCE) created a modified version of the Energy Exascale Earth System Model (E3SM) to represent the forested boreal peatlands, referred to as ELM-SPRUCE. SPRUCE researchers have collected extensive data from the S1 Bog located in the Marcell Experimental Forest, where a forested boreal bog undergoes temperature and CO_2 manipulations to train ELM-SPRUCE. Current research at the SPRUCE site has found increased labile carbon outputs and methane

emissions with elevated temperature conditions (R. M. Wilson et al., 2021). This suggests that peatlands under warming will trend toward increasing vascular plant cover such as spruce and larch trees, and there is a need to broadly characterize canopy structure. Currently, the ELM-SPRUCE model predicts LAI of the main conifer trees, the eastern larch and black spruce, using multiple parameters of vegetation productivity. Some of these parameters are: specific leaf area, fraction of leaf N in RuBisCO (flnr), leaf carbon to nitrogen ratio, stem to leaf ratio, and fine root to leaf ratio (Shi et al., 2020a). However, the model requires empirical data to constrain current model uncertainties.

Terrestrial Laser Scanning

Collecting a comprehensive temporal and fine scale spatial dataset of canopy structure can be challenging using traditional methods of canopy evaluation. TLS is capable of quantifying vertical and horizontal canopy structure over time at a fine scale. Previously, SPRUCE researchers used other methods of canopy structure assessment to develop allometric relationships between canopy and tree structural measurements including tree basal area and height (Griffiths et al., 2017). However, more recent work has revealed losses in foliage, especially from the lower branches of trees under SPRUCE treatments, causing the distribution of the canopy to change. Additionally, a freeze event caused losses of foliage and tree top dieback in plots. The changes in canopy prevent the use of the previous allometric relationships as they will no longer hold or work as predictors. This issue requires the use of an indirect canopy analysis method that is independent of allometric relationships to measure the trees at SPRUCE.

Research Objectives

Further research is needed to quantify boreal canopy traits over time at a species-level and cumulative stand scale. The research goal of this study was to use TLS to apply a voxel-based contact frequency (VCP) model to quantify conifer LAI, leaf area density, and leaf inclination angle distribution in 12 SPRUCE plots under elevated and ambient CO_2 and temperature conditions from August 2015 - August 2022. Specifically, we asked, how are the spruce and larch tree canopy structures within 12 SPRUCE plots changing from 2015 - 2022? Under elevated CO_2 and temperature, we expected LAI to significantly increase, leaf area density to decrease in lower canopies, and leaf inclination angles to become more vertical. At the species level, we expected the spruce and larch trees would respond with opposing trends for each metric under the same treatment. This study will extend previous work evaluating trends in canopy structure over time and reveal the capacity for species to respond to an altered climate over time.

Methods

Study Site

The SPRUCE experiment takes place in the boreal forested S1 bog Marcell Experimental Forest in Northern Minnesota, USA (N47°30′19″, W93°27′18″). The acidic, ombrotrophic bog is 8.1 ha with an average peat depth of 2.27 m and a perched water table, 418 m above sea level. From 1961 - 2005 the mean annual air temperature was 3.3°C and mean annual precipitation was 768 mm (Sebestyen, 2011). Average temperature has risen by approximately 1.76° C over the last 40 years. The Greenwood series soil is low drainage with a deep peat age of 5,100 - 11,100 (Sebestyen & Griffiths, 2016) with average peat depths at 2 - 3 m, down to the Wisconsin glacial-age

lakebed (Hanson et al., 2009). The dominant vegetation includes the two dominant conifers, ericaceous shrubs, herbaceous species, and a bryophyte layer consisting mostly of *Sphagnum spp.* Mosses. For belowground peat profile and geochemistry see Tfaily et al. (2014).

The dominant conifers within the peatland are the *Picea mariana* (Mill.) B.S.P. (black spruce) and *Larix laricina* (Du Roi) K. Koch (eastern larch or tamarack). The larch and spruce trees were harvested in strip cuts in 1969 and 1974 to test the effects of seeding on the spruce's regeneration. Natural vegetative processes or seeding events followed to generate regeneration post-strip cuts. Plot saplings greater than 1 cm in diameter and 1.3 m above the *Sphagnum* surface are considered trees in this study. Both the larch and spruce tree's growth season begins in early to late spring, May, and ends in late autumn, or November. The SPRUCE plots contain a range of 10 larger trees in plot 10 to a maximum of 27 trees in plot 20 for a mean number of trees per plot of between 18 and 19 whole trees. Currently, canopy heights are 8 - 9 m tall, with some treetops being cut during 2021 as they outgrew the chamber walls. In 2016, the full range of diameter at breast height values were 1.2 to 11.1 cm. On average, there are 10 spruce trees (range: 3 - 17 trees) per plot and 3 larch trees (range: 1 - 5 trees) per plot.

Sections of the peatland are under elevated carbon dioxide and temperature conditions resulting in aboveground and belowground warming effects (**Figure 3.1**, Hanson et al., 2016). The warming effects take place using 12.8 m diameter and 7 m tall open-top chambers, with a total area of 114.8 m^2 per chamber. Air warming via blowing heated air 1 m above the bog surface and peat warming via heating elements inserted 3 m into the peat layer, occur at a range of temperatures: +0°C, +2.25°C, +4.5°C,

+6.75°C, and +9°C. Peat warming began in June 2014 and air warming began in August 2015 (Hanson et al., 2016). Throughout chambers, there are two of each temperature treatment. One temperature treatment undergoes elevated carbon dioxide by injecting CO_2 to a concentration of +500 ppm above ambient. The injections began in June 2016. Additionally, the study includes two unchambered control plots. The present study focuses on tree structural trait responses to elevated temperatures, elevated CO_2 (eCO_2), ambient CO_2 (aCO_2), and ambient temperature from 2015 to 2022. Four of the plots are under eCO_2 and elevated temperatures, plots 4, 10, 11, and 16. One plot is under eCO_2 and blowers with unheated air only, plot 19. Four plots are under aCO_2 and elevated temperatures, plots 8, 13, 17, and 20. One plot is under aCO_2 and blowers with unheated air only, plot 6. Two plots are controls with no chamber, no eCO_2, and no blowers plots 7 and 21.

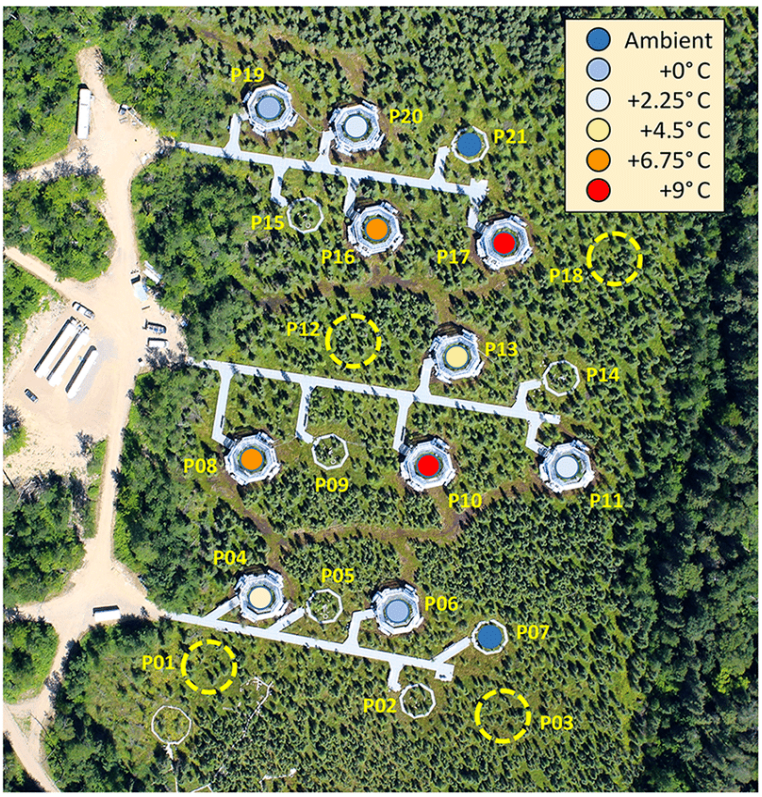

Figure 3.1. Aerial view of the SPRUCE plots with their respective treatment conditions (Adapted from Hanson et al., 2016).

TLS Data Collection

We used a Riegl VZ-1000 TLS with a 1550 nm laser and an angular resolution of 0.04 degrees to collect scans of the 12 SPRUCE plots. Scans were taken biyearly from 2015 - 2022 during the beginning of the growth period and the maximum growth period. Only scans taken during the maximum growth period were used for the analyses in this study. Around each plot, we symmetrically placed 5 - 8 scan positions depending on the necessary amount needed to reduce occlusion effects (**Figure 3.2**). Scans were coregistered to an error less than 1 cm using RiSCAN PRO. We applied a point deviation filter to reduce poor returns and corrected the intensity by the range to obtain the point reflectance values. Georegistration of plots was performed in CloudCompare v2.12.

Figure 3.2. Nadir view of a chambered plot at the SPRUCE site. Red circles indicate TLS scan position locations.

VCP Model Canopy Structure Estimation

After obtaining 12 SPRUCE plot point clouds each year from 2015 - 2022 we generated plot scale canopy height models and applied them to the modified VCP model (Almeida et al., 2019; Hosoi & Omasa, 2006; S. Li et al., 2017; Yan et al., 2021) based on J. W. Wilson, (1960)'s contact frequency theory. Ground points were removed using the Cloth Simulation Filter (CSF) tool (Zhang et al., 2016) in CloudCompare. The tool extracts ground points from discrete lidar point clouds. We removed any remaining nontree points manually. To separate the leaf and wood components in the plots we applied a random forest that uses number of returns and reflectance values as features for component separation. The model produces a leaf-only cloud of all the trees in the plot (**Figure 3.3 & 3.4 A&B**).

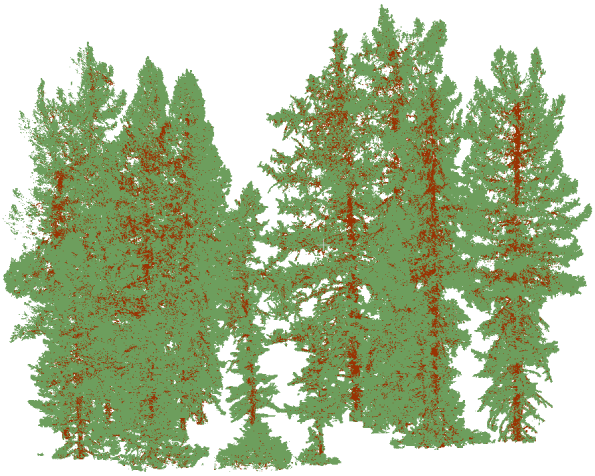

Figure 3.3. SPRUCE plot 16, 2022 with classified wood components.

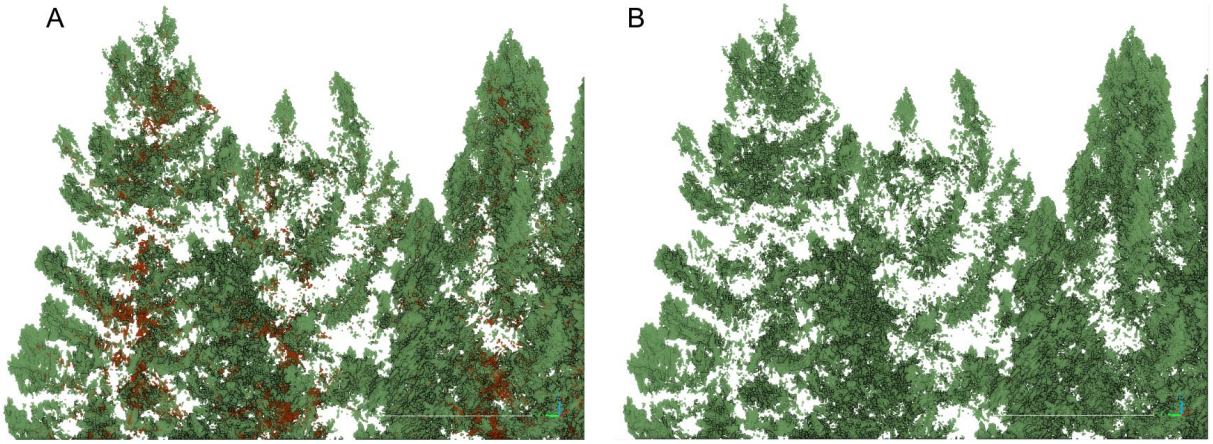

Figure 3.4A. SPRUCE plot 16, 2022 treetops before wood component removal. B. SPRUCE plot 16, 2022 treetops after wood component removal.

Following the removal of wood, the trees within each of the plots for each year were manually separated into larch and spruce species (**Figure 3.5A, B, & C**). This separation allowed us to analyze how each species' canopy was changing over time at the plot scale. Each leaf point cloud was then run through the VCP model. 288 total plots were applied to the model. The model performed 10 iterations to predict leaf canopy metrics and quantify uncertainty in the LAI estimation for all plots. Approximately 1,616

tree canopies, 1,184 spruce and 432 larch, were iteratively evaluated at the plot scale for all species and at the plot scale where species were separated.

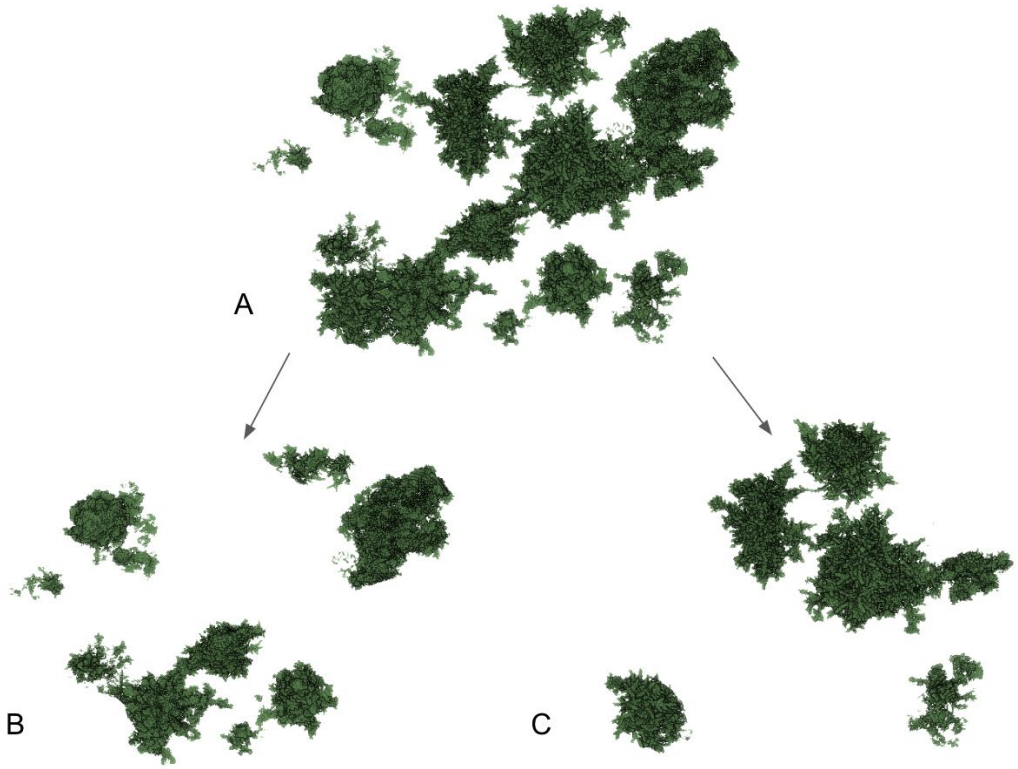

Figure 3.5A. SPRUCE plot 17, 2022 from above, all tree species together. B. Black spruce trees separated at the plot scale. C. Larch trees separated at the plot scale.

The VCP model is based on the contact frequency theory for estimating LAI (J. W. Wilson, 1960). The model estimates the probability that a laser beam will hit a voxel or pass through a voxel, resulting in a vertical estimate of leaf area density that can be summed to calculate the LAI of the plot (Almeida et al., 2019) (**Equations 3.1 & 3.2**). The workflow begins by applying a volumetric pixel grid to the tree to generate a standardized point cloud with which volume and area can be estimated. In this study, we used 3.25 cm voxels based on iterative voxel tests during model development. For each group of 3.25 cm voxels in a 0.5 m layer of the tree canopy we calculated the leaf

inclination angle using the leaf normal and the zenith angle of the TLS beam. These leaf inclination angles were used to calculate the mean projection coefficient and the correction factor (**Equation 3.3**), which is based on the leaf angle distribution at the TLS zenith angles. A convex hull was used to calculate the total possible number of voxels that would occupy the plot area, 66.44 m^2. This number was subtracted from the actual number of voxels to calculate the voxels where a laser beam passed through ($n_p(k)$). This calculation provided the contact frequencies, or the leaf area densities at each 0.5 m portion of the canopy. These densities were summed to find the cumulative LAI.

$$LAdensity(h, \Delta H) = \alpha(\theta)\frac{1}{\Delta H} \cdot \sum_{k\,=\,m_h}^{m_h+\Delta H} \frac{n_l(k)}{n_l(k) + n_p(k)} \tag{3.1}$$

Where $LAdensity$ is the leaf area density in m^2/m^3, $\alpha(\theta)$ is the leaf angle-based correction factor, m_h is a single canopy profile layer, ΔH is the thickness of each canopy profile in m, $n_l(k)$ is the number of laser beams intercepted at a voxel in a canopy layer, and $n_p(k)$ is the number of laser beams passing through a voxel in a canopy layer, and m_{HT} is the treetop height.

$$LAI(h) = \alpha(\theta) \cdot \sum_{k\,=\,m_h}^{m_{HT}} \frac{n_l(k)}{n_l(k) + n_p(k)} \tag{3.2}$$

$$\alpha(\theta) = \frac{cos\theta}{G(\theta)} \tag{3.3}$$

Where θ is the laser zenith angle and G is the mean projection coefficient (Hosoi & Omasa, 2006).

Statistical Analyses

After quantifying the canopy structural measurements for each of these SPRUCE plots, we performed statistical analyses to identify monotonic trends through time in each metric between species and treatments. We grouped plots including both species into 3 categories: elevated CO_2 increased temperature & blowers, ambient CO_2 increased temperature & blowers, and control plots. The same categories were generated for plots with only spruce species and plots with only larch species. Data was normalized using the min-max method to better visualize trends. Additionally, we used normalized data to perform least squares regressions across the experimental temperature gradient and reveal any linear trends between the metrics and temperature.

Each category of non-normalized LAI values was analyzed through time using Mann-Kendall tests. The Mann-Kendall tests applied a pre-whitening procedure to account for the presence of serial-correlation in the dataset. This test identified if there was an increasing or decreasing trend in the data and if it was statistically significant. To analyze the temperature gradient, we performed linear regressions between temperature and LAI, grouping and normalizing LAI by carbon dioxide treatment.

Leaf area density measurements were analyzed through the vertical canopy and over time for each category of plots. The plot canopies were broken into three categories: upper ($\geq$ 6 m), middle ($<$ 6 m & $\geq$ 3 m), and lower ($<$ 3 m). We applied the same Mann-Kendall tests to reveal any significant monotonic trends through time. The leaf area density data was then normalized by temperature, carbon dioxide treatment, and canopy section for comparison using least squares linear regression tests to determine if there were trends between leaf area density and the plot temperature gradient.

We analyzed leaf inclination angle distributions in terms of their functional representation and dynamics with height, species, time, and category. Using kernel density functions, we found the frequency of mean leaf inclination angles. The frequency of the mean leaf angles was used to identify what leaf inclination distribution functions the trees represented. We again applied Mann Kendall tests to leaf inclination angles at each section of the canopy, for each species, grouped by carbon dioxide treatment to determine if there were monotonic trends through time. Additionally, we performed regressions with the same normalization technique as used for the leaf area density analysis to evaluate if there was a relationship between leaf angle and the temperature gradient across the SPRUCE plots.

Results

LAI Dynamics

We used a VCP model to evaluate LAI over time of peatland conifers cumulatively and at the species level under three treatment categories: elevated CO_2 increased temperature & blowers, ambient CO_2 increased temperature & blowers, and control plots. We also analyzed LAI across the different plot temperature levels, +0°C, +2.25°C, +4.5°C, +6.75°C, and +9°C under ambient or elevated CO_2. We found that the average LAI across SPRUCE plots over the past eight years was 1.9 and had a right skewed distribution (see Appendix B for LAI distribution figure).

Based on a least squares regression analysis, we found that plots in elevated CO_2 and ambient CO_2 with increased temperatures or with blowers had significantly increasing LAI values over time. Additionally, we found plots under control conditions exhibited a significant trend through time (**Figure 3.6, Table 3.1**). Time explained 41%

of the LAI trends in ambient CO_2 plots while time explained less than 25% of the LAI trends in elevated CO_2 and control plots. Ambient CO_2 plots exhibited the greatest increase in LAI through time (**Table 3.1**). Plots under elevated CO_2 and elevated temperature conditions had a mean LAI of 1.9 and a range of 0.9 to 3.9. Under ambient CO_2 and elevated temperatures, the plots had a mean LAI of 1.7 and a range of 0.9 to 4.3. The mean plot LAI under control conditions was 1.9 and the range was 1.2 to 3.0 (see Appendix B for LAI distributions under different carbon dioxide treatments).

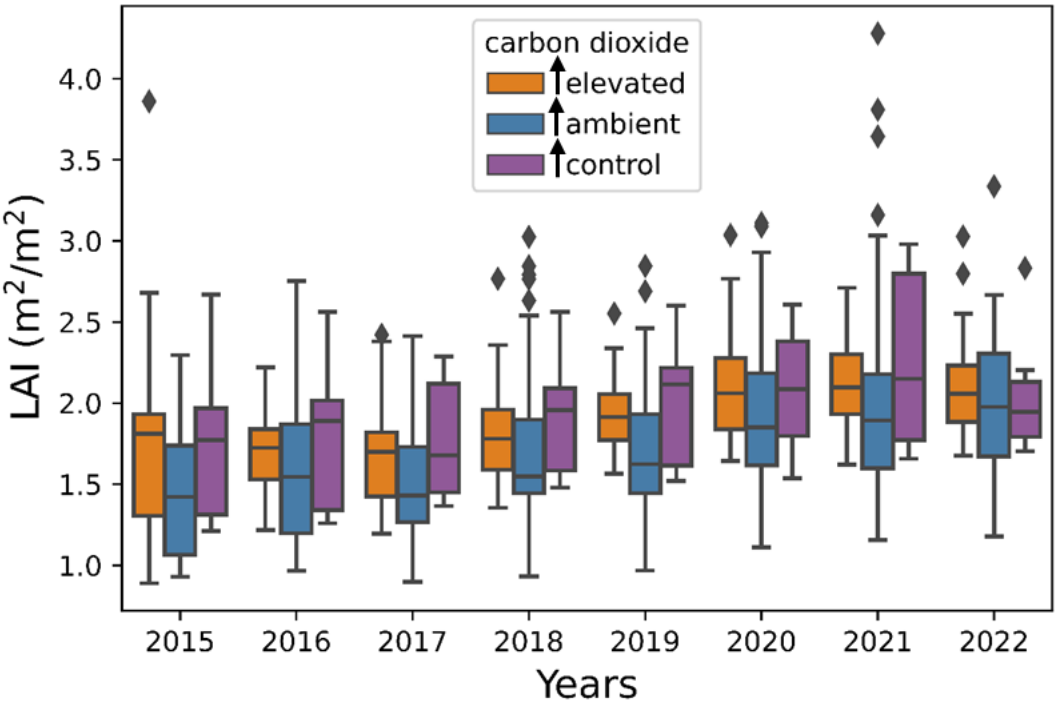

Figure 3.6. LAI of all trees across SPRUCE plots under elevated CO_2 and ambient CO_2 conditions with elevated temperatures or with blowers both demonstrated increasing trends. LAI increased significantly under control conditions. Whisker lengths represent the minimum and maximum value that lies within 1.5 times the interquartile range. Diamonds represent outliers. Arrows in the legend indicate the direction of significant trends.

Using regression analysis and the min-max normalization method, we analyzed plot LAIs and their relationship to temperature. The basis for the temperature regression

dependent variable was the mean air temperature at 2 m (Hanson et al., 2016) from May to September in each year (2016, 2017, 2018, 2019, 2020, 2021, and 2022) to reflect the temperatures encompassing the full growing season. As mean temperatures increased, under ambient CO_2 conditions, LAI decreased. Plots under elevated CO_2 conditions exhibited no significant trends with temperature (**Table 3.1, Figure 3.7**). We performed regression tests on LAI across temperature treatments and time. We found that the greatest increases in normalized LAI over time were occurring in the +9°C elevated CO_2 plots (**Table 3.1, Figure 3.8**) with a slope of 0.11. The lowest increases in LAI were occurring in the +6.75°C elevated CO_2 plots with a slope of 0.02. Both trends were significant. Plots under elevated CO_2 and +0°C did not demonstrate a significant trend through time (**Table 3.1**, **Figure 3.9**).

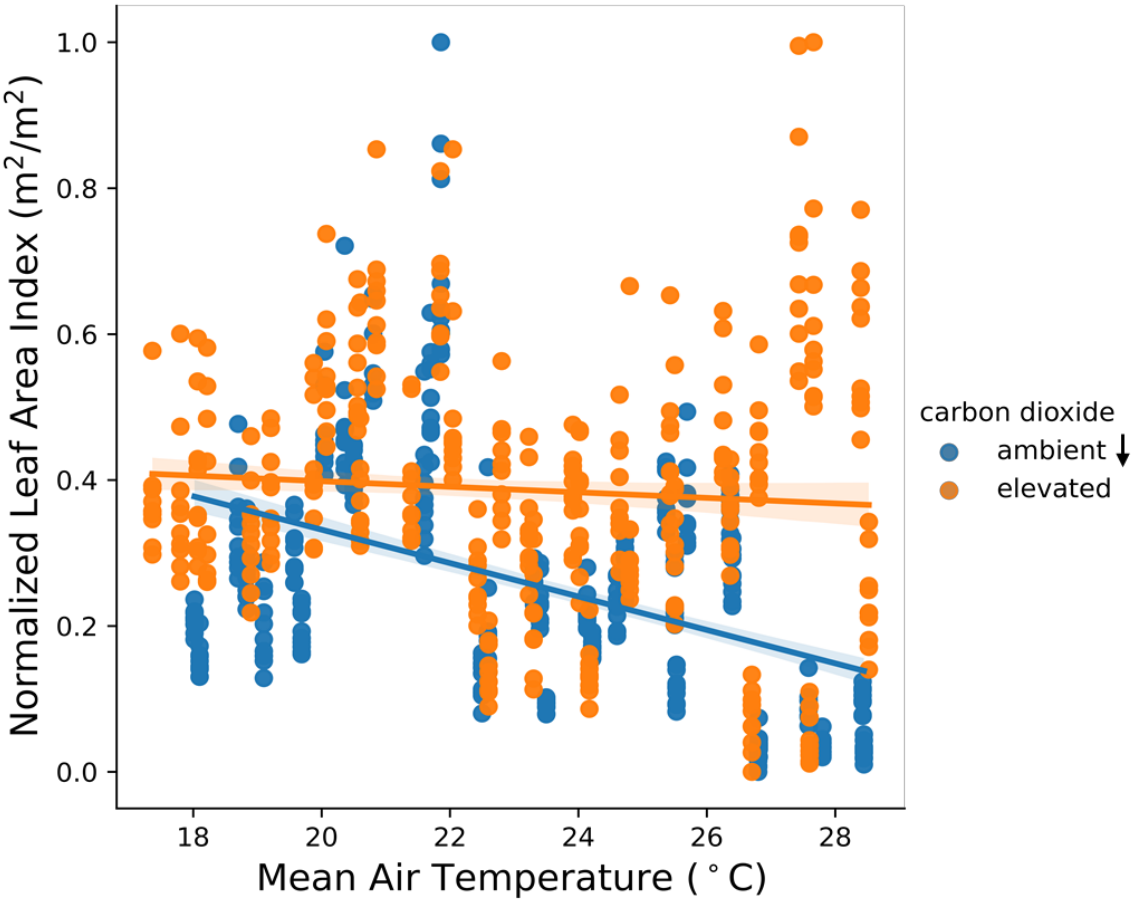

Figure 3.7. Normalized LAI in ambient CO_2 plots exhibited a decreasing trend (R^2 = 0.19, m = -0.02, $p < 0.001$) with temperature. Elevated CO_2 plot LAI presented no significant trend with temperature ($p > 0.05$). Shading indicates a 95% confidence interval and arrows in the legend indicate the direction of a significant trend.

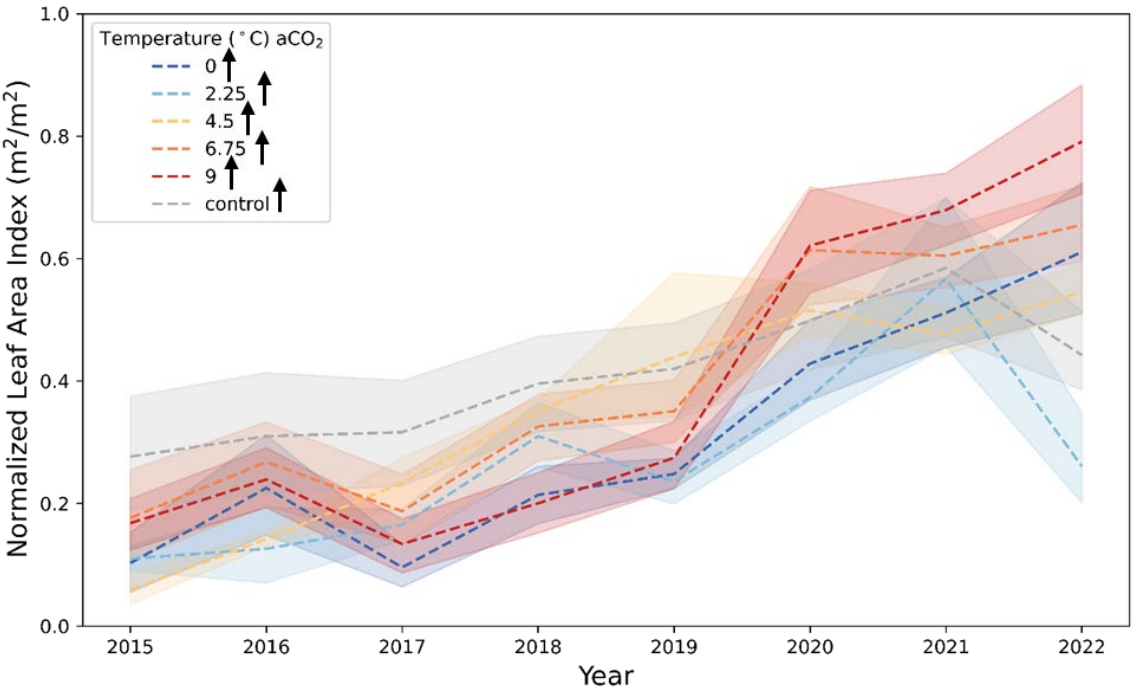

Figure 3.8. The greatest increases in LAI among the ambient CO_2 plots were in the + 9°C plot ($R^2 = 0.70$, $p < 0.001$, $m = 0.10$). The lowest increases were in the + 2.25°C plots ($R^2 = 0.36$, $p < 0.001$, $m = 0.05$). All plots overall increased more significantly over time than in control plots. Significant trends ($p < 0.001$) and their direction are indicated by arrows in the legend. Shading indicates a 95% confidence interval.

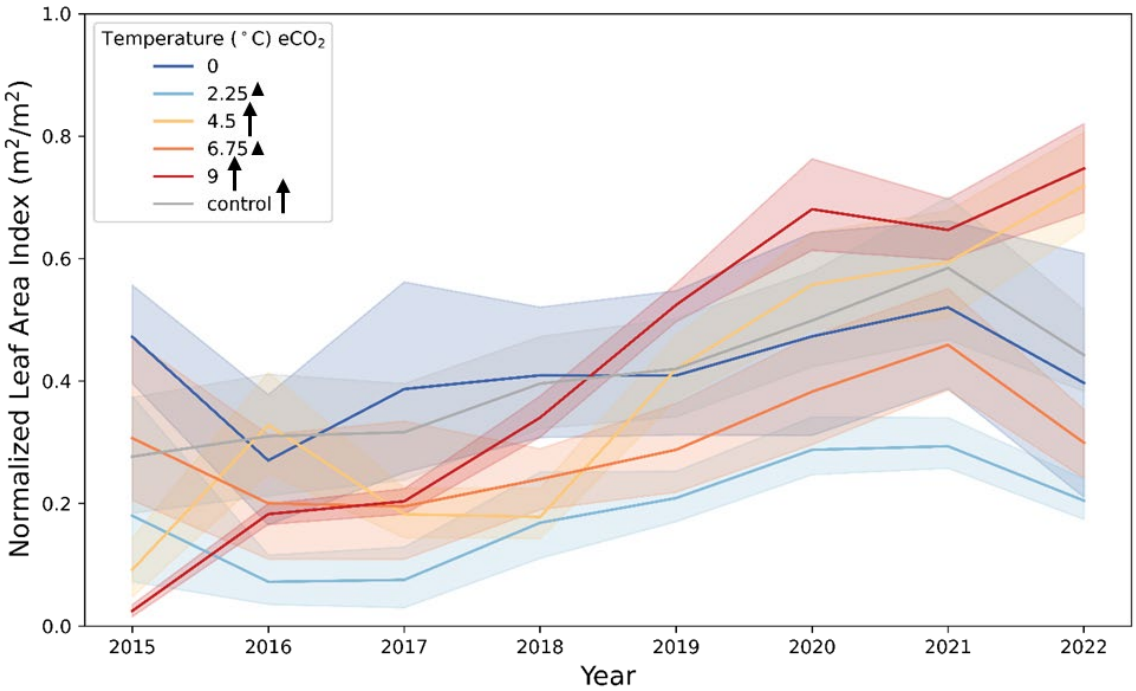

Figure 3.9. Plots under elevated CO_2 and +9°C had the greatest increase in LAI over time ($R^2 = 0.88$, $p < 0.001$, $m = 0.11$). The lowest increase in LAI was found in the

+6.75°C plot (R^2 = 0.08, $p < 0.05$, m = 0.02). + 0°C plot did not exhibit a significant trend through time. Significant trends ($p < 0.001$) and their direction are indicated by arrows in the legend. Less significant trends ($p < 0.05$) and their direction are indicated by triangles in the legend. Shading indicates a 95% confidence interval.

We performed an LAI analysis across plots with species separated, using CloudCompare to segment the species apart. We found that the mean spruce LAI was 1.5 and the species' range was 0.7 to 3.2. Larch LAI was lower, with an average of 0.5 and a range of 0.005 to 1.2. Distributions of spruce LAI followed similar patterns to the cumulative plot LAIs. Black spruce LAI demonstrated a right skewed distribution while the larch LAI had a bimodal distribution, with many trees having an LAI less than 1 (see Appendix B for LAI distributions for spruce and larch species).

We applied ordinary least squares regression tests to perform a species-specific time series analysis on normalized groups. Similar trends resulted for the larch and spruce trees under both CO_2 conditions through time. In ambient CO_2 conditions, larch and spruce LAI followed statistically significant increasing trends. The larch LAI increased with a slope of 0.04 while the spruce had a slope of 0.02 (**Table 3.2**). Under elevated CO_2 conditions, spruce LAI demonstrated increasing trends, slightly greater than in ambient CO_2 conditions with a slope of 0.03. Larch LAI under elevated CO_2 resulted in a less significant increasing trend ($p < 0.05$) with a slope of 0.01 (**Table 3.2, Figure 3.10**). Between the two control plots, spruce LAI resulted in significant increases (m = 0.07) in LAI over time and larch LAI increased with a slope of 0.03 (**Table 3.2, Figure 3.11**).

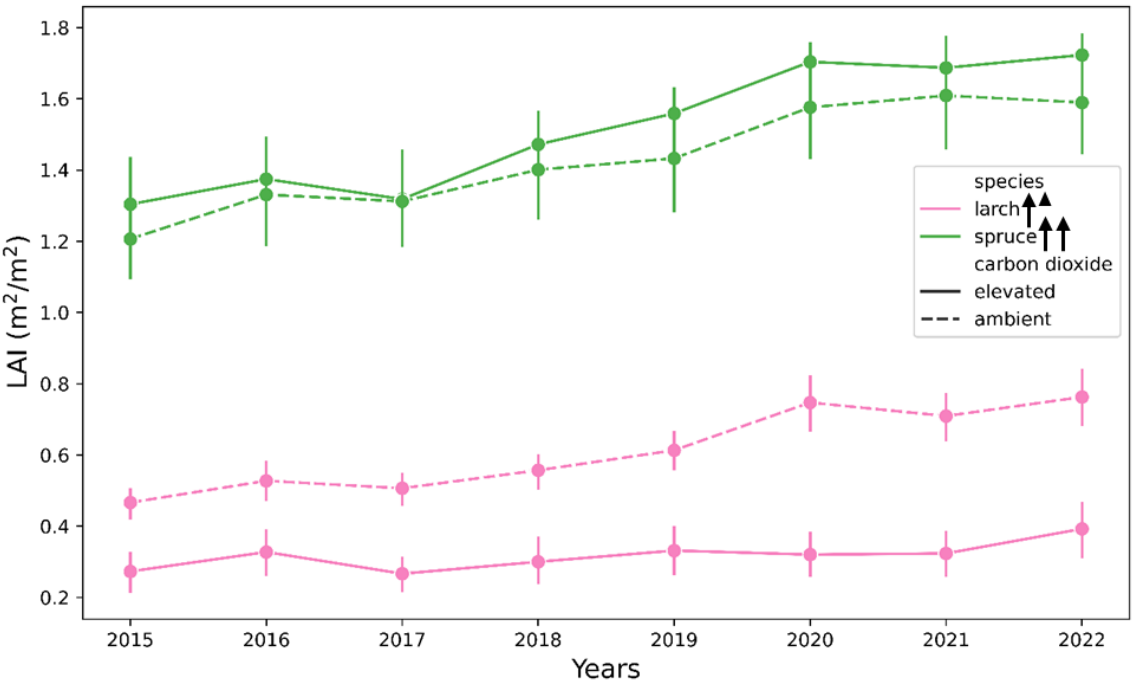

Figure 3.10. In ambient CO_2 conditions, larch and spruce LAI had statistically significant increasing trends. Under elevated CO_2 conditions, spruce LAI increased significantly ($p < 0.001$) while the larch had a less significant increasing trend ($p < 0.05$). Error bars represent a 95% confidence interval. Full arrows indicate significant trends ($p < 0.001$) under both CO_2 conditions. One arrow and a triangle indicate most significant trends ($p < 0.001$) in ambient CO_2 and less significant trends in elevated CO_2 ($p < 0.05$).

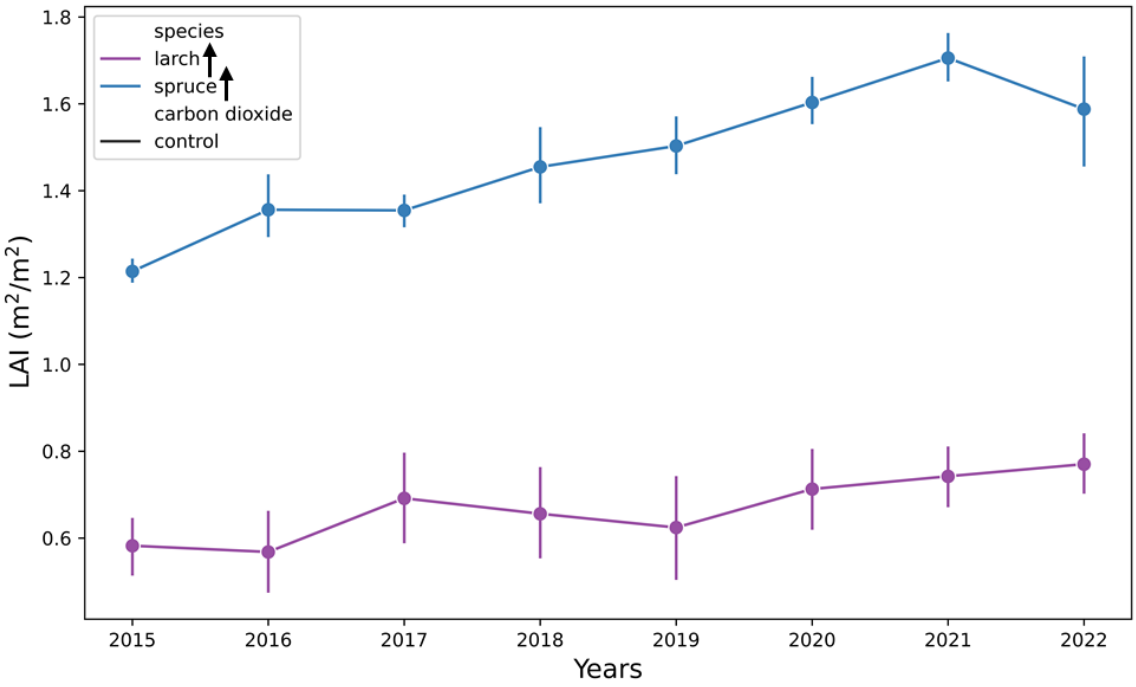

Figure 3.11. Black spruce LAI between the unchambered control plots increased over time ($p < 0.001$, $m = 0.42$). Larch LAI also increased significantly over time in the control plots ($p < 0.001$, $m = 0.08$). Error bars indicate a 95% confidence interval. Arrows indicate the direction of significant trends.

Leaf Area Density Trends

We evaluated the leaf area density trends through time and through the vertical canopy profile for the larch and spruce species. The average spruce leaf area density was 0.35 m^2/m^3 and the range was 0.03 m^2/m^3 to 1.5 m^2/m^3 with the lowest density of leaves being in the lower 0.5 m portion of the tree and the highest density being, on average, 1 m from the top of the canopy. Larch leaf area density averaged 0.21 m^2/m^3 and ranged from 0.004 m^2/m^3 to 0.83 m^2/m^3. The maximum leaf area density was estimated to be 2 m from the top of the canopy (see Appendix B for leaf area density distributions for spruce and larch species).

From contact frequency estimates, we evaluated leaf area density over time for three portions of the spruce and larch canopies under different treatment

conditions. We performed Mann-Kendall tests to determine if the upper, middle, or lower plot canopy of either species was increasing or decreasing in leaf density over time.

Spruce leaf area densities exhibited no statistically significant trends through time under each treatment condition ($p > 0.05$). Larch leaf area density through time exhibited two statistically significant leaf area density trends while the rest were not significant. Upper larch leaf densities under ambient CO_2 conditions resulted in increasing trends through time with a slope of 0.002 and middle larch canopies under control conditions increased with a slope of 0.001. Fluctuations in leaf area density over time were most notable in the upper canopies of trees (see Appendix B for leaf area density temporal trends by species figures and table).

Using least squares regression tests across temperature treatments we found normalized leaf area density was increasing in upper and middle canopies as temperatures got warmer in ambient CO_2 plots and lower canopies did not have a significant trend. In elevated CO_2 plots, upper and lower canopy leaf area density was significantly increasing across the experimental temperature gradient while middle canopies were decreasing across the temperature gradient (see Appendix B for leaf area density trends with temperature figures and table).

Leaf Inclination Angle Trends

To analyze distributions and changes in leaf inclination angles of the spruce and larch trees we estimated the normal vectors of each 3.25 cm voxel and calculated the average inclination angle by estimating the angle between the normal vector and the instrument zenith angle (**Equation 2.5**). We analyzed the distribution of leaf angles across plots for each species (see Appendix B for leaf angle distributions for

the spruce and larch species). Additionally, we used Mann-Kendall tests to determine if leaf inclination angle was shifting through time in the upper, middle, and lower canopy profiles at the plot scale under different treatments for either species.

Spruce leaf angles had more vertical leaf angles in the lower canopy and more planar leaf angles in the upper canopy. On average, leaves were inclined at 59°, ranging from 41° to 68°. Larger angles represent more vertically angled leaves. Under eCO_2 and elevated temperature conditions, spruce angles exhibited differing distributions through the vertical canopy. Upper leaf angles were more symmetrically distributed, having a mean angle of 58°, and the angle distribution ranged from 55° to 63°. The middle and lower canopies exhibited more vertical distributions of leaves where the mean angle was 60°. Leaf angles in the middle canopy ranged from 60° to 68° and in the lower canopy they ranged from 61° to 67°. Under ambient conditions, leaf angle distributions were consistently more symmetrical on average. Upper canopy spruce inclination angles under ambient conditions had a mean of 57° and a range of 46° to 62°. Middle and lower leaf angles were on average, 59° and 56° respectively. Their respective ranges were 45° to 66° in the middle canopy and 42° to 66° in the lower canopy. Under control conditions, spruce upper canopies had a mean inclination angle of 57° and a range of 45° to 65°, indicating a symmetrical upper portion on average. Similar to the plots under treatment conditions, on average, leaf inclination angles in control conditions in middle and lower canopies had more vertical leaf angles. Middle spruce canopies in the control plot exhibited mean angles of 59° with a range of 43° to 66° and lower spruce canopies had an average angle of 61° with a range of 42° to 66° (see Appendix B for leaf angle distributions by species).

We used Mann-Kendall tests to evaluate if spruce and larch leaf angle distributions were shifting through time in the different treatment plots. Only lower spruce canopies under warming and ambient CO_2 had statistically significant decreases in leaf inclination angle, indicating that leaf angles were becoming more planar over time. We noted novel fluctuations toward more downward leaf angles for all canopy sections in 2016 under eCO_2. Additionally, we saw abnormal fluctuations downward in 2021 under aCO_2 conditions and in 2020 and 2021 under control conditions. Needle inclination angles in elevated CO_2 and control plots did not have any significant trends through time (see Appendix B for leaf angle temporal trends by species figures and table).

Larch leaf inclination angles were similar to spruce, showing spherical and vertical inclination angles on average. Cumulatively, larch trees across the site had an average leaf inclination angle of 58° and ranged from 45° to 71°. Under the elevated CO_2 and temperature conditions with blowers, larch tree upper canopies had average leaf inclination angles of 57° having a range of 54° to 63°. Middle and lower canopies under elevated CO_2 and temperature had average inclination angles of 58°, with middle canopies ranging from 48° to 66° and lower canopies ranging from 52° to 71°. Under ambient CO_2 larch canopies had spherically distributed leaf angles on average. Upper canopy leaf inclination angles were an average of 57° with a range of 50° to 65°. Middle larch (μ = 58°) and lower larch (μ = 59°) canopy leaf angles had the same range, 45° to 65°, under the ambient CO_2 conditions. Within control conditions, upper and middle canopy larch leaf angles had more spherical distributions, with averages of 56° and 58° and ranges of 51° to 59° and 50° to 62° respectively. Low canopy leaf distributions were

slightly more vertical on average, with a mean of 60° and a range of 51° to 63° (see Appendix B for distributions).

Mann-Kendall test trend analyses revealed that larch leaf inclination angles were not shifting with statistical significance in any one direction. Similar to the spruce trees, we saw noticeable trends downward in leaf inclination angle in 2021 ambient CO_2 plots and in 2020 and 2021 in the control plots (see Appendix B for figures).

We found that the normalized leaf inclination angles of the upper, middle, and lower canopies shifted significantly as plots got warmer. Only middle canopies under elevated CO_2 did not show a significant trend across the temperature gradient. We found that leaf inclination angles decreased the most in middle canopies under ambient CO_2 as plots got warmer with a slope of -0.04. Upper and lower canopies also had significant decreasing trends in average leaf inclination angle as the temperature of the plot increased (**Figure 3.12, Table 3.3**). As plots got warmer under elevated CO_2 conditions, we found that upper canopy leaf inclination differed from the other canopy sections and treatment groups as its angles significantly increased, having a coefficient of 0.03. Lower canopy leaf inclination angles had decreasing trends with temperature (**Figure 3.13, Table 3.3**).

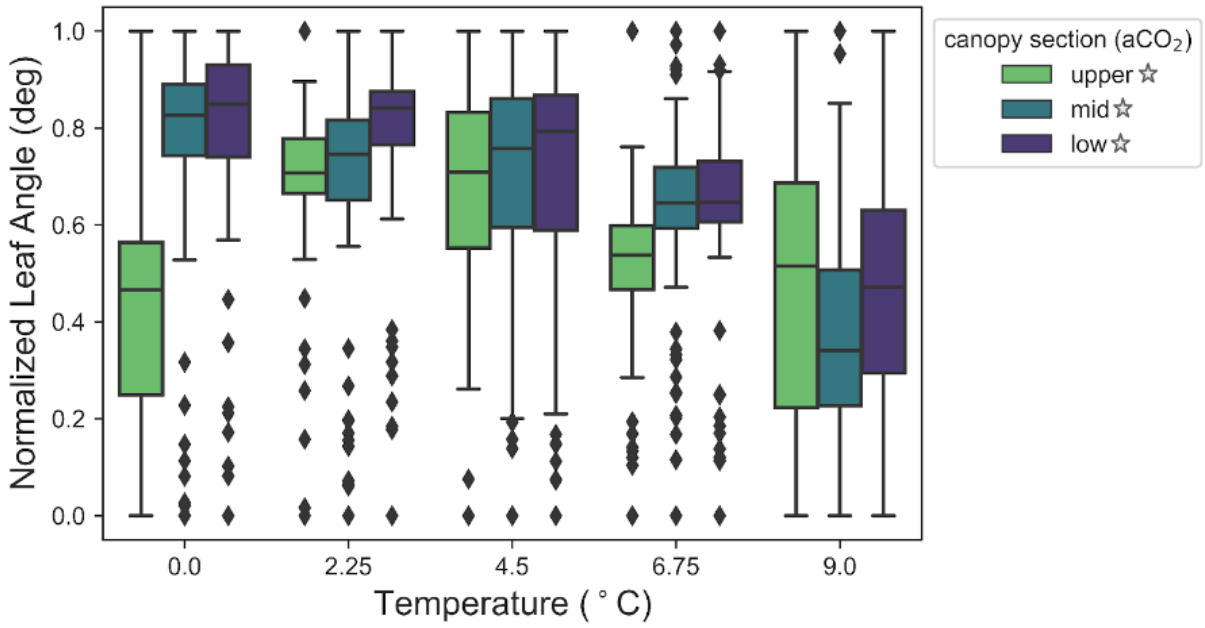

Figure 3.12. Normalized leaf inclination angles under ambient CO_2 conditions exhibited significantly decreasing trends as temperatures increased in the upper canopy ($R^2 = 0.08$, $p < 0.001$, $m = -0.02$), middle canopy ($R^2 = 0.21$, $p < 0.001$, $m = -0.04$), and the lower canopy ($R^2 = 0.18$, $p < 0.001$, $m = -0.03$). Stars in the legend indicate significant trends.

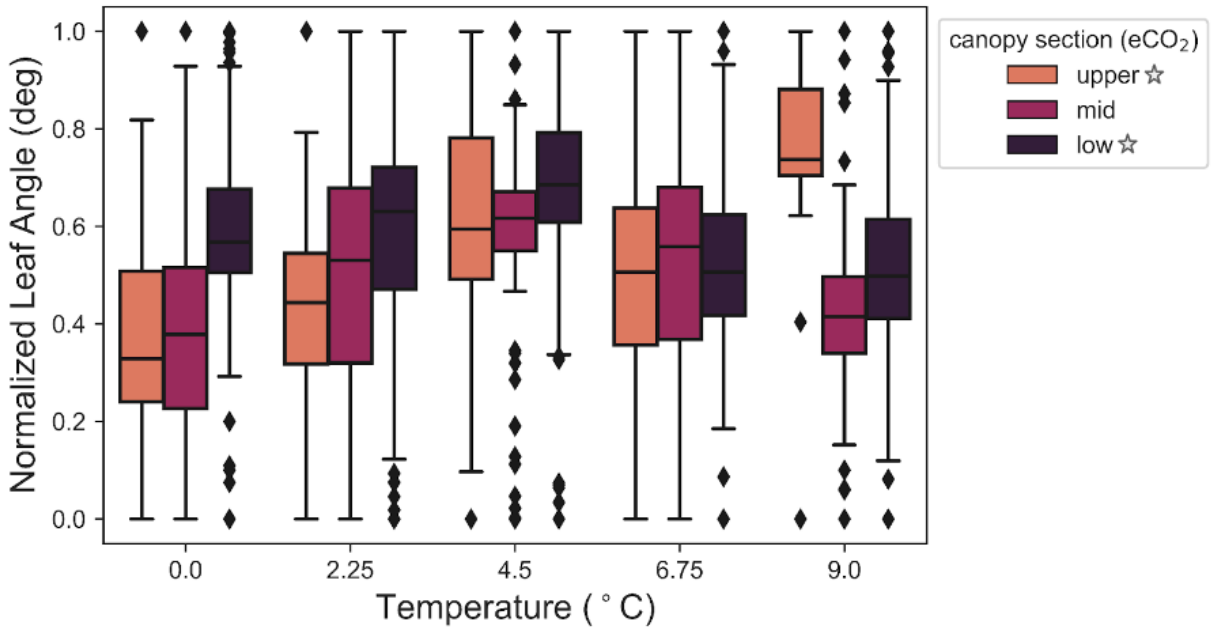

Figure 3.13. Normalized leaf inclination angles under elevated CO_2 conditions exhibited significantly increasing trends as temperatures increased in the upper canopy ($R^2 = 0.14$, $p < 0.001$, $m = 0.03$. The middle canopy leaf inclination angles did not demonstrate any significant trends. Lower canopy leaf angles significantly decreased ($R^2 = 0.016$, $p < 0.05$, $m = -0.009$). Stars in the legend indicate significant trends.

Table 3.1. Ordinary least squares regression analysis LAI results for all species and treatments.

Species	Treatment	Independent Metric	Dependent Metric	p	R^2	coefficient	95% CI
All	Ambient CO_2 & warming	Time	LAI	< 0.001	0.41	0.06	0.056 - 0.068
All	Elevated CO_2 & warming	Time	LAI	< 0.001	0.21	0.05	0.039 - 0.054
All	Control	Time	LAI	< 0.001	0.14	0.04	0.02 - 0.05

All	Ambient CO_2	Temperature	LAI	< 0.001	0.19	-0.02	-0.026 - -0.019
All	Elevated CO_2	Temperature	LAI	0.06	0.005	-0.004	-0.008 - 0.000
All	0°C & aCO_2	Time	LAI	< 0.001	0. 63	0.07	0.059 - 0.084
All	2.25°C & aCO_2	Time	LAI	< 0.001	0.36	0.05	0.032 - 0.059
All	4.5°C & aCO_2	Time	LAI	< 0.001	0.73	0.07	0.062 - 0.081
All	6.75°C & aCO_2	Time	LAI	< 0.001	0.65	0.08	0.063 - 0.088
All	9°C & aCO_2	Time	LAI	< 0.001	0.70	0.10	0.082 - 0.111
All	0°C & eCO_2	Time	LAI	0.31	0.01	0.01	-0.011 - 0.034
All	2.25°C & eCO_2	Time	LAI	< 0.05	0.14	0.02	0.01 - 0.04
All	4.5°C & eCO_2	Time	LAI	< 0.001	0.66	0.08	0.071 - 0.098
All	6.75°C & eCO_2	Time	LAI	< 0.05	0.08	0.02	0.005 - 0.039
All	9°C & eCO_2	Time	LAI	< 0.001	0.88	0.11	0.098 - 0.116

Table 3.2. Ordinary least squares regression analysis evaluating trends between LAI and time for the spruce and larch species.

Species	Treatment	Independent Metric	Dependent Metric	p	R^2	coefficient	95% CI
spruce	Ambient CO_2	Time	LAI	< 0.001	0.06	0.02	0.014 – 0.032
larch	Ambient CO_2	Time	LAI	< 0.001	0.19	0.04	0.036 – 0.054
spruce	Elevated CO_2	Time	LAI	< 0.001	0.22	0.03	0.024 – 0.035
larch	Elevated CO_2	Time	LAI	< 0.05	0.02	0.01	0.003 – 0.026
spruce	Control	Time	LAI	< 0.001	0.42	0.07	0.056 – 0.082
larch	Control	Time	LAI	< 0.001	0.08	0.03	0.016 – 0.052

Table 3.3. Ordinary least squares regression analysis average leaf inclination angle results for all species across the temperature gradient.

Species	Treatment	Independent Metric	Dependent Metric	p	r^2	coefficient	95% CI
All, Upper Canopy	Ambient CO_2	Temperature	Leaf Angle	< 0.001	.08	-0.02	-0.035 - -0.012
All, Middle Canopy	Ambient CO_2	Temperature	Leaf Angle	< 0.001	.21	-0.04	-0.043 - -0.030
All, Lower Canopy	Ambient CO_2	Temperature	Leaf Angle	< 0.001	.18	-0.03	-0.041 - -0.027
All, Upper Canopy	Elevated CO_2	Temperature	Leaf Angle	< 0.001	.14	0.03	0.018 - 0.040
All, Middle Canopy	Elevated CO_2	Temperature	Leaf Angle	0.68	.00	0.00	-0.009 - 0.006
All, Low Canopy	Elevated CO_2	Temperature	Leaf Angle	< 0.05	.02	-0.01	-0.015 - -0.002

Discussion

We used a voxel contact frequency-based model to answer the research question, to what degree are the spruce and larch tree canopy structures changing from 2015 - 2022 across 12 SPRUCE plots. The VCP method enabled us to characterize LAI, leaf area density, and leaf inclination angles across horizontal and vertical spatial scales,

through time, and within different temperature and CO_2 treatments. Within elevated CO_2, we expected cumulative LAI to increase significantly, leaf area density to decrease significantly in the understory portion of canopies, and leaf inclination angles to become more vertical, on average, over time and temperature gradients. At the species level, we expected the spruce and larch trees to respond with opposing trends for each structural metric under the same treatment.

Our data supported our hypothesis that under elevated temperature and CO_2, cumulative LAI increased significantly over time. However, we also found that under ambient CO_2 and warming cumulative LAI increased at a faster rate over time on average. Across the temperature gradient, we found that LAI increased the most significantly in the warmest plot under elevated CO_2, supporting our hypothesis. Regarding leaf area density trends, our data did not support the hypothesis with statistical significance over time or across the temperature gradient. Leaf densities in the lower canopy under elevated CO_2 and warming did not show any significant trends through time. Under elevated CO_2 as temperatures increased, we found lower canopy leaf area density increased, but middle canopies decreased significantly. The data did not support our hypothesis that leaf inclination angles would become steeper with elevated CO_2 across time or with warming. Monotonic trend tests revealed that, in general, leaf angles did not change significantly in one direction over time. Across the temperature gradient we found that the upper canopy leaf angles under elevated CO_2 increased with warming, supporting our hypothesis, but lower canopy needles had decreasing trends, negating the hypothesis. At the species level, our data negated the hypothesis that larch and spruce would have opposing trends when in any of the same treatments. Spruce and larch trees

both had increasing trends in LAI under ambient CO_2 conditions, with the larch increasing at a greater rate. While in elevated CO_2 and control conditions, spruce LAI increased at a greater rate than the larch. Leaf area density and leaf inclination angle species data through time did not reveal significant trends through time for the tree species to be compared.

These data reveal that conifer canopy structure may not be comprehensively represented by two-dimensional LAI values and there are complex processes changing the vertical profile of tree canopies across temperature gradients. We noted anomalous fluctuations in the time series data. This enhances previous study findings that the impact of elevated CO_2 and temperature varies across plant stages (Sabagh et al., 2020).

LAI Across CO_2 Treatment, Time, Species, and Temperature Treatments

Our time series analyses of LAI at the SPRUCE site across elevated temperatures under ambient and elevated CO_2 conditions support current findings that elevated CO_2 causes significant increases in LAI over time (Dermody et al., 2006). We additionally bolster this finding with evidence that LAI in SPRUCE control plots is, cumulatively, not increasing at as great of a rate over time. Previous studies have found that elevated CO_2 enables plants to maximize photosynthesis with better water use efficiency (Sperry et al., 2019), leading to increased LAI.

Our species-based LAI data adds to the currently documented measurements of black spruce and eastern larch currently available. The LAI ranges in this study corroborate with previous studies of black spruce studies reporting a range of 0.178 - 8.97. Our plot-based black spruce LAI data ranges were 0.7 - 3.2. We reported values currently inside the recorded eastern larch range. The current recorded range is 0.68 -

2.29 and we reported 0.005 – 1.2. We found larch LAI tended to only increase over time at a greater rate than spruce trees under the ambient CO_2 conditions, while the spruce outperformed the larch over time in the other two conditions. This may point to the larch being shaded out due to increased rates of spruce growth like in previous studies (Evans et al., 2016).

Recently, LAI time series analysis experiments have shown that under warmer temperatures LAI has increased or is projected to increase (Chen et al., 2019; Ramezani et al., 2020). Initial declines in LAI seen across some plots in 2016 were likely an artifact of trees being at stages where they are more susceptible to stress and plot temperature treatments beginning. Other studies have found that, in earlier stages, plants under elevated CO_2 and temperature have decreased leaf area initially, but subsequently developed greater water use efficiency and nutrient use efficiency with time (Kadam et al., 2014). We identified temperature thresholds where CO_2 may have been modulating conifer heat tolerance. At mean air temperatures greater than 18°C, conifer LAI under warming conditions and ambient CO_2 significantly decreased as temperatures increased, but under elevated CO_2 LAI remained constant. These temperature results add new insights about potential temperature thresholds where conifer LAI is liable to be most impacted by warming, and how elevated CO_2 could potentially improve heat tolerance in plants. Previous studies of corn and wheat LAI have found that elevated temperatures (+ 1.8 to 2.9°C) with no elevated CO_2 caused decreasing LAI trends (Chakrabarti et al., 2013). Pan et al. (2018) found that tomato plants under heat stress resulted in decreased photosynthetic rates, but elevated CO_2 combined with heat stress led to more efficient carboxylation rates, photochemical efficiency rates, and less oxidative stress. Our plot

temperature time-series data support these findings as we saw that plots under ambient CO_2 decreased in LAI as temperatures increased, and under elevated CO_2 LAI remained constant.

Leaf Area Density Across CO_2 Treatment, Species, Temperature Treatments, and Time

Current leaf area density trends in the literature indicate that leaf area density is, in general, increasing with higher CO_2 levels (Lalic & Mihailovic, 2004). We attempted to refine this finding by describing leaf area density changes in the upper, middle, and lower canopy in conifers under warming and elevated or ambient CO_2 conditions over time. However, we found little statistical evidence that leaf area density in the different canopy sections were changing through time. Only upper larch canopies in ambient CO_2 and warming and middle canopy larch tree densities in the control conditions demonstrated increased leaf area density over time. Importantly though, this significant leaf area density increase in the larch middle canopy under control conditions supplements the finding that the larch LAI was not changing through time in control conditions. This data supports previous studies showing that LAI alone does not always provide comprehensive canopy structural data (Sterba et al., 2019).

Our leaf area density analysis across temperature treatments adds new insight about changes in leaves under different levels of warming. Current data reveals that leaf tissue density and stomatal density typically increase with warming (Zhu et al., 2020). We extend this data by providing insight about where in the canopy leaf area density may accumulate at warmer temperature levels. As plot temperatures increased in ambient CO_2 conditions, upper and middle leaf area density increased significantly. In the elevated CO_2 conditions only upper and lower leaf area densities increased while middle canopy

leaf densities decreased with warming. The middle canopy leaf density decrease may help explain why LAI tended to decrease in certain levels of warming in the elevated CO_2 plots. Upper canopy leaf area density increases may be shading out middle canopy leaves, and the middle canopy's leaf area density decrease subsequently led to the lower canopy increase across temperature gradients. This finding provides evidence that three-dimensional vertical canopy profile data can help more comprehensively explain changes in two-dimensional data.

Leaf Inclination Angles Across CO_2 Treatment, Species, Temperature Treatments, and Time

Leaf inclination angle studies currently show that species tend to shift their leaf angles toward a more vertical distribution under elevated carbon dioxide levels of +700 ppm (Jayawardena et al., 2019) and leaf angle response to disturbance or stress varies by species (Ginebra-Solanellas et al., 2020; Holder et al., 2020; Reza Kasury et al., 2020). Our data contradicts these findings as we rarely saw trends showing significant change in leaf inclination angle over time. Only the lower spruce canopies under ambient CO_2 and warming conditions showed a trend toward flatter leaf angles over time. We did note anomalous trends in leaf angle inclination in 2016 and 2020 - 2021, but these were similar across species and treatments, suggesting that they were artifacts of treatments beginning in 2016 and a drought year in 2020 and 2021. Other studies have also found that leaves adjust their angles frequently in response to sunlight, drought, and precipitation adhesion (Kattenborn et al., 2022). Our findings of needles trending toward more spherical or less vertical distributions can be explained by previous studies finding that leaves become more equally distributed over time, leading to spherical angles (J. Wu

et al., 2022). Additionally, our study applies +500 ppm of CO_2, and in Jayawardena et al. (2019)'s study, they did not see any significant changes in leaf angles at +400 ppm, suggesting +500 ppm may not be a threshold for significant needle angle change through time. We found little evidence of significantly different distributions of average leaf inclination angles between the larch and the spruce trees at a cumulative level, but this is supported by recent studies finding boreal conifers having similar angles (Huemmrich, 2013). These data will add to the current database of larch, spruce, and boreal conifer leaf angle measurements which currently range from planar to vertical distributions depending on the study.

Across the temperature treatments we found that leaf inclination angles tended to decrease except in upper canopy elevated CO_2 treatments. The literature currently shows that as leaves undergo greater drought stress, they often become more vertical until they reach a wilting threshold. (Briglia et al., 2020) found that grapevine leaf angles increased by 30% under drought conditions as compared to well-watered conditions. In the ambient CO_2 conditions, leaf inclination angles decreased on average as plots warmed. Additionally, lower canopy leaf angles across temperatures decreased in elevated CO_2 plots, contradictory to the upper canopy inclination angles. Tendencies for leaf angles to become more planar with the most extreme levels of warming may indicate where leaves reach a wilting threshold (Kenchanmane Raju et al., 2020), with the lower and middle canopies reaching it first.

Implications and Next Steps

Our main findings consist of significant increases in LAI over time under warming and that three-dimensional leaf area density provides data that helps

comprehensively explain LAI data. We found that leaf area density and leaf inclination angle trends over time were complex and often not statistically significant according to monotonic trend tests. However, we highlighted where the lower canopy leaf density increased while LAI did not, providing evidence that the vertical canopy profile is useful to have as an additional canopy change metric. Additionally, we provided further evidence that the leaf area density profile assists in explaining LAI trends by showing changes in elevated CO_2 plots where upper and lower canopy leaf area density increased with temperature while the middle section did not. This helps to explain mechanistically why the two-dimensional LAI value may not be increasing as much under elevated CO_2 and warming as the ambient CO_2 trees. Upper leaf area density may be causing decreases in middle section leaf resources. Our leaf inclination angle data provides possible evidence of trees reaching wilting thresholds in the warmest plots.

Our findings capture minute differences in vegetation metrics that add to the literature supporting the utility of TLS to comprehensively evaluate tree stands. We are unable to make conclusions about the relationship between the treatments and these structural measurements due to unresolved confounding factors, but we have comprehensively evaluated these trees across time and temperature gradients. With these evaluations, we have suggested possible processes at work causing the changes, but they cannot be considered conclusive. The application of mixed effects models with this data would assist in revealing more conclusive relationships between CO_2, temperature, time, and species. However, our data supports the highly complex structural system that are treed peatland bogs and the necessity for detailed analyses to capture dynamics through time and space. Differing canopy section trends highlight the need to expand on canopy

structure beyond LAI alone as these impact photosynthesis, understory resources, and hydrologic inputs.

Conclusion

As the climate continues to warm and CO_2 levels rise, it is important to monitor and quantify how tree canopies change through time. By quantifying black spruce and eastern larch LAI, leaf area density, and leaf inclination angle, this study established that LAI is significantly increasing in warmer conditions and increasing a slower rate in control conditions over time. Leaf area density trends revealed that upper, middle, and lower canopies did not always have the same trends, underscoring the need for vertical canopy profile analyses. There were many confounding factors in this study, making it difficult to associate any canopy structural changes to treatment conditions alone. It would be useful to incorporate a seasonality component by estimating canopy structural metrics in the winter to evaluate boreal forests' leaf physiology sensitivity to seasonality. Additionally, normalizing the height of the plot-scale canopy would likely prevent disagreement between canopy section heights at the plot vs the individual tree scale, preventing possible outliers from skewing canopy section metrics. This data provides the opportunity to further constrain uncertainties in larger climate models, such as ELM-SPRUCE and future mixed effects models. This study extends evidence that TLS is a useful tool for quantifying large amounts of canopy structural data to scales at a sub centimeter level.

CHAPTER 4: CONCLUSIONS

Canopy structure is complex, and its variation is capable of impacting peatland function (Strack et al., 2019). Monitoring how peatland canopy structure changes under different environmental conditions is necessary to better understand how terrestrial carbon budgets may change with rising temperatures and CO_2 levels. Quantifying canopy structure accurately under different treatment conditions is challenging due to inconsistent structural-based validation metrics across treatment conditions. This underscores the need for models that can estimate canopy structure with parameters that maintain accuracy across inputs. Additionally, the complex changes that canopy structures can undergo under these differing environmental treatment conditions emphasizes the need for canopy structural estimations that quantify the entire vertical canopy profile. In this thesis, we used TLS data to build and validate a model to explore canopy structure accurately and comprehensively at the SPRUCE site.

The first study of this thesis was a methods-based analysis where we used TLS point cloud data to develop a model to estimate LAI, leaf area density, and leaf inclination angle based on J. W. Wilson, (1960)'s contact frequency principle and workflows from Almeida et al. (2019); Hosoi & Omasa (2006); S. Li et al. (2017); Yan et al. (2021) to modify a voxel-based model (VCP). We validated the model against eight individual tree destructively harvested-based LAI estimates and two plot DHP-based LAI estimates. We found that incorporating correction workflows for wood component removal, clumping, leaf inclination angle, and projection coefficient calculation resulted in a model that maintained moderate accuracy across the voxel size input parameter, suggesting that the model would be effective at estimating canopy structure under

different conditions. Based on an error analysis, we also found that the leaf inclination angle corrected for the most error in LAI estimation and wood component removal corrected for the least amount of error.

In the second study, we applied the modified and validated VCP model from the previous chapter to quantify the canopy structure across twelve plots at the SPRUCE site. We analyzed the structural data across the vertical and horizontal canopy profile, time, and temperature gradient. We found that the normalized LAI increased significantly and at a greater rate in plots under warming conditions over time as compared to plots under controlled conditions. Additionally, LAI increased the most significantly in the warmest plots under elevated and ambient CO_2. Leaf area density trends did not indicate significant changes in the understory plot canopies, but they did offer insight about why plots under elevated CO_2 occasionally had no significant trends in LAI under some temperature treatments. The data indicated that the leaf area density was decreasing in the middle canopy section across the temperature gradient, suggesting that while leaf area density builds in the upper canopy, middle canopies may be shaded out, better explaining LAI trends. Leaf inclination angle trends indicated that leaf angle tended to decrease across the temperature gradient except in the upper canopy. The spruce and larch species generally had similar canopy structural trends, which was not expected. However, in the control and elevated CO_2 plots, larch LAI tended to have lower increases in LAI compared to spruce LAI over time. This suggests further data collection may resolve that these species respond differently under different CO_2 conditions. From this study we extended previous canopy structural analyses and made predictions about what processes are affected and at work as the canopy changes.

There were various limitations, implications, and future proposals in each of these studies. The small validation sample size limited our ability to confirm the model's accuracy using direct estimates of LAI in treatment plots. However, the current model was moderately accurate across parameter inputs. We recommend a future study that collects and destructively harvests at least 4 larch and 4 spruce trees to quantify how the model's predictive accuracy may change over time and in the different treatment conditions. Additionally, future research should work to develop allometric relationships between LAI and structure of trees across different treatment conditions. In the second study we performed a comprehensive canopy structure analysis at the plot scale. We proposed what mechanisms may be at work or changing under the different treatment conditions to generate canopy changes. However, the confounding variables made it difficult to identify treatments as the main reason for these changes. The empirical data from this study can be used in the ELM-SPRUCE model or a mixed effects model to make firmer conclusions about the extent that the treatments are affecting canopy structure. The modified VCP workflow and TLS data comprehensively quantify canopy structure and provide metrics that help to better explain LAI trends across time and different environmental treatments. We recommend evaluating the model's time series analysis capacity by standardizing vertical canopy height metrics using plot height distributions to adjust upper, middle, and lower canopy thresholds. This will make analyses less prone to possible outliers. The method should be modified, validated, and applied in this peatland ecosystem in the future and in other terrestrial ecosystems where traditional methods of canopy structure estimation may be limited due to spatial scales or time constraints.

REFERENCES

Alexandridis, T., Stavridou, D., Strati, S., Monachou, S., & Silleos, N. (2013, September 9). *LAI measurement with hemispherical photographs at variable conditions for assessment of remotely sensed estimations*.

Almeida, D. R. A. de, Stark, S. C., Shao, G., Schietti, J., Nelson, B. W., Silva, C. A., Gorgens, E. B., Valbuena, R., Papa, D. de A., & Brancalion, P. H. S. (2019). Optimizing the Remote Detection of Tropical Rainforest Structure with Airborne Lidar: Leaf Area Profile Sensitivity to Pulse Density and Spatial Sampling. *Remote Sensing*, *11*(1), Article 1. https://doi.org/10.3390/rs11010092

Alonzo, M., Bookhagen, B., McFadden, J. P., Sun, A., & Roberts, D. A. (2015). Mapping urban forest leaf area index with airborne lidar using penetration metrics and allometry. *Remote Sensing of Environment*, *162*, 141–153. https://doi.org/10.1016/j.rse.2015.02.025

Angstmann, J. L., Ewers, B. E., & Kwon, H. (2012). Size-mediated tree transpiration along soil drainage gradients in a boreal black spruce forest wildfire chronosequence. *Tree Physiology*, *32*(5), 599–611. https://doi.org/10.1093/treephys/tps021

Asaadi, A., Arora, V. K., Melton, J. R., & Bartlett, P. (2018). An improved parameterization of leaf area index (LAI) seasonality in the Canadian Land Surface Scheme (CLASS) and Canadian Terrestrial Ecosystem Model (CTEM) modelling framework. *Biogeosciences*, *15*(22), 6885–6907. https://doi.org/10.5194/bg-15-6885-2018

Atik, M. E., Duran, Z., & Seker, D. Z. (2021). Machine Learning-Based Supervised Classification of Point Clouds Using Multiscale Geometric Features. *ISPRS International Journal of Geo-Information*, *10*(3), 187. https://doi.org/10.3390/ijgi10030187

Barclay, H. J., Trofymow, J. A., & Leach, R. I. (2000). Assessing bias from boles in calculating leaf area index in immature Douglas-fir with the LI-COR canopy

analyzer. *Agricultural and Forest Meteorology*, *100*(2), 255–260. https://doi.org/10.1016/S0168-1923(99)00091-X

Beaulne, J., Garneau, M., Magnan, G., & Boucher, É. (2021). Peat deposits store more carbon than trees in forested peatlands of the boreal biome. *Scientific Reports*, *11*(1), Article 1. https://doi.org/10.1038/s41598-021-82004-x

Béland, M., Baldocchi, D. D., Widlowski, J.-L., Fournier, R. A., & Verstraete, M. M. (2014). On seeing the wood from the leaves and the role of voxel size in determining leaf area distribution of forests with terrestrial LiDAR. *Agricultural and Forest Meteorology*, *184*, 82–97. https://doi.org/10.1016/j.agrformet.2013.09.005

Béland, M., & Kobayashi, H. (2021). Mapping forest leaf area density from multiview terrestrial lidar. *Methods in Ecology and Evolution*, *12*(4), 619–633. https://doi.org/10.1111/2041-210X.13550

Bond-Lamberty, B., Wang, C., Gower, S. T., & Norman, J. (2002). Leaf area dynamics of a boreal black spruce fire chronosequence. *Tree Physiology*, *22*(14), 993–1001. https://doi.org/10.1093/treephys/22.14.993

Briglia, N., Williams, K., Wu, D., Li, Y., Tao, S., Corke, F., Montanaro, G., Petrozza, A., Amato, D., Cellini, F., Doonan, J. H., Yang, W., & Nuzzo, V. (2020). Image-Based Assessment of Drought Response in Grapevines. *Frontiers in Plant Science*, *11*, 595. https://doi.org/10.3389/fpls.2020.00595

Brusa, A., & Bunker, D. (2014). Increasing the precision of canopy closure estimates from hemispherical photography: Blue channel analysis and under-exposure. *Agricultural and Forest Meteorology*, *s 195–196*, 102–107. https://doi.org/10.1016/j.agrformet.2014.05.001

Burgess, A. J., Retkute, R., Herman, T., & Murchie, E. H. (2017). Exploring Relationships between Canopy Architecture, Light Distribution, and Photosynthesis in Contrasting Rice Genotypes Using 3D Canopy Reconstruction. *Frontiers in Plant Science*, *8*. https://www.frontiersin.org/articles/10.3389/fpls.2017.00734

Calders, K., Origo, N., Disney, M., Nightingale, J., Woodgate, W., Armston, J., & Lewis, P. (2018). Variability and bias in active and passive ground-based measurements of effective plant, wood and leaf area index. *Agricultural and Forest Meteorology*, *252*, 231–240. https://doi.org/10.1016/j.agrformet.2018.01.029

Carrell, A. A., Lawrence, T. J., Cabugao, K. G. M., Carper, D. L., Pelletier, D. A., Lee, J. H., Jawdy, S. S., Grimwood, J., Schmutz, J., Hanson, P. J., Shaw, A. J., & Weston, D. J. (2022). Habitat-adapted microbial communities mediate Sphagnum peatmoss resilience to warming. *New Phytologist*, *234*(6), 2111–2125. https://doi.org/10.1111/nph.18072

Cerreta, J., Burgess, S., & Coleman, J. (2020). UAS for Public Safety Operations: A Comparison of UAS Point Clouds to Terrestrial LIDAR Point Cloud Data using a FARO Scanner. *International Journal of Aviation, Aeronautics, and Aerospace*. https://doi.org/10.15394/ijaaa.2020.1432

Chakrabarti, B., Singh, S. D., Kumar, V., Harit, R. C., & Misra, S. (2013). Growth and yield response of wheat and chickpea crops under high temperature. *Indian Journal of Plant Physiology*, *18*(1), 7–14. https://doi.org/10.1007/s40502-013-0002-6

Chen, J. M., Ju, W., Ciais, P., Viovy, N., Liu, R., Liu, Y., & Lu, X. (2019). Vegetation structural change since 1981 significantly enhanced the terrestrial carbon sink. *Nature Communications*, *10*(1), Article 1. https://doi.org/10.1038/s41467-019-12257-8

Chianucci, F. (2019). An overview of in situ digital canopy photography in forestry. *Canadian Journal of Forest Research*. https://doi.org/10.1139/cjfr-2019-0055

Chianucci, F., & Cutini, A. (2013). Estimation of canopy properties in deciduous forests with digital hemispherical and cover photography. *Agricultural and Forest Meteorology*, *168*, 130–139. https://doi.org/10.1016/j.agrformet.2012.09.002

Cifuentes, R., Van der Zande, D., Farifteh, J., Salas, C., & Coppin, P. (2014). Effects of voxel size and sampling setup on the estimation of forest canopy gap fraction

from terrestrial laser scanning data. *Agricultural and Forest Meteorology*, *194*, 230–240. https://doi.org/10.1016/j.agrformet.2014.04.013

Clawges, R., Vierling, L., Calhoon, M., & Toomey, M. (2007). Use of a ground-based scanning lidar for estimation of biophysical properties of western larch (Larix occidentalis). *International Journal of Remote Sensing*, *28*(19), 4331–4344. https://doi.org/10.1080/01431160701243460

Computree Core Team. 2017. Plugin Base for Computree. Office National des Forêts,

RDI Department. http://rdinnovation.onf.fr/projects/computree.

de Godoy Fernandes, P. H., de Souza, A. L. T., Tanaka, M. O., & Sebastiani, R. (2021). Decomposition and stabilization of organic matter in an old-growth tropical riparian forest: Effects of soil properties and vegetation structure. *Forest Ecosystems*, *8*(1), 13. https://doi.org/10.1186/s40663-021-00293-0

Dechant, B., Ryu, Y., Badgley, G., Zeng, Y., Berry, J. A., Zhang, Y., Goulas, Y., Li, Z., Zhang, Q., Kang, M., Li, J., & Moya, I. (2020). Canopy structure explains the relationship between photosynthesis and sun-induced chlorophyll fluorescence in crops. *Remote Sensing of Environment*, *241*, 111733. https://doi.org/10.1016/j.rse.2020.111733

Dermody, O., Long, S. P., & DeLucia, E. H. (2006). How does elevated CO2 or ozone affect the leaf-area index of soybean when applied independently? *The New Phytologist*, *169*(1), 145–155. https://doi.org/10.1111/j.1469-8137.2005.01565.x

Disney, M. (2019). Terrestrial LiDAR: A three-dimensional revolution in how we look at trees. *New Phytologist*, *222*(4), 1736–1741. https://doi.org/10.1111/nph.15517

Dusenge, M. E., Duarte, A. G., & Way, D. A. (2019). Plant carbon metabolism and climate change: Elevated CO2 and temperature impacts on photosynthesis, photorespiration and respiration. *New Phytologist*, *221*(1), 32–49. https://doi.org/10.1111/nph.15283

Evans, C., DeSotle, R., Mattilio, C., Yankowsky, E., Chenaille, A.-A., & Whiston, A. (2016). A Fine-Scale Examination of Larix laricina and Picea mariana Abundances along Abiotic Gradients in an Adirondack Peatland. *Northeastern Naturalist*, *23*(3), 420–433. https://doi.org/10.1656/045.023.0312

Fang, H., Baret, F., Plummer, S., & Schaepman-Strub, G. (2019). An Overview of Global Leaf Area Index (LAI): Methods, Products, Validation, and Applications. *Reviews of Geophysics*, *57*(3), 739–799. https://doi.org/10.1029/2018RG000608

Flynn, Wi. R. M., Owen, H. J. F., Grieve, S. W. D., & Lines, E. R. (2022). *Quantifying vegetation indices using TLS: Methodological complexities and ecological insights from a Mediterranean forest* [Preprint]. Biodiversity and Ecosystem Function: Terrestrial. https://doi.org/10.5194/egusphere-2022-1055

Gilardelli, C., Orlando, F., Movedi, E., & Confalonieri, R. (2018). Quantifying the Accuracy of Digital Hemispherical Photography for Leaf Area Index Estimates on Broad-Leaved Tree Species. *Sensors (Basel, Switzerland)*, *18*(4), 1028. https://doi.org/10.3390/s18041028

Ginebra-Solanellas, R. M., Holder, C. D., Lauderbaugh, L. K., & Webb, R. (2020). The influence of changes in leaf inclination angle and leaf traits during the rainfall interception process. *Agricultural and Forest Meteorology*, *285–286*, 107924. https://doi.org/10.1016/j.agrformet.2020.107924

Giuliani, R., Koteyeva, N., Voznesenskaya, E., Evans, M. A., Cousins, A. B., & Edwards, G. E. (2013). Coordination of Leaf Photosynthesis, Transpiration, and Structural Traits in Rice and Wild Relatives (Genus Oryza). *PLANT PHYSIOLOGY*, *162*(3), 1632–1651. https://doi.org/10.1104/pp.113.217497

Glatthorn, J., & Beckschäfer, P. (2014). Standardizing the Protocol for Hemispherical Photographs: Accuracy Assessment of Binarization Algorithms. *PLoS ONE*, *9*(11), e111924. https://doi.org/10.1371/journal.pone.0111924

Goel, N. S. (1988). Models of vegetation canopy reflectance and their use in estimation of biophysical parameters from reflectance data. *Remote Sensing Reviews*, *4*(1), 1–212. https://doi.org/10.1080/02757258809532105

GONZALEZ-MELER, M. A., TANEVA, L., & TRUEMAN, R. J. (2004). Plant Respiration and Elevated Atmospheric CO2 Concentration: Cellular Responses and Global Significance. *Annals of Botany*, *94*(5), 647–656. https://doi.org/10.1093/aob/mch189

Graham, J. D. (2020). *Using Terrestrial Laser Scanning to Characterize Peatland Microtopography and Assess Tree Growth Responses to Elevated Temperature and CO 2* [Doctor of Philosophy in Geosciences, Boise State University]. https://doi.org/10.18122/td/1729/boisestate

Graham, J. D., Ricciuto, D. M., Glenn, N. F., & Hanson, P. J. (2022). Incorporating Microtopography in a Land Surface Model and Quantifying the Effect on the Carbon Cycle. *Journal of Advances in Modeling Earth Systems*, *14*(2), e2021MS002721. https://doi.org/10.1029/2021MS002721

Grau, E., Durrieu, S., Fournier, R., Gastellu-Etchegorry, J.-P., & Yin, T. (2017). Estimation of 3D vegetation density with Terrestrial Laser Scanning data using voxels. A sensitivity analysis of influencing parameters. *Remote Sensing of Environment*, *191*, 373–388. https://doi.org/10.1016/j.rse.2017.01.032

Griffiths, N. A., Hanson, P. J., Ricciuto, D. M., Iversen, C. M., Jensen, A. M., Malhotra, A., McFarlane, K. J., Norby, R. J., Sargsyan, K., Sebestyen, S. D., Shi, X., Walker, A. P., Ward, E. J., Warren, J. M., & Weston, D. J. (2017). Temporal and Spatial Variation in Peatland Carbon Cycling and Implications for Interpreting Responses of an Ecosystem-Scale Warming Experiment. *Soil Science Society of America Journal*, *81*(6), 1668–1688. https://doi.org/10.2136/sssaj2016.12.0422

Hanson, P. J., Griffiths, N. A., Iversen, C. M., Norby, R. J., Sebestyen, S. D., Phillips, J. R., Chanton, J. P., Kolka, R. K., Malhotra, A., Oleheiser, K. C., Warren, J. M., Shi, X., Yang, X., Mao, J., & Ricciuto, D. M. (2020). Rapid Net Carbon Loss From a Whole-Ecosystem Warmed Peatland. *AGU Advances*, *1*(3), e2020AV000163. https://doi.org/10.1029/2020AV000163

Hanson, P. J., Riggs, J. S., Nettles, W. R., Phillips, J. R., Krassovski, M. B., Hook, L. A., Gu, L., Richardson, A. D., Aubrecht, D. M., Ricciuto, D. M., Warren, J. M., &

Barbier, C. (2016). *Attaining Whole-Ecosystem Warming Using Air and Deep Soil Heating Methods with an Elevated CO₂ Atmosphere* [Preprint]. Biogeochemistry: Wetlands. https://doi.org/10.5194/bg-2016-449

Hanson, P. J., Staff, U. S. F., & Team, S. (2009). *SPRUCE S1 Bog Vegetation Survey and Peat Depth Data: 2009*. https://knb.ecoinformatics.org/view/doi%3A10.3334%2FCDIAC%2FSPRUCE.003

Hickey, L. J., Nave, L. E., Nadelhoffer, K. J., Clay, C., Marini, A. I., & Gough, C. M. (2022). Mechanistically-grounded pathways connect remotely sensed canopy structure to soil respiration. *Science of The Total Environment*, *851*, 158267. https://doi.org/10.1016/j.scitotenv.2022.158267

Holder, C. D., Lauderbaugh, L. K., Ginebra-Solanellas, R. M., & Webb, R. (2020). Changes in leaf inclination angle as an indicator of progression toward leaf surface storage during the rainfall interception process. *Journal of Hydrology*, *588*, 125070. https://doi.org/10.1016/j.jhydrol.2020.125070

Holmgren, M., Lin, C.-Y., Murillo, J. E., Nieuwenhuis, A., Penninkhof, J., Sanders, N., van Bart, T., van Veen, H., Vasander, H., Vollebregt, M. E., & Limpens, J. (2015). Positive shrub–tree interactions facilitate woody encroachment in boreal peatlands. *Journal of Ecology*, *103*(1), 58–66.

Hosoi, F., Nakai, Y., & Omasa, K. (2013). Voxel tree modeling for estimating leaf area density and woody material volume using 3-D LIDAR data. *ISPRS Annals of the Photogrammetry, Remote Sensing and Spatial Information Sciences*, *II-5/W2*, 115–120. https://doi.org/10.5194/isprsannals-II-5-W2-115-2013

Hosoi, F., & Omasa, K. (n.d.). *ESTIMATING VERTICAL LEAF AREA DENSITY PROFILES OF TREE CANOPIES USING THREE-DIMENSIONAL PORTABLE LIDAR IMAGING*.

Hosoi, F., & Omasa, K. (2006). Voxel-Based 3-D Modeling of Individual Trees for Estimating Leaf Area Density Using High-Resolution Portable Scanning Lidar.

IEEE Transactions on Geoscience and Remote Sensing, *44*(12), 3610–3618. https://doi.org/10.1109/TGRS.2006.881743

Hu, R., Yan, G., Mu, X., & Luo, J. (2014). Indirect measurement of leaf area index on the basis of path length distribution. *Remote Sensing of Environment*, *155*, 239–247. https://doi.org/10.1016/j.rse.2014.08.032

Hu, R., Yan, G., Nerry, F., Liu, Y., Jiang, Y., Wang, S., Chen, Y., Mu, X., Zhang, W., & Xie, D. (2018). Using Airborne Laser Scanner and Path Length Distribution Model to Quantify Clumping Effect and Estimate Leaf Area Index. *IEEE Transactions on Geoscience and Remote Sensing*, *56*(6), 3196–3209. https://doi.org/10.1109/TGRS.2018.2794504

Huemmrich, K. F. (2013). Simulations of Seasonal and Latitudinal Variations in Leaf Inclination Angle Distribution: Implications for Remote Sensing. *Advances in Remote Sensing*, *02*(02), 93–101. https://doi.org/10.4236/ars.2013.22013

Hugelius, G., Loisel, J., Chadburn, S., Jackson, R. B., Jones, M., MacDonald, G., Marushchak, M., Olefeldt, D., Packalen, M., Siewert, M. B., Treat, C., Turetsky, M., Voigt, C., & Yu, Z. (2020). Large stocks of peatland carbon and nitrogen are vulnerable to permafrost thaw. *Proceedings of the National Academy of Sciences*, *117*(34), 20438–20446. https://doi.org/10.1073/pnas.1916387117

IIO, A., & ITO, A. (2014). *A Global Database of Field-observed Leaf Area Index in Woody Plant Species, 1932-2011*. 1.616815 MB. https://doi.org/10.3334/ORNLDAAC/1231

Indirabai, I., Nair, M. V. H., Nair, J. R., & Nidamanuri, R. R. (2020). Direct estimation of leaf area index of tropical forests using LiDAR point cloud. *Remote Sensing Applications: Society and Environment*, *18*, 100295. https://doi.org/10.1016/j.rsase.2020.100295

Islam, M. A., MacDonald, S. E., & Zwiazek, J. J. (2003). Responses of black spruce (Picea mariana) and tamarack (Larix laricina) to flooding and ethylene. *Tree Physiology*, *23*(8), 545–552. https://doi.org/10.1093/treephys/23.8.545

Itakura, K., & Hosoi, F. (2019). Estimation of Leaf Inclination Angle in Three-Dimensional Plant Images Obtained from Lidar. *Remote Sensing*, *11*(3), Article 3. https://doi.org/10.3390/rs11030344

Jayawardena, D. M., Heckathorn, S. A., Bista, D. R., & Boldt, J. K. (2019). Elevated carbon dioxide plus chronic warming causes dramatic increases in leaf angle in tomato, which correlates with reduced plant growth. *Plant, Cell & Environment*, *42*(4), 1247–1256. https://doi.org/10.1111/pce.13489

Jensen, A. M., Warren, J. M., King, A. W., Ricciuto, D. M., Hanson, P. J., & Wullschleger, S. D. (2019). Simulated projections of boreal forest peatland ecosystem productivity are sensitive to observed seasonality in leaf physiology†. *Tree Physiology*, *39*(4), 556–572. https://doi.org/10.1093/treephys/tpy140

Joosten, H., & Clarke, D. (2002). *Wise use of mires and peatlands: Background and principles including a framework for decision-making*. International Peat Society ; International Mire Conservation Group.

Kadam, N. N., Xiao, G., Melgar, R. J., Bahuguna, R. N., Quinones, C., Tamilselvan, A., Prasad, P. V. V., & Jagadish, K. S. V. (2014). Chapter Three—Agronomic and Physiological Responses to High Temperature, Drought, and Elevated CO2 Interactions in Cereals. In D. Sparks (Ed.), *Advances in Agronomy* (Vol. 127, pp. 111–156). Academic Press. https://doi.org/10.1016/B978-0-12-800131-8.00003-0

Kattenborn, T., Richter, R., Guimarães-Steinicke, C., Feilhauer, H., & Wirth, C. (2022). AngleCam: Predicting the temporal variation of leaf angle distributions from image series with deep learning. *Methods in Ecology and Evolution*, *13*(11), 2531–2545. https://doi.org/10.1111/2041-210X.13968

Kenchanmane Raju, S. K., Adkins, M., Enersen, A., Santana de Carvalho, D., Studer, A. J., Ganapathysubramanian, B., Schnable, P. S., & Schnable, J. C. (2020). Leaf Angle eXtractor: A high-throughput image processing framework for leaf angle measurements in maize and sorghum. *Applications in Plant Sciences*, *8*(8), e11385. https://doi.org/10.1002/aps3.11385

Kettridge, N., Thompson, D. K., Bombonato, L., Turetsky, M. R., Benscoter, B. W., & Waddington, J. M. (2013). The ecohydrology of forested peatlands: Simulating the effects of tree shading on moss evaporation and species composition. *Journal of Geophysical Research: Biogeosciences*, *118*(2), 422–435. https://doi.org/10.1002/jgrg.20043

Krishna Moorthy, S. M., Calders, K., Vicari, M. B., & Verbeeck, H. (2020). Improved Supervised Learning-Based Approach for Leaf and Wood Classification From LiDAR Point Clouds of Forests. *IEEE Transactions on Geoscience and Remote Sensing*, *58*(5), 3057–3070. https://doi.org/10.1109/TGRS.2019.2947198

Laine, A. M., Tolvanen, A., Mehtätalo, L., & Tuittila, E. (2016). Vegetation structure and photosynthesis respond rapidly to restoration in young coastal fens. *Ecology and Evolution*, *6*(19), 6880–6891. https://doi.org/10.1002/ece3.2348

Lalic, B., & Mihailovic, D. T. (2004). An Empirical Relation Describing Leaf-Area Density inside the Forest for Environmental Modeling. *Journal of Applied Meteorology and Climatology*, *43*(4), 641–645. https://doi.org/10.1175/1520-0450(2004)043<0641:AERDLD>2.0.CO;2

Leblanc, S. G. (2002). Correction to the plant canopy gap-size analysis theory used by the Tracing Radiation and Architecture of Canopies instrument. *Applied Optics*, *41*(36), 7667–7670. https://doi.org/10.1364/ao.41.007667

Lemeur, R., & Blad, B. L. (1975). A Critical Review of Light Models for Estimating the Shortwave Radiation Regime of Plant Canopies* *Published as Paper No. 3702, Journal Series, Nebraska Agricultural Experiment Station. In J. F. Stone (Ed.), *Developments in Agricultural and Managed Forest Ecology* (Vol. 1, pp. 255–286). Elsevier. https://doi.org/10.1016/B978-0-444-41273-7.50025-8

Leppä, K., Korkiakoski, M., Nieminen, M., Laiho, R., Hotanen, J.-P., Kieloaho, A.-J., Korpela, L., Laurila, T., Lohila, A., Minkkinen, K., Mäkipää, R., Ojanen, P., Pearson, M., Penttilä, T., Tuovinen, J.-P., & Launiainen, S. (2020). Vegetation controls of water and energy balance of a drained peatland forest: Responses to

alternative harvesting practices. *Agricultural and Forest Meteorology*, *295*, 108198. https://doi.org/10.1016/j.agrformet.2020.108198

Li, L., Mu, X., Soma, M., Wan, P., Qi, J., Hu, R., Zhang, W., Tong, Y., & Yan, G. (2021). An Iterative-Mode Scan Design of Terrestrial Laser Scanning in Forests for Minimizing Occlusion Effects. *IEEE Transactions on Geoscience and Remote Sensing*, *59*(4), 3547–3566. https://doi.org/10.1109/TGRS.2020.3018643

Li, S., Dai, L., Wang, H., Wang, Y., He, Z., & Lin, S. (2017). Estimating Leaf Area Density of Individual Trees Using the Point Cloud Segmentation of Terrestrial LiDAR Data and a Voxel-Based Model. *Remote Sensing*, *9*(11), 1202. https://doi.org/10.3390/rs9111202

Li, S., Fang, H., & Zhang, Y. (2023). Determination of the Leaf Inclination Angle (LIA) through Field and Remote Sensing Methods: Current Status and Future Prospects. *Remote Sensing*, *15*(4), 946. https://doi.org/10.3390/rs15040946

Li, Y., Guo, Q., Su, Y., Tao, S., Zhao, K., & Xu, G. (2017). Retrieving the gap fraction, element clumping index, and leaf area index of individual trees using single-scan data from a terrestrial laser scanner. *ISPRS Journal of Photogrammetry and Remote Sensing*, *130*, 308–316. https://doi.org/10.1016/j.isprsjprs.2017.06.006

Li, Y., Shi, H., Zhou, L., Eamus, D., Huete, A., Li, L., Cleverly, J., Hu, Z., Harahap, M., Yu, Q., He, L., & Wang, S. (2018). Disentangling Climate and LAI Effects on Seasonal Variability in Water Use Efficiency Across Terrestrial Ecosystems in China. *Journal of Geophysical Research: Biogeosciences*, *123*(8), 2429–2443. https://doi.org/10.1029/2018JG004482

Lin, Y., & West, G. (2016). Retrieval of effective leaf area index (LAIe) and leaf area density (LAD) profile at individual tree level using high density multi-return airborne LiDAR. *International Journal of Applied Earth Observation and Geoinformation*, *50*, 150–158. https://doi.org/10.1016/j.jag.2016.03.014

Liu, J., Liu, H., Chen, H., Yu, Z., Piao, S., Smol, J. P., Zhang, J., Huang, L., Wang, T., Yang, B., Zhao, Y., & Chen, F. (2022). Anthropogenic warming reduces the

carbon accumulation of Tibetan Plateau peatlands. *Quaternary Science Reviews*, *281*, 107449. https://doi.org/10.1016/j.quascirev.2022.107449

Liu, L.-X., Xu, S.-M., & Woo, K. C. (2003). Influence of leaf angle on photosynthesis and the xanthophyll cycle in the tropical tree species Acacia crassicarpa. *Tree Physiology*, *23*(18), 1255–1261. https://doi.org/10.1093/treephys/23.18.1255

Long, S. P., Zhu, X.-G., Naidu, S. L., & Ort, D. R. (2006). Can improvement in photosynthesis increase crop yields? *Plant, Cell & Environment*, *29*(3), 315–330. https://doi.org/10.1111/j.1365-3040.2005.01493.x

Luomala, E.-M., Laitinen, K., Sutinen, S., Kellomäki, S., & Vapaavuori, E. (2005). Stomatal density, anatomy and nutrient concentrations of Scots pine needles are affected by elevated CO2 and temperature. *Plant, Cell & Environment*, *28*(6), 733–749. https://doi.org/10.1111/j.1365-3040.2005.01319.x

Lynch, J. A., Clark, J. S., Bigelow, N. H., Edwards, M. E., & Finney, B. P. (2002). Geographic and temporal variations in fire history in boreal ecosystems of Alaska. *Journal of Geophysical Research*, *108*(D1), 8152. https://doi.org/10.1029/2001JD000332

Mahowald, N., Lo, F., Zheng, Y., Harrison, L., Funk, C., Lombardozzi, D., & Goodale, C. (2016). Projections of leaf area index in earth system models. *Earth System Dynamics*, *7*(1), 211–229. https://doi.org/10.5194/esd-7-211-2016

Malhotra, A., Brice, D. J., Childs, J., Graham, J. D., Hobbie, E. A., Vander Stel, H., Feron, S. C., Hanson, P. J., & Iversen, C. M. (2020). Peatland warming strongly increases fine-root growth. *Proceedings of the National Academy of Sciences*, *117*(30), 17627–17634. https://doi.org/10.1073/pnas.2003361117

Mantilla-Perez, M. B., & Salas Fernandez, M. G. (2017). Differential manipulation of leaf angle throughout the canopy: Current status and prospects. *Journal of Experimental Botany*, *68*(21–22), 5699–5717. https://doi.org/10.1093/jxb/erx378

McFarlane, K. J., Hanson, P. J., Iversen, C. M., Phillips, J. R., & Brice, D. J. (2018). Local Spatial Heterogeneity of Holocene Carbon Accumulation throughout the

Peat Profile of an Ombrotrophic Northern Minnesota Bog. *Radiocarbon*, *60*(3), 941–962. https://doi.org/10.1017/RDC.2018.37

Miller, J. (1967). A formula for average foliage density. *Australian Journal of Botany*, *15*(1), 141. https://doi.org/10.1071/BT9670141

Montague, T. G., & Givnish, T. J. (1996). Distribution of black spruce versus eastern larch along peatland gradients: Relationship to relative stature, growth rate, and shade tolerance. *Canadian Journal of Botany*, *74*(9), 1514–1532. https://doi.org/10.1139/b96-182

Nguyen, V.-T., Fournier, R. A., Côté, J.-F., & Pimont, F. (2022). Estimation of vertical plant area density from single return terrestrial laser scanning point clouds acquired in forest environments. *Remote Sensing of Environment*, *279*, 113115. https://doi.org/10.1016/j.rse.2022.113115

Niinemets, Ü. (2010). A review of light interception in plant stands from leaf to canopy in different plant functional types and in species with varying shade tolerance. *Ecological Research*, *25*(4), 693–714. https://doi.org/10.1007/s11284-010-0712-4

Norby, R. J., Sholtis, J. D., Gunderson, C. A., & Jawdy, S. S. (2003). Leaf dynamics of a deciduous forest canopy: No response to elevated CO2. *Oecologia*, *136*(4), 574–584. https://doi.org/10.1007/s00442-003-1296-2

Norby, R. J., Warren, J. M., Iversen, C. M., Childs, J., Jawdy, S. S., & Walker, A. P. (2022). Forest stand and canopy development unaltered by 12 years of CO2 enrichment*. *Tree Physiology*, *42*(3), 428–440. https://doi.org/10.1093/treephys/tpab107

Olsoy, P. J., Glenn, N. F., Clark, P. E., & Derryberry, D. R. (2014). Aboveground total and green biomass of dryland shrub derived from terrestrial laser scanning. *ISPRS Journal of Photogrammetry and Remote Sensing*, *88*, 166–173. https://doi.org/10.1016/j.isprsjprs.2013.12.006

Olsoy, P. J., Mitchell, J. J., Levia, D. F., Clark, P. E., & Glenn, N. F. (2016). Estimation of big sagebrush leaf area index with terrestrial laser scanning. *Ecological Indicators*, *61*, 815–821. https://doi.org/10.1016/j.ecolind.2015.10.034

Oshio, H., Asawa, T., Hoyano, A., & Miyasaka, S. (2015). Estimation of the leaf area density distribution of individual trees using high-resolution and multi-return airborne LiDAR data. *Remote Sensing of Environment*, *166*, 116–125. https://doi.org/10.1016/j.rse.2015.05.001

Pan, C., Ahammed, G. J., Li, X., & Shi, K. (2018). Elevated CO2 Improves Photosynthesis Under High Temperature by Attenuating the Functional Limitations to Energy Fluxes, Electron Transport and Redox Homeostasis in Tomato Leaves. *Frontiers in Plant Science*, *9*, 1739. https://doi.org/10.3389/fpls.2018.01739

Pisek, J., Sonnentag, O., Richardson, A. D., & Mõttus, M. (2013). Is the spherical leaf inclination angle distribution a valid assumption for temperate and boreal broadleaf tree species? *Agricultural and Forest Meteorology*, *169*, 186–194. https://doi.org/10.1016/j.agrformet.2012.10.011

Qu, Y., & Zhuang, Q. (2018). Modeling leaf area index in North America using a process-based terrestrial ecosystem model. *Ecosphere*, *9*(1), e02046. https://doi.org/10.1002/ecs2.2046

Qu, Y., & Zhuang, Q. (2020). Evapotranspiration in North America: Implications for water resources in a changing climate. *Mitigation and Adaptation Strategies for Global Change*, *25*(2), 205–220. https://doi.org/10.1007/s11027-019-09865-6

Raabe, K., Pisek, J., Sonnentag, O., & Annuk, K. (2015). Variations of leaf inclination angle distribution with height over the growing season and light exposure for eight broadleaf tree species. *Agricultural and Forest Meteorology*, *214–215*, 2–11. https://doi.org/10.1016/j.agrformet.2015.07.008

Ramezani, M. R., Massah Bavani, A. R., Jafari, M., Binesh, A., & Peters, S. (2020). Investigating the leaf area index changes in response to climate change (case study: Kasilian catchment, Iran). *SN Applied Sciences*, *2*(3), 501. https://doi.org/10.1007/s42452-020-2290-6

Reza Kasury, A., Sujono, J., & Jayadi, R. (2020). Effect of leaf inclination and rainfall intensity on the Canopy Wetness Index of Artocarpus Heterophyllus. *IOP*

Conference Series: Earth and Environmental Science, *437*(1), 012023. https://doi.org/10.1088/1755-1315/437/1/012023

Ringgaard, R., Herbst, M., & Friborg, T. (2014). Partitioning forest evapotranspiration: Interception evaporation and the impact of canopy structure, local and regional advection. *Journal of Hydrology*, *517*, 677–690. https://doi.org/10.1016/j.jhydrol.2014.06.007

Rouzbeh Kargar, A., MacKenzie, R., Asner, G. P., & van Aardt, J. (2019). A Density-Based Approach for Leaf Area Index Assessment in a Complex Forest Environment Using a Terrestrial Laser Scanner. *Remote Sensing*, *11*(15), 1791. https://doi.org/10.3390/rs11151791

Ruiz-Pérez, G., & Vico, G. (2020). Effects of Temperature and Water Availability on Northern European Boreal Forests. *Frontiers in Forests and Global Change*, *3*. https://www.frontiersin.org/articles/10.3389/ffgc.2020.00034

Ryu, Y., Verfaillie, J., Macfarlane, C., Kobayashi, H., Sonnentag, O., Vargas, R., Ma, S., & Baldocchi, D. D. (2012). Continuous observation of tree leaf area index at ecosystem scale using upward-pointing digital cameras. *Remote Sensing of Environment*, *126*, 116–125. https://doi.org/10.1016/j.rse.2012.08.027

Sabagh, A. E., Hossain, A., Islam, M. S., Iqbal, M. A., Raza, A., Karademir, Ç., Karademir, E., Rehman, A., Rahman, M. A., Singhal, R. K., Llanes, A., Raza, M. A., Mubeen, M., Nasim, W., Barutçular, C., Meena, R. S., Saneoka, H., Sabagh, A. E., Hossain, A., … Saneoka, H. (2020). Elevated CO_2 Concentration Improves Heat-Tolerant Ability in Crops. In *Abiotic Stress in Plants*. IntechOpen. https://doi.org/10.5772/intechopen.94128

Schädel, C., Richardson, A. D., Hufkens, K., Milliman, T., Seyednasrollah, B., Nettles, W. R., Krassovski, M. B., & Hanson, P. J. (2020). *SPRUCE Vegetation Phenology in Experimental Plots from Phenocam Imagery, 2015-2019*. Oak Ridge National Lab. (ORNL), Oak Ridge, TN (United States). https://doi.org/10.25581/spruce.086/1693418

Scott, R. L., Huxman, T. E., Cable, W. L., & Emmerich, W. E. (2006). Partitioning of evapotranspiration and its relation to carbon dioxide exchange in a Chihuahuan Desert shrubland. *Hydrological Processes*, *20*(15), 3227–3243. https://doi.org/10.1002/hyp.6329

Sebestyen, S. D. (2011). *Long-Term Monitoring Sites and Trends at the Marcell Experimental Forest*. 57.

Sebestyen, S. D., & Griffiths, N. A. (2016). *SPRUCE Enclosure Corral and Sump System: Description, Operation, and Calibration*. https://doi.org/10.3334/CDIAC/SPRUCE.030

Seidel, D., Fleck, S., & Leuschner, C. (2012). Analyzing forest canopies with ground-based laser scanning: A comparison with hemispherical photography. *Agricultural and Forest Meteorology*, *154–155*, 1–8. https://doi.org/10.1016/j.agrformet.2011.10.006

Shi, X., Ricciuto, D. M., Thornton, P. E., Xu, X., Yuan, F., Norby, R. J., Walker, A. P., Warren, J., Mao, J., Hanson, P. J., Meng, L., Weston, D., & Griffiths, N. A. (2020a). *Modeling the hydrology and physiology of <i>Sphagnum</i> moss in anorthern temperate bog* [Preprint]. Biogeochemistry: Modelling, Terrestrial. https://doi.org/10.5194/bg-2020-90

Shi, X., Ricciuto, D., Thornton, P., Xu, X., Yuan, F., Norby, R., Walker, A., Warren, J., Mao, J., Hanson, P., Meng, L., Weston, D., & Griffiths, N. (2020b). *Modeling the hydrology and physiology of Sphagnum moss in a northern temperate bog*. https://doi.org/10.5194/bg-2020-90

Souza, D. C., Jardine, K. J., Rodrigues, J. V. F. C., Gimenez, B. O., Rogers, A., McDowell, N., Walker, A. P., Higuchi, N., Sampaio-Filho, I. J., & Chambers, J. (2021). Canopy Position Influences the Degree of Light Suppression of Leaf Respiration in Abundant Tree Genera in the Amazon Forest. *Frontiers in Forests and Global Change*, *4*. https://www.frontiersin.org/articles/10.3389/ffgc.2021.723539

Sperry, J. S., Venturas, M. D., Todd, H. N., Trugman, A. T., Anderegg, W. R. L., Wang, Y., & Tai, X. (2019). The impact of rising CO2 and acclimation on the response of US forests to global warming. *Proceedings of the National Academy of Sciences*, *116*(51), 25734–25744. https://doi.org/10.1073/pnas.1913072116

Sterba, H., Dirnberger, G., & Ritter, T. (2019). Vertical Distribution of Leaf Area of European Larch (Larix decidua Mill.) and Norway Spruce (Picea abies (L.) Karst.) in Pure and Mixed Stands. *Forests*, *10*(7), Article 7. https://doi.org/10.3390/f10070570

Strack, M., Hayne, S., Lovitt, J., McDermid, G. J., Rahman, M. M., Saraswati, S., & Xu, B. (2019). Petroleum exploration increases methane emissions from northern peatlands. *Nature Communications*, *10*(1), Article 1. https://doi.org/10.1038/s41467-019-10762-4

Su, W., Zhu, D., Huang, J., & Guo, H. (2018). Estimation of the vertical leaf area profile of corn (Zea mays) plants using terrestrial laser scanning (TLS). *Computers and Electronics in Agriculture*, *150*(C), 5–13. https://doi.org/10.1016/j.compag.2018.03.037

Sun, J., Wang, P., Gao, Z., Liu, Z., & Li, Y. (2021). *Wood-leaf classification of tree point cloud based on intensity and geometrical information*. 41.

Tang, H., Brolly, M., Zhao, F., Strahler, A. H., Schaaf, C. L., Ganguly, S., Zhang, G., & Dubayah, R. (2014). Deriving and validating Leaf Area Index (LAI) at multiple spatial scales through lidar remote sensing: A case study in Sierra National Forest, CA. *Remote Sensing of Environment*, *143*, 131–141. https://doi.org/10.1016/j.rse.2013.12.007

Tfaily, M. M., Cooper, W. T., Kostka, J. E., Chanton, P. R., Schadt, C. W., Hanson, P. J., Iversen, C. M., & Chanton, J. P. (2014). Organic matter transformation in the peat column at Marcell Experimental Forest: Humification and vertical stratification. *Journal of Geophysical Research: Biogeosciences*, *119*(4), 661–675. https://doi.org/10.1002/2013JG002492

Tian, H., Lu, C., Yang, J., Banger, K., Huntzinger, D. N., Schwalm, C. R., Michalak, A. M., Cook, R., Ciais, P., Hayes, D., Huang, M., Ito, A., Jain, A. K., Lei, H., Mao, J., Pan, S., Post, W. M., Peng, S., Poulter, B., … Zeng, N. (2015). Global patterns and controls of soil organic carbon dynamics as simulated by multiple terrestrial biosphere models: Current status and future directions. *Global Biogeochemical Cycles*, *29*(6), 775–792. https://doi.org/10.1002/2014GB005021

Tian, L., Qu, Y., & Qi, J. (2021). Estimation of Forest LAI Using Discrete Airborne LiDAR: A Review. *Remote Sensing*, *13*(12), Article 12. https://doi.org/10.3390/rs13122408

Uchytil, R. (1991). *Larix laricina*. https://www.fs.fed.us/database/feis/plants/tree/larlar/all.html

Vicari, M. B., Disney, M., Wilkes, P., Burt, A., Calders, K., & Woodgate, W. (2019). Leaf and wood classification framework for terrestrial LiDAR point clouds. *Methods in Ecology and Evolution*, *10*(5), 680–694. https://doi.org/10.1111/2041-210X.13144

von Arx, G., Graf Pannatier, E., Thimonier, A., & Rebetez, M. (2013). Microclimate in forests with varying leaf area index and soil moisture: Potential implications for seedling establishment in a changing climate. *Journal of Ecology*, *101*(5), 1201–1213. https://doi.org/10.1111/1365-2745.12121

Wallace, K. J., Laughlin, D. C., Clarkson, B. D., & Schipper, L. A. (2018). Forest canopy restoration has indirect effects on litter decomposition and no effect on denitrification. *Ecosphere*, *9*(12). https://doi.org/10.1002/ecs2.2534

Wang, Y., & Fang, H. (2020). Estimation of LAI with the LiDAR Technology: A Review. *Remote Sensing*, *12*(20), 3457. https://doi.org/10.3390/rs12203457

Wedeux, B., & Coomes, D. (2015). Landscape-scale changes in forest canopy structure across a partially logged tropical peat swamp. *Biogeosciences*, *12*, 6707–6719. https://doi.org/10.5194/bg-12-6707-2015

Wilson, J. W. (1960). Inclined Point Quadrats. *The New Phytologist*, *59*(1), 1–8.

Wilson, R. M., Tfaily, M. M., Kolton, M., Johnston, E. R., Petro, C., Zalman, C. A., Hanson, P. J., Heyman, H. M., Kyle, J. E., Hoyt, D. W., Eder, E. K., Purvine, S. O., Kolka, R. K., Sebestyen, S. D., Griffiths, N. A., Schadt, C. W., Keller, J. K., Bridgham, S. D., Chanton, J. P., & Kostka, J. E. (2021). Soil metabolome response to whole-ecosystem warming at the Spruce and Peatland Responses under Changing Environments experiment. *Proceedings of the National Academy of Sciences of the United States of America*, *118*(25). https://doi.org/10.1073/pnas.2004192118

Wit, C. T. de. (1965). *Photosynthesis of leaf canopies* (No. 663; p.). Pudoc. https://library.wur.nl/WebQuery/wurpubs/413358

Woodgate, W., Armston, J. D., Disney, M., Suarez, L., Jones, S. D., Hill, M. J., Wilkes, P., & Soto-Berelov, M. (2017). Validating canopy clumping retrieval methods using hemispherical photography in a simulated Eucalypt forest. *Agricultural and Forest Meteorology*, *247*, 181–193. https://doi.org/10.1016/j.agrformet.2017.07.027

Wu, D., Phinn, S., Johansen, K., Robson, A., Muir, J., & Searle, C. (2018). Estimating Changes in Leaf Area, Leaf Area Density, and Vertical Leaf Area Profile for Mango, Avocado, and Macadamia Tree Crowns Using Terrestrial Laser Scanning. *Remote Sensing*, *10*(11), Article 11. https://doi.org/10.3390/rs10111750

Wu, J., Wen, S., Lan, Y., Yin, X., Zhang, J., & Ge, Y. (2022). Estimation of cotton canopy parameters based on unmanned aerial vehicle (UAV) oblique photography. *Plant Methods*, *18*(1), 129. https://doi.org/10.1186/s13007-022-00966-z

Xu, J., Morris, P. J., Liu, J., & Holden, J. (2018). PEATMAP: Refining estimates of global peatland distribution based on a meta-analysis. *CATENA*, *160*, 134–140. https://doi.org/10.1016/j.catena.2017.09.010

Yan, G., Hu, R., Luo, J., Weiss, M., Jiang, H., Mu, X., Xie, D., & Zhang, W. (2019). Review of indirect optical measurements of leaf area index: Recent advances,

challenges, and perspectives. *Agricultural and Forest Meteorology*, *265*, 390–411. https://doi.org/10.1016/j.agrformet.2018.11.033

Yan, G., Jiang, H., Luo, J., Mu, X., Li, F., Qi, J., Hu, R., Xie, D., & Zhou, G. (2021). Quantitative Evaluation of Leaf Inclination Angle Distribution on Leaf Area Index Retrieval of Coniferous Canopies. *Journal of Remote Sensing*, *2021*. https://doi.org/10.34133/2021/2708904

Yazaki, T., Hirano, T., & Sano, T. (2016). Biomass Accumulation and Net Primary Production during the Early Stage of Secondary Succession after a Severe Forest Disturbance in Northern Japan. *Forests*, *7*(11), Article 11. https://doi.org/10.3390/f7110287

Yin, T., Qi, J., Cook, B. D., Morton, D. C., Wei, S., & Gastellu-Etchegorry, J.-P. (2020). Modeling Small-Footprint Airborne Lidar-Derived Estimates of Gap Probability and Leaf Area Index. *Remote Sensing*, *12*(1), Article 1. https://doi.org/10.3390/rs12010004

Yun, T., An, F., Li, W., Sun, Y., Cao, L., & Xue, L. (2016). A Novel Approach for Retrieving Tree Leaf Area from Ground-Based LiDAR. *Remote Sensing*, *8*(11), Article 11. https://doi.org/10.3390/rs8110942

Zhang, W., Qi, J., Wan, P., Wang, H., Xie, D., Wang, X., & Yan, G. (2016). An Easy-to-Use Airborne LiDAR Data Filtering Method Based on Cloth Simulation. *Remote Sensing*, *8*(6), Article 6. https://doi.org/10.3390/rs8060501

Zhao, X., Shi, S., Yang, J., Gong, W., Sun, J., Chen, B., Guo, K., & Chen, B. (2020). Active 3D Imaging of Vegetation Based on Multi-Wavelength Fluorescence LiDAR. *Sensors (Basel, Switzerland)*, *20*(3), 935. https://doi.org/10.3390/s20030935

Zhou, Q.-Y., Park, J., & Koltun, V. (2018). *Open3D: A Modern Library for 3D Data Processing* (arXiv:1801.09847). arXiv. https://doi.org/10.48550/arXiv.1801.09847

Zhu, X., Liu, J., Skidmore, A. K., Premier, J., & Heurich, M. (2020). A voxel matching method for effective leaf area index estimation in temperate deciduous forests

from leaf-on and leaf-off airborne LiDAR data. *Remote Sensing of Environment*, *240*, 111696. https://doi.org/10.1016/j.rse.2020.111696

Zhu, X., Skidmore, A. K., Darvishzadeh, R., Niemann, K. O., Liu, J., Shi, Y., & Wang, T. (2018). Foliar and woody materials discriminated using terrestrial LiDAR in a mixed natural forest. *International Journal of Applied Earth Observation and Geoinformation*, *64*, 43–50. https://doi.org/10.1016/j.jag.2017.09.004

Zou, J., Zhong, P., Hou, W., Zuo, Y., & Leng, P. (2021). Estimating Needle and Shoot Inclination Angle Distributions and Projection Functions in Five Larix principis-rupprechtii Plots via Leveled Digital Camera Photography. *Forests*, *12*(1), Article 1. https://doi.org/10.3390/f12010030

Zou, X., Mõttus, M., Tammeorg, P., Torres, C. L., Takala, T., Pisek, J., Mäkelä, P., Stoddard, F. L., & Pellikka, P. (2014). Photographic measurement of leaf angles in field crops. *Agricultural and Forest Meteorology*, *184*, 137–146. https://doi.org/10.1016/j.agrformet.2013.09.010

APPENDIX A

Chapter 2 Supplementary Figures

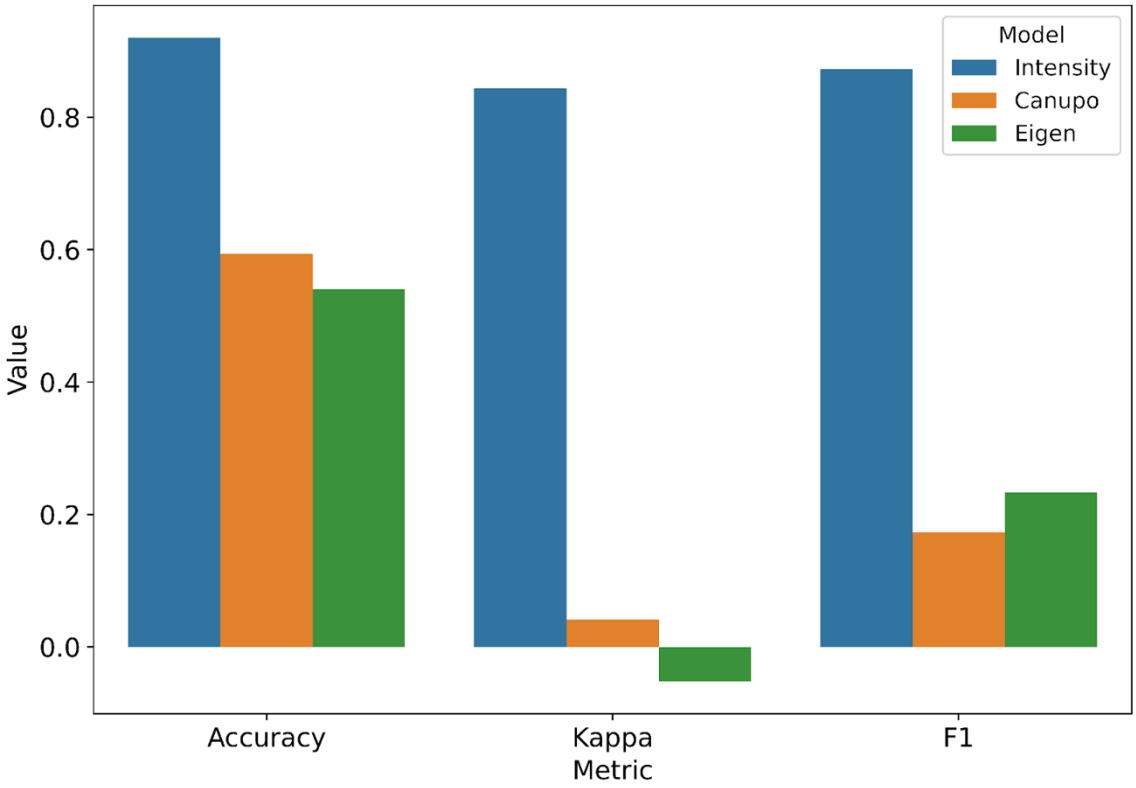

Figure A.1. The intensity-based random forest was more effective at separating leaf and wood components than the CANUPO and eigen feature-based algorithms.

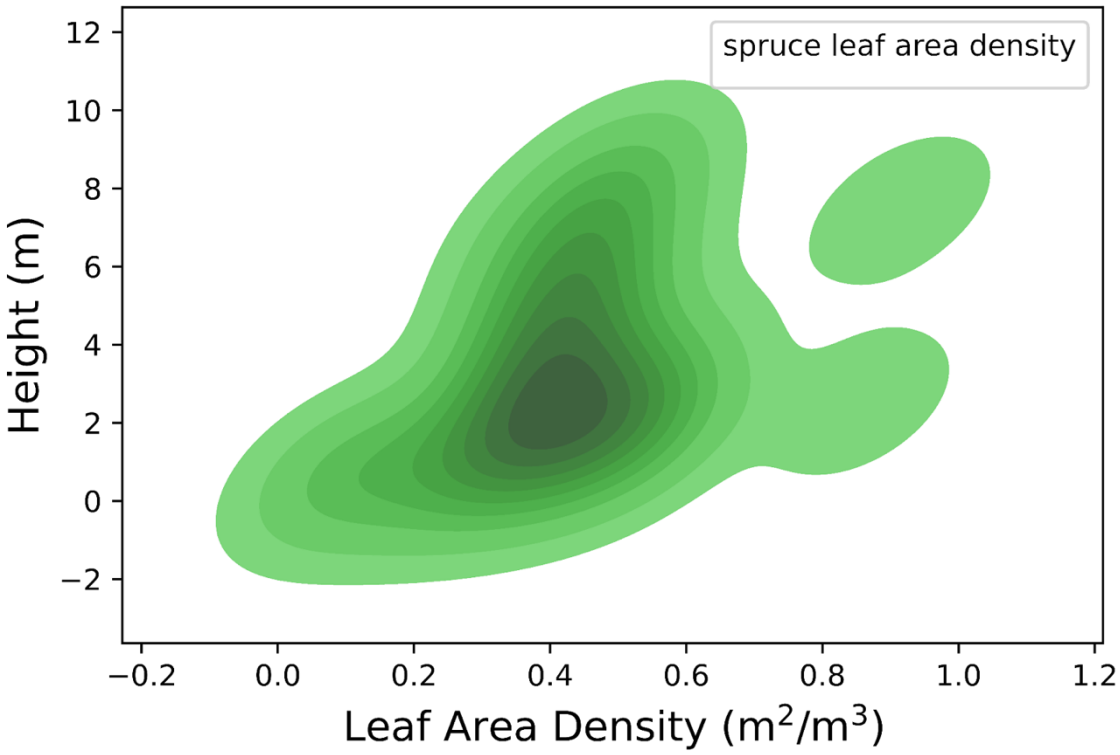

Figure A.2. Individual tree TLS-based leaf area density vertical distribution for the largest spruce (8.93 m). Densities increased in the center and upper portions of the canopy. The average density (0.49 m^2/m^3) for the majority of the vertical tree canopy profile was found most often in the low to middle canopy.

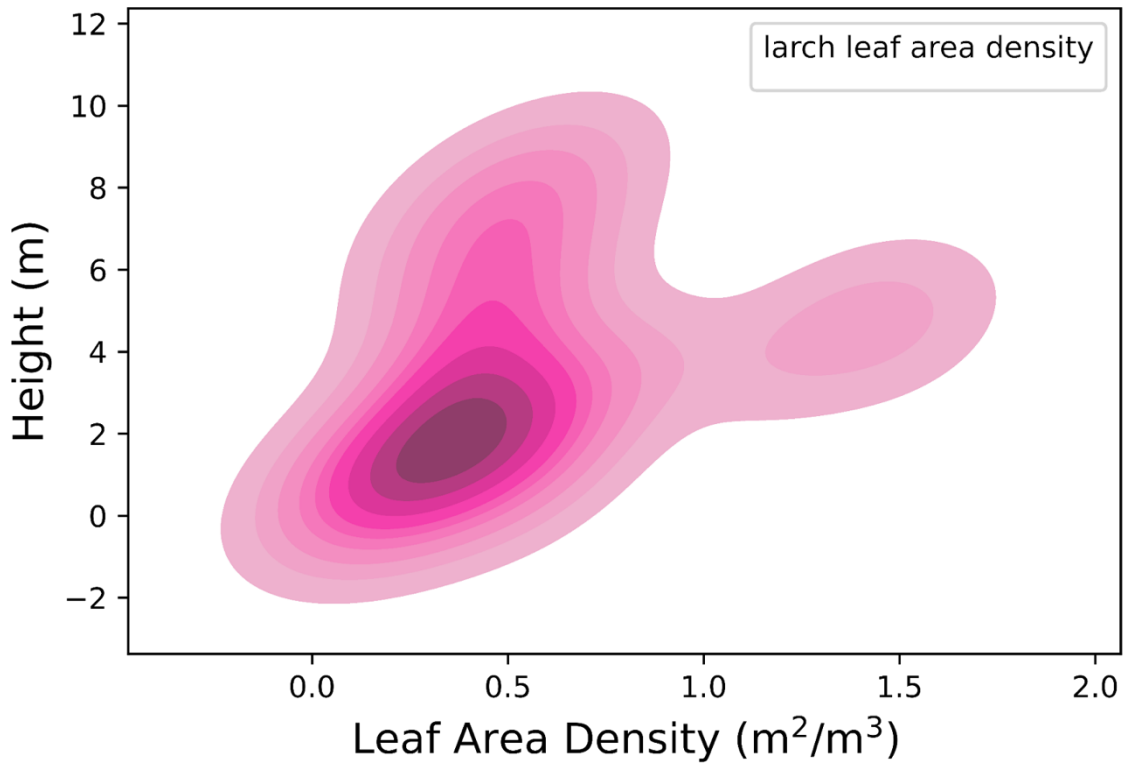

Figure A.3. Individual tree TLS-based leaf area density vertical distribution for the largest larch tree (8.95 m). Densities increased in the center of the canopy. The average density (0.40 m2/m3) for the majority of the vertical tree canopy profile was found most often in the lower canopy.

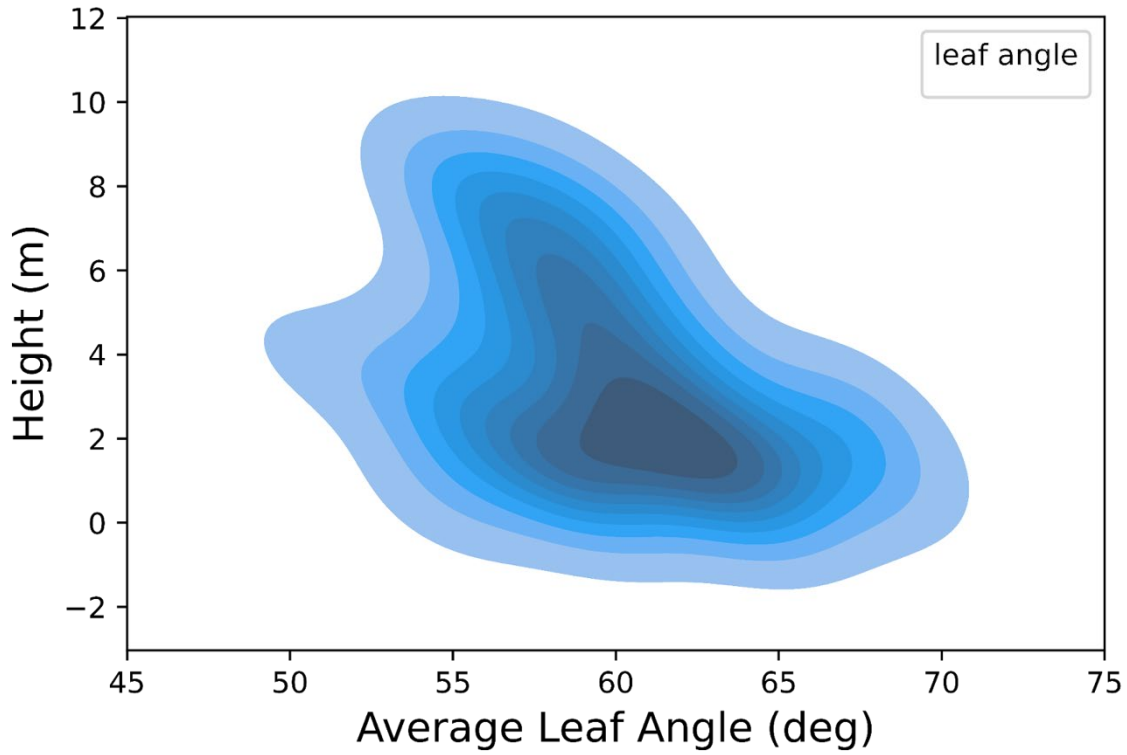

Figure A.4. Leaf inclination angle estimations made through the vertical canopy for the largest spruce and larch trees. Higher regions of the canopy of both trees tended to have a more symmetrical distribution of leaves and the lowest portion had a more vertical distribution of leaf angles.

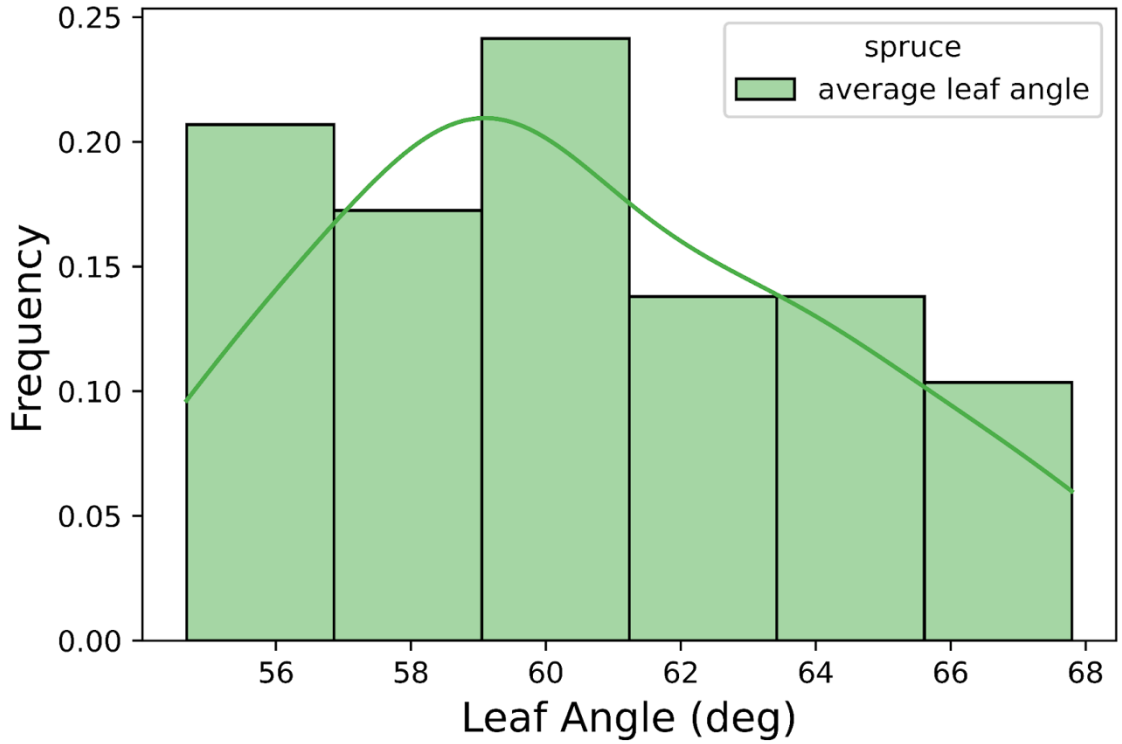

Figure A.5. Leaf inclination angle estimations made for the individually destructively harvested and scanned spruce trees. The average leaf angle was 60.5° and the median was 59.6°, resulting in a tendency toward vertically distributed leaves at the individual scale.

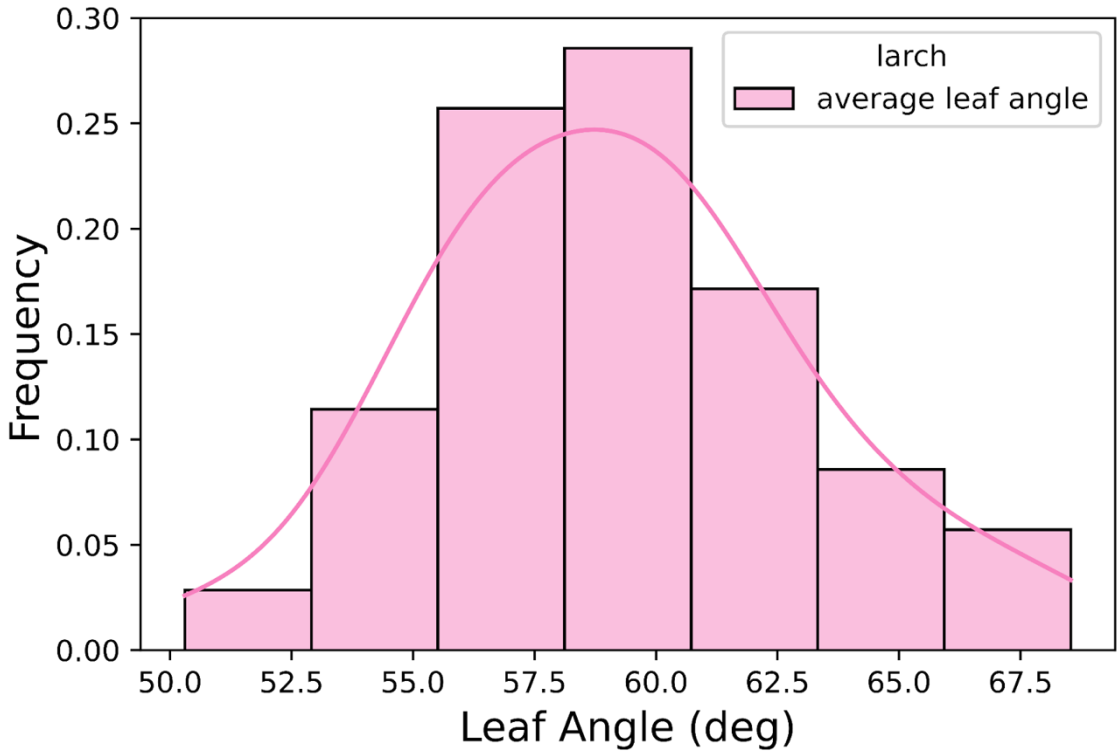

Figure A.6. Leaf inclination angle estimations made for the individually destructively harvested and scanned larch trees. The average leaf angle was 59.06° and the median was 58.43°, resulting in a tendency toward spherically distributed leaves at the individual scale.

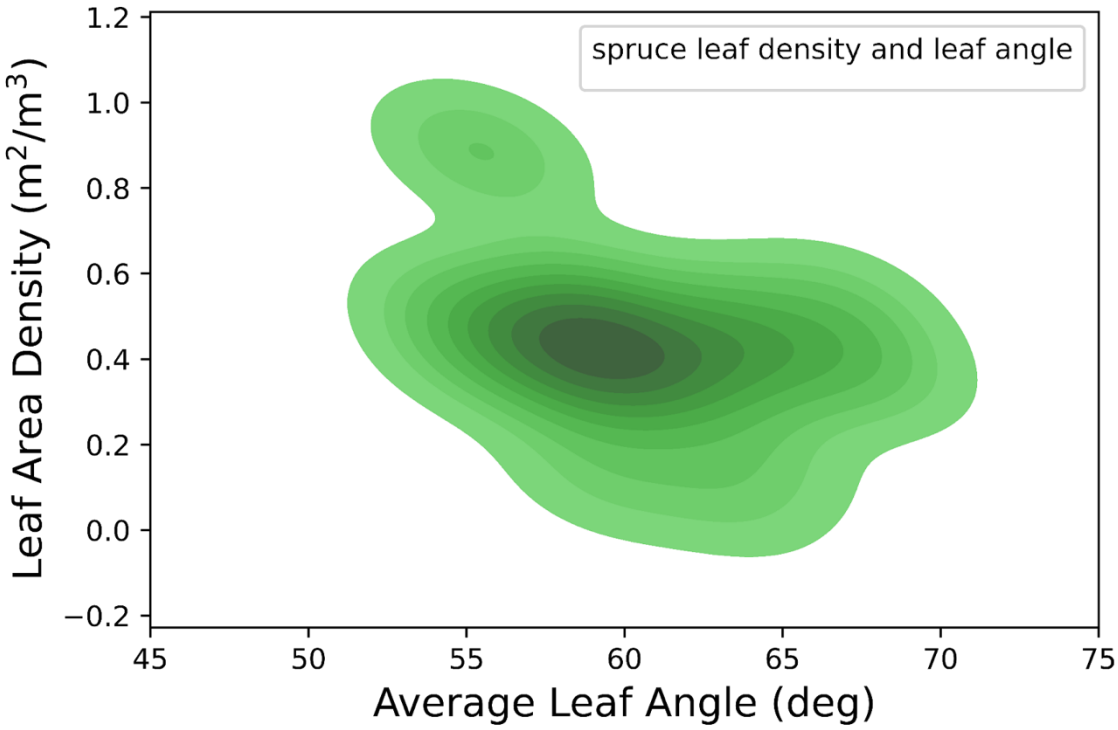

Figure A.7. Leaf density and leaf inclination angle relationship for spruce trees. On average, as leaf density decreases needles become more vertically distributed.

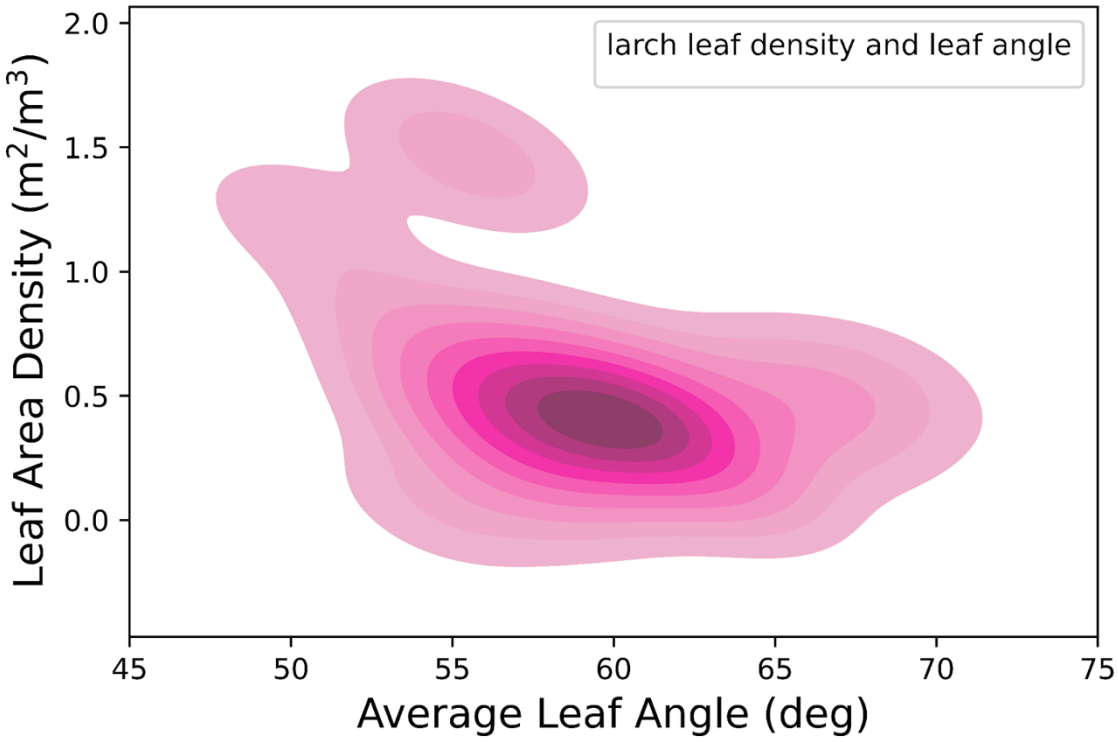

Figure A.8. Leaf density and leaf inclination angle relationship for larch. On average, as leaf density decreases needles become more vertically distributed

APPENDIX B

Chapter 3 Supplementary Figures

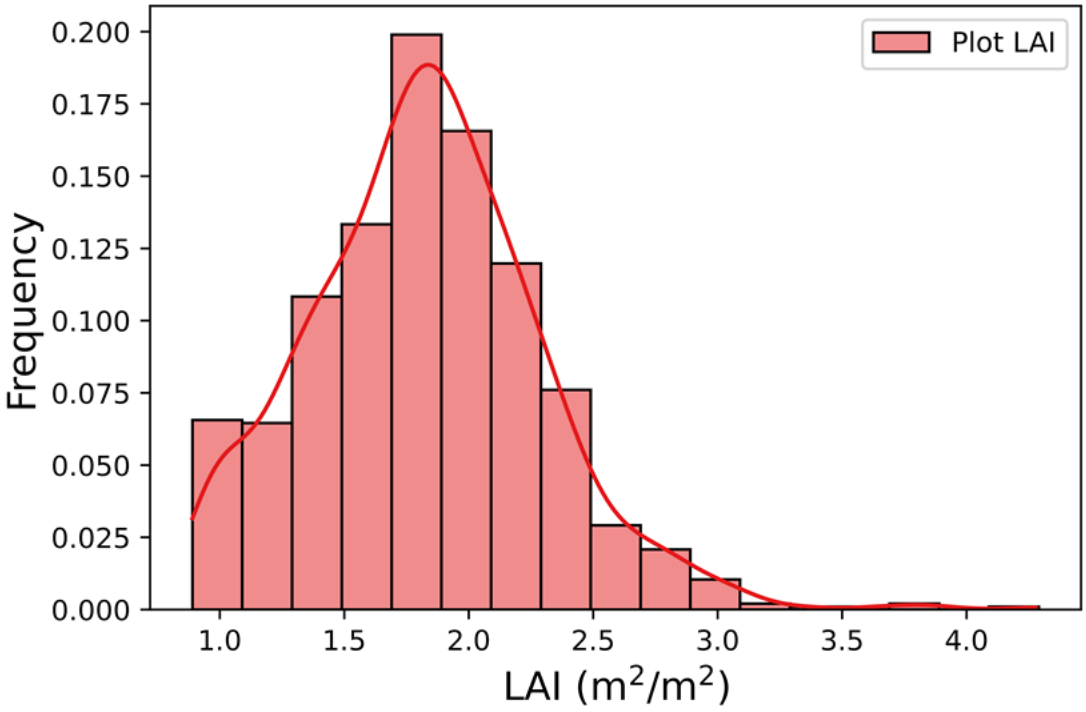

Figure B.1. Histogram with the LAI distribution for 12 SPRUCE plots across the experimental site, including from August 2015 - August 2022. μ = 1.9.

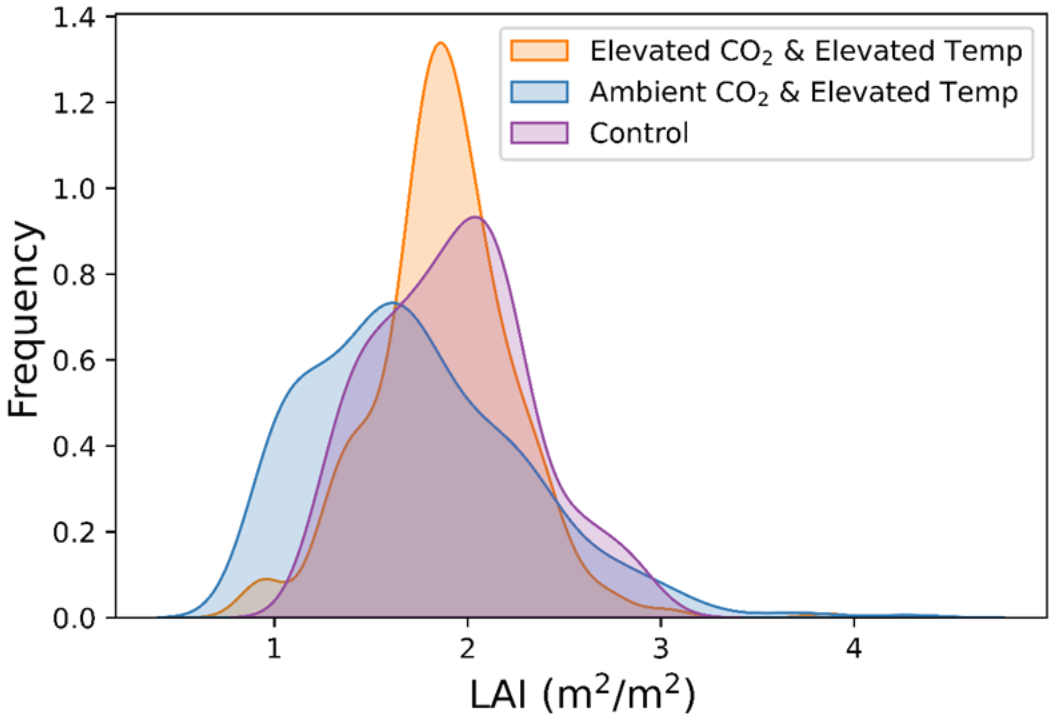

Figure B.2. The mean plot LAI across elevated carbon dioxide and elevated temperature plots was 1.9. The mean plot LAI under ambient carbon dioxide and elevated temperature plots was 1.7. The mean plot LAI under control conditions was 1.9.

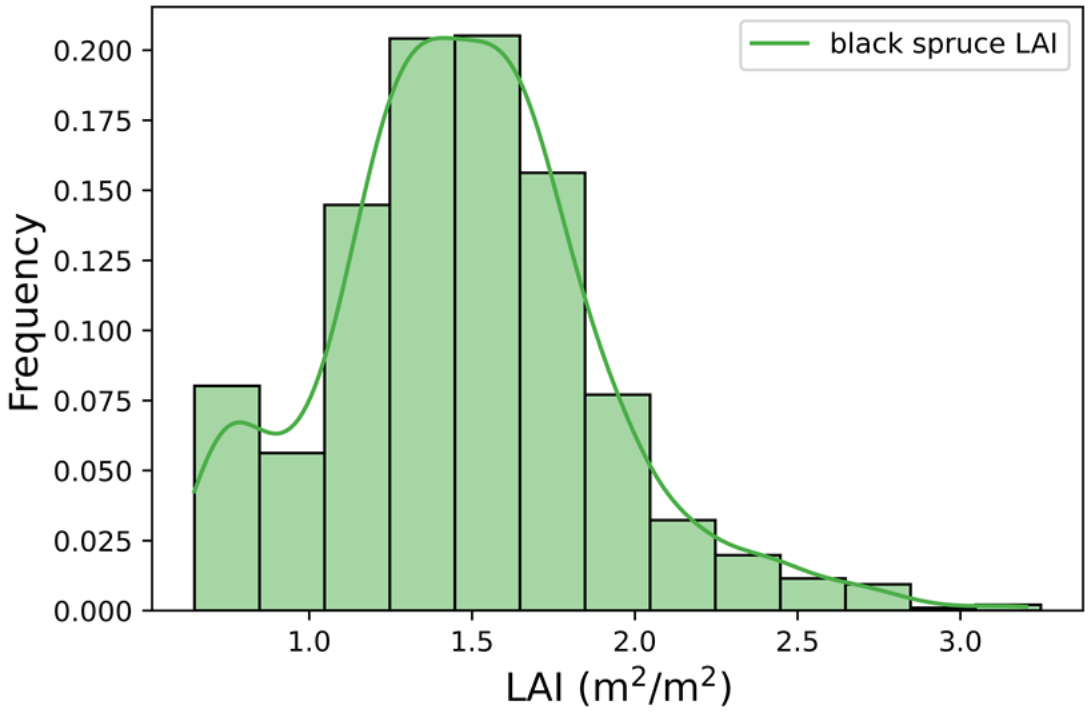

Figure B.3. Histogram with the LAI distribution for all black spruce trees across the experimental site. N = 1,184, μ = 1.5.

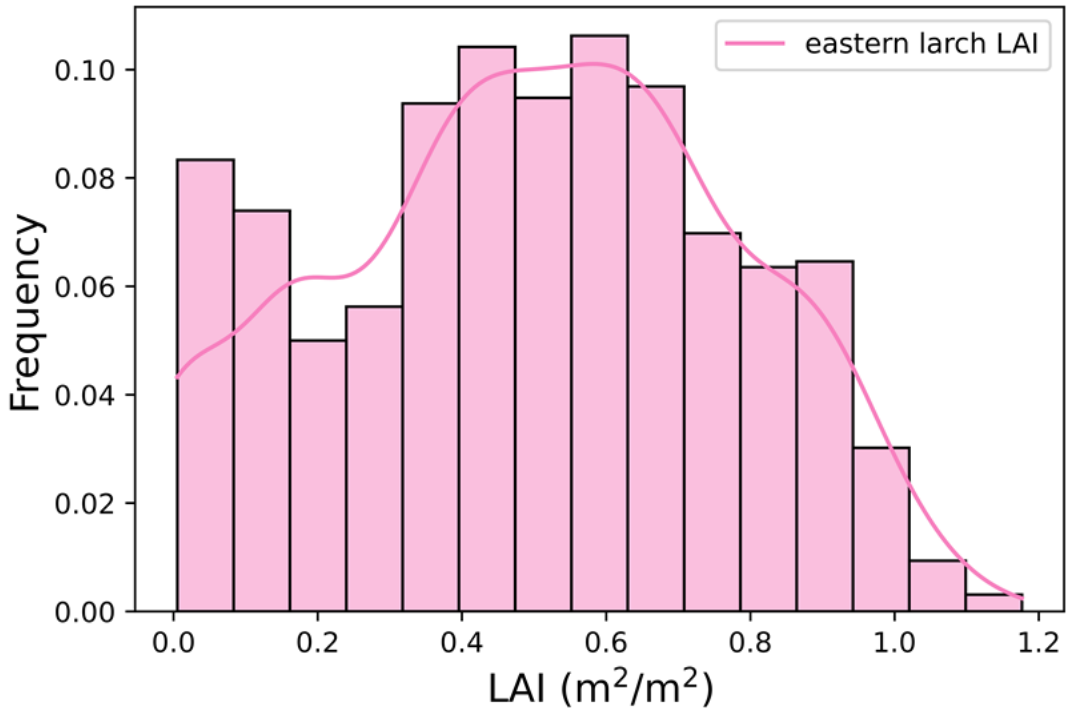

Figure B.4. Histogram with the LAI distribution for all eastern larch trees across the experimental site. $N = 432$, $\mu = 0.5$.

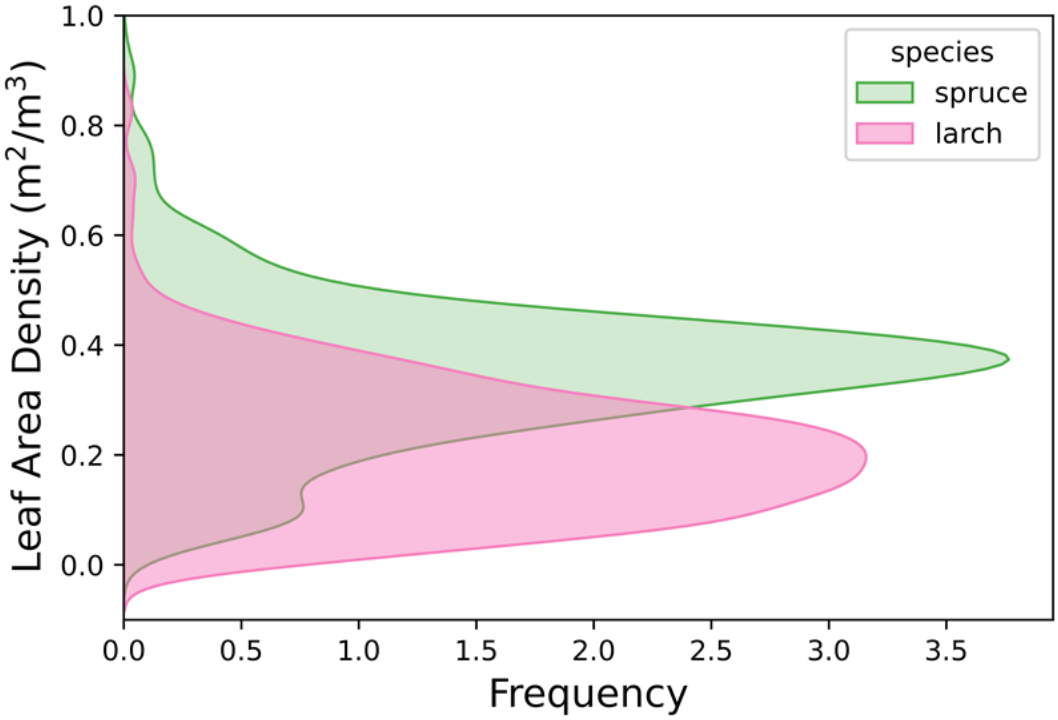

Figure B.5. Vertical distributions of leaf area density for the black spruce and the eastern larch across the SPRUCE site.

Table B.1. Mann-Kendall tests evaluating trends between leaf area density and time for the spruce and larch species.

Species	Treatment	Independent Metric	Dependent Metric	p	coefficient
upper spruce	Elevated CO_2	Time	Leaf Area Density	0.29	0.00
upper larch	Elevated CO_2	Time	Leaf Area Density	0.47	0.00
upper spruce	Control	Time	Leaf Area Density	0.06	0.00

upper larch	Control	Time	Leaf Area Density	0.10	0.00
upper spruce	Ambient CO_2	Time	Leaf Area Density	0.97	0.00
upper larch	Ambient CO_2	Time	Leaf Area Density	< 0.05	0.002
middle spruce	Elevated CO_2	Time	Leaf Area Density	0.09	0.00
middle larch	Elevated CO_2	Time	Leaf Area Density	0.88	0.00
middle spruce	Control	Time	Leaf Area Density	0.40	0.00
middle larch	Control	Time	Leaf Area Density	< 0.05	0.001
middle spruce	Ambient CO_2	Time	Leaf Area Density	0.79	0.00
middle larch	Ambient CO_2	Time	Leaf Area Density	0.54	0.00
lower spruce	Elevated CO_2	Time	Leaf Area Density	0.89	0.00
lower larch	Elevated CO_2	Time	Leaf Area Density	0.23	0.00
lower spruce	Control	Time	Leaf Area Density	0.62	0.00

lower larch	Control	Time	Leaf Area Density	0.73	0.00
lower spruce	Ambient CO_2	Time	Leaf Area Density	0.38	0.00
lower larch	Ambient CO_2	Time	Leaf Area Density	0.92	0.00

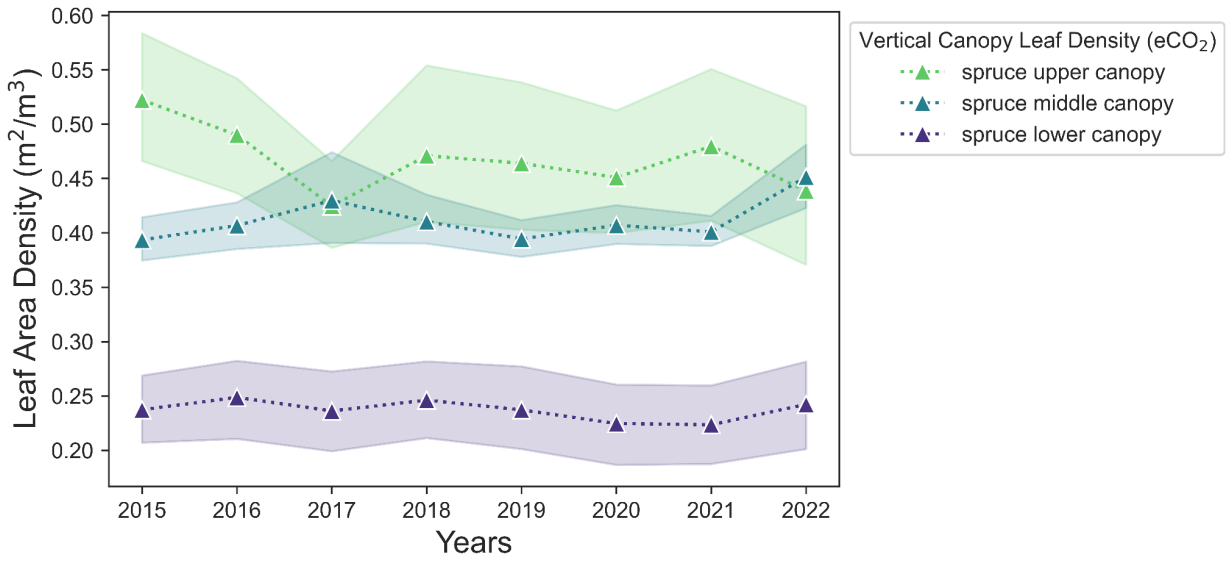

Figure B.6. Spruce leaf area density through time under elevated CO_2 did not show significant trends.

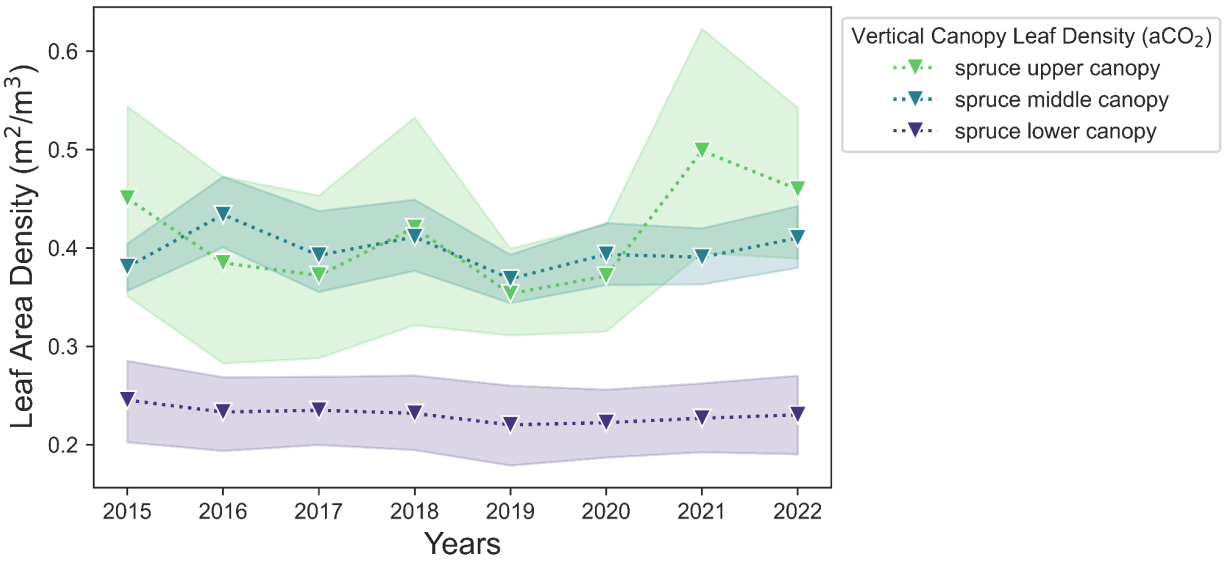

Figure B.7. Spruce leaf area density through time under ambient CO_2 did not show significant trends.

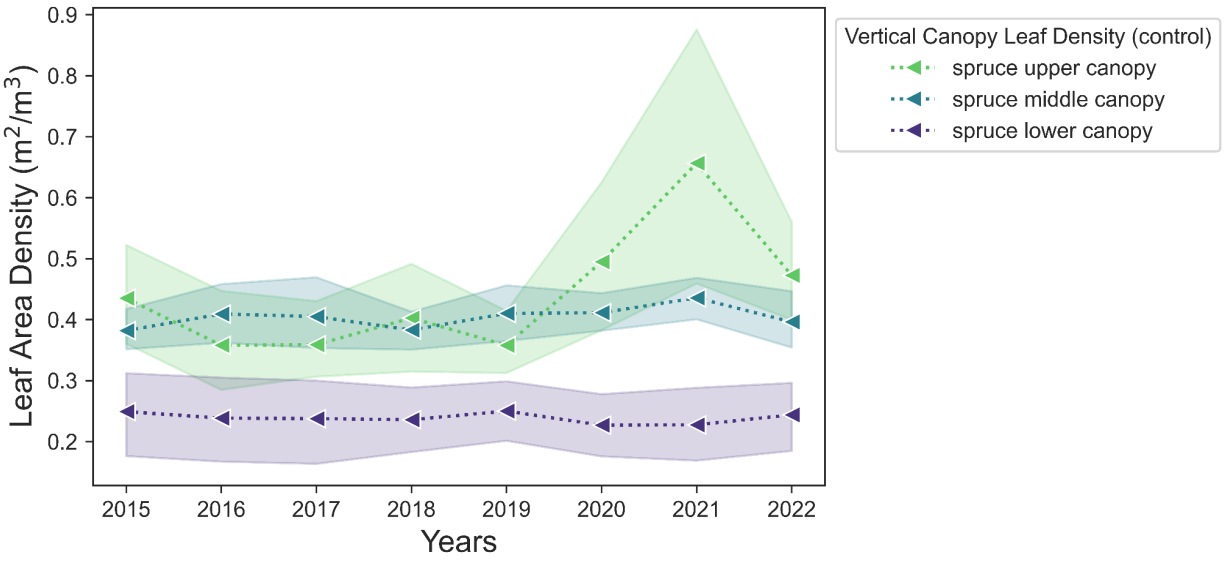

Figure B.8. Spruce leaf area density through time under controlled conditions did not show significant trends.

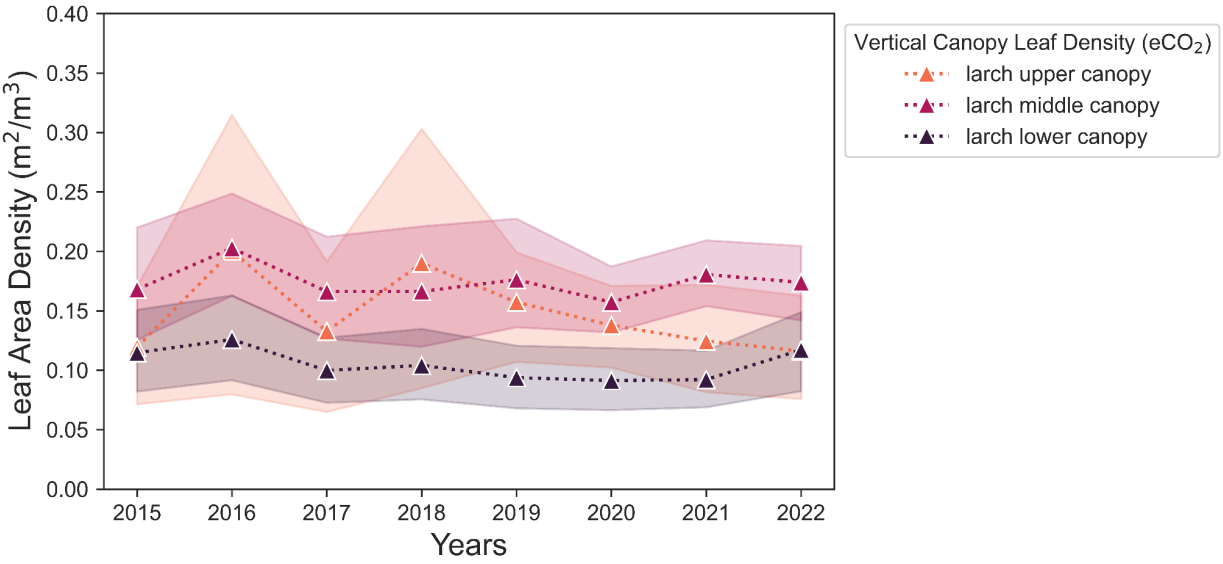

Figure B.9. Larch leaf area density through time under elevated CO_2 did not show significant trends

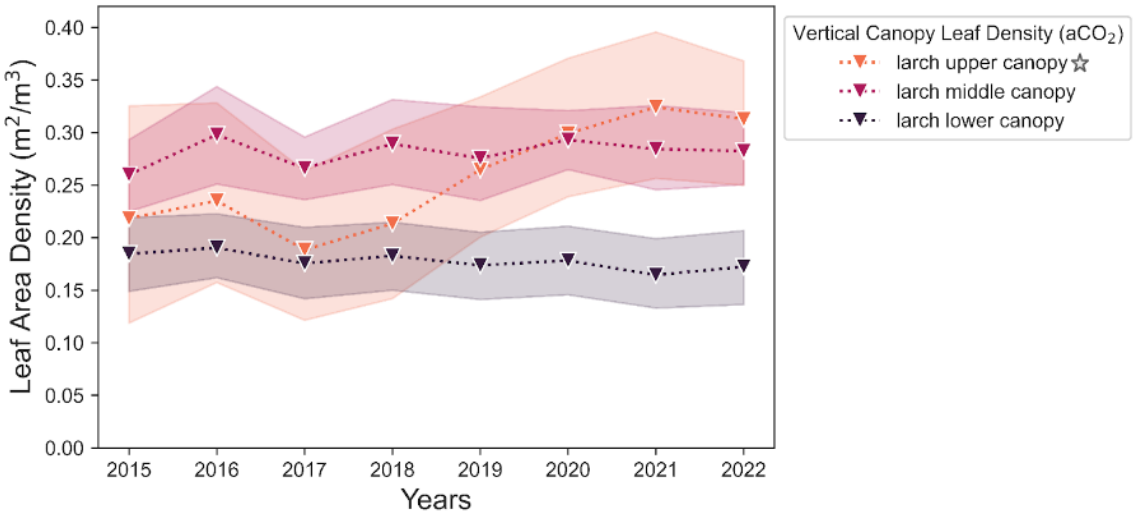

Figure B.10. Across the ambient CO_2 , elevated temperature plots, the upper larch canopy leaf density increased with a slope of 0.002 ($p < 0.05$). Stars indicate a significant trend.

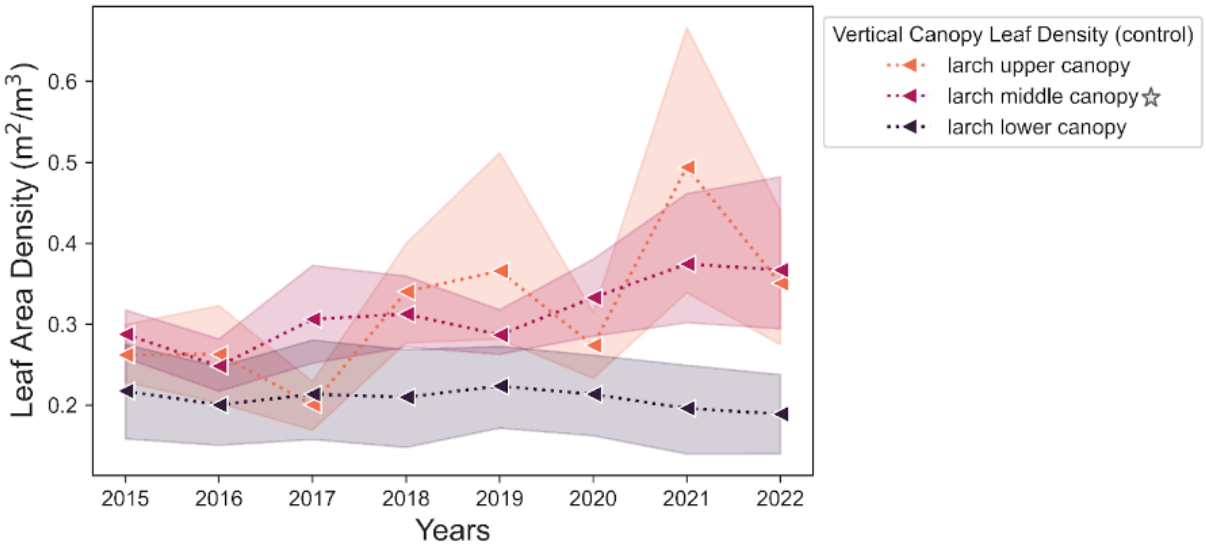

Figure B.11. Middle larch canopy leaf densities had increasing trends with a slope of 0.001 ($p < 0.05$). Stars indicate a significant trend.

Table B.2. Ordinary least squares regression analysis results for leaf area density and temperature.

Species	Treatment	Independent Metric	Dependent Metric	p	R^2	coefficient	95% CI
All, Upper Canopy	Ambient CO_2	Temperature	Leaf Area Density	< 0.001	0.17	0.04	0.028 - 0.053
All, Middle Canopy	Ambient CO_2	Temperature	Leaf Area Density	< 0.01	0.02	0.01	0.004 - 0.016
All, Lower Canopy	Ambient CO_2	Temperature	Leaf Area Density	0.098	0.01	-0.01	-0.016 - 0.001
All, Upper Canopy	Elevated CO_2	Temperature	Leaf Area Density	< 0.05	0.02	0.01	0.001 - 0.025
All, Middle Canopy	Elevated CO_2	Temperature	Leaf Area Density	< 0.05	0.02	-0.01	-0.020 - - 0.004

All, Lower Canopy	Elevated CO_2	Temperature	Leaf Area Density	< 0.01	0.02	0.01	0.004 - 0.024

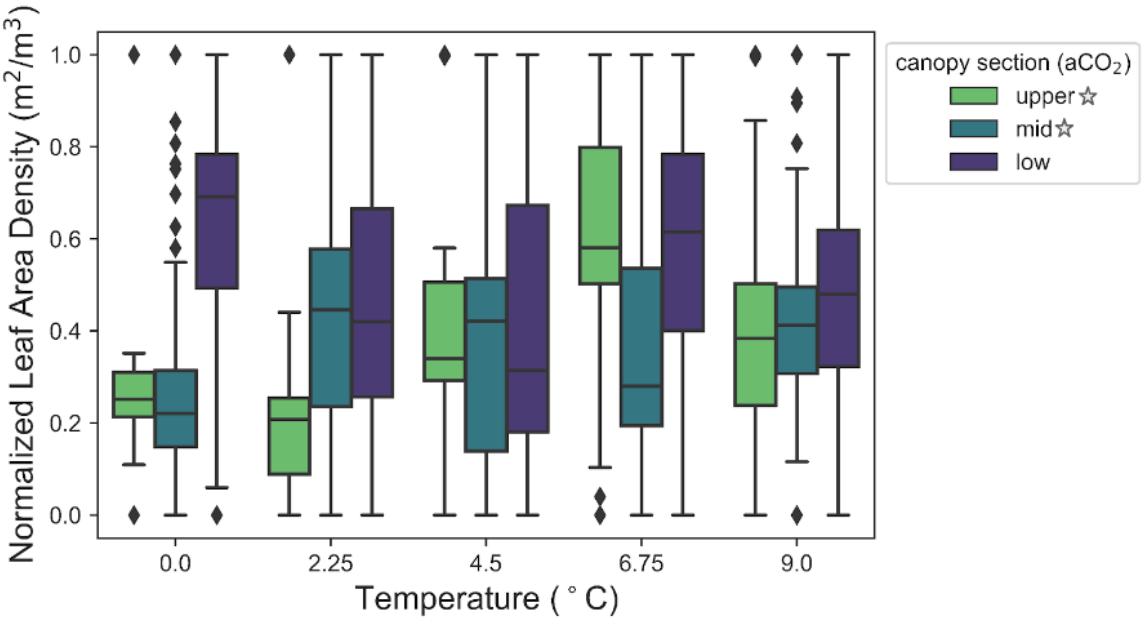

Figure B.12. Normalized leaf area density in ambient CO_2 plots exhibited increasing leaf area densities in upper ($R^2 = 0.17$, $p < 0.001$, $m = 0.04$) and middle canopies ($R^2 = 0.02$, $p < 0.01$, $m = 0.009$). Lower canopy leaf densities did not have a significant trend across temperatures. Stars indicate a significant trend.

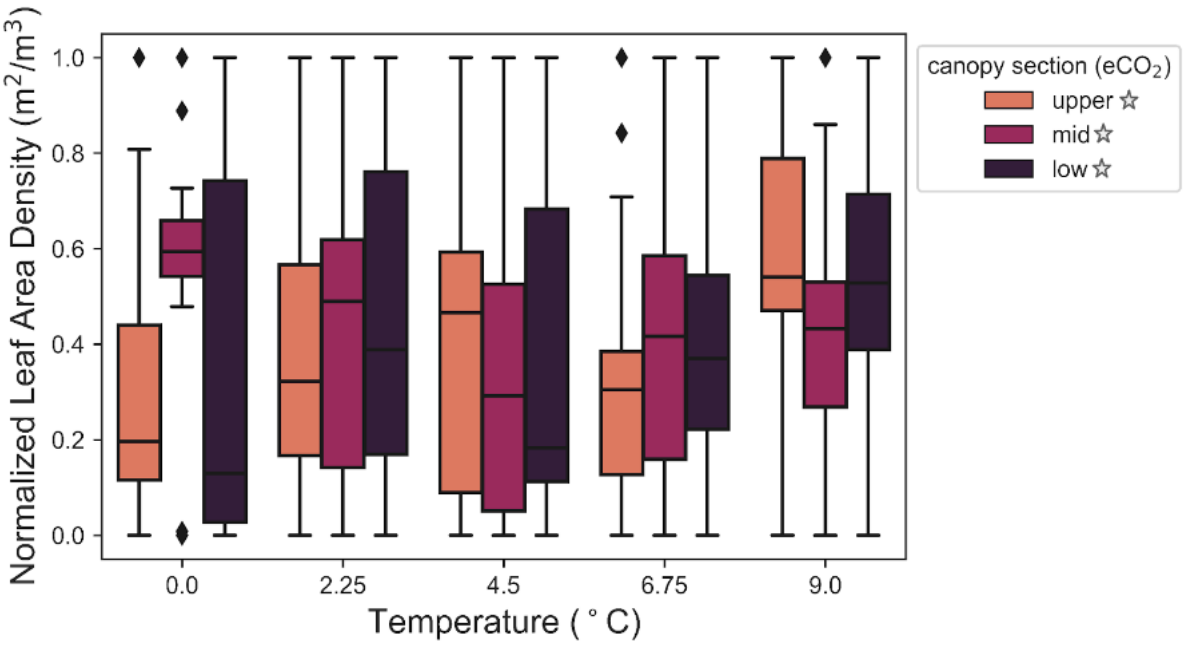

Figure B.13. Normalized leaf area density in elevated CO_2 plots exhibited increasing leaf area densities in upper ($R^2 = 0.022$, $p < 0.05$, $m = 0.01$) and lower canopies ($R^2 = 0.019$, $p < 0.01$, $m = 0.01$). Middle canopy leaf area densities had a significant decreasing trend across the temperature gradient ($R^2 = 0.019$, $p < 0.05$, $m = -0.01$). Stars indicate a significant trend.

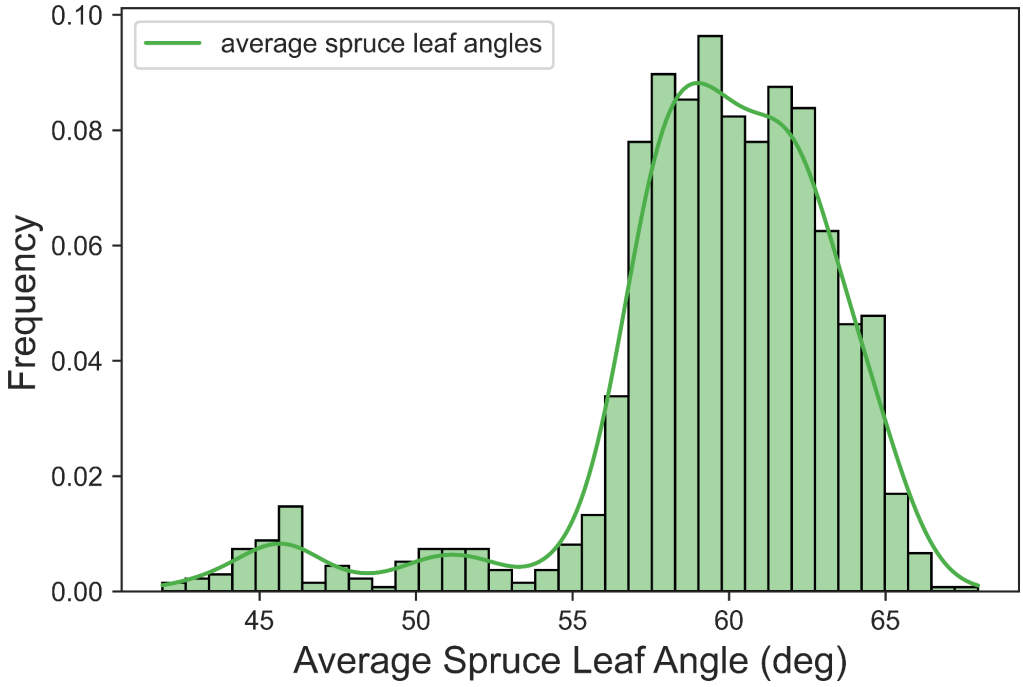

Figure B.14. Histogram with the average leaf inclination angle distribution for all black spruce trees across the experimental site. *N* = 1,184, μ = 59°, the range was 41° to 68°. Cumulatively, spruce trees tended to represent either spherical or vertical leaf angle distribution patterns.

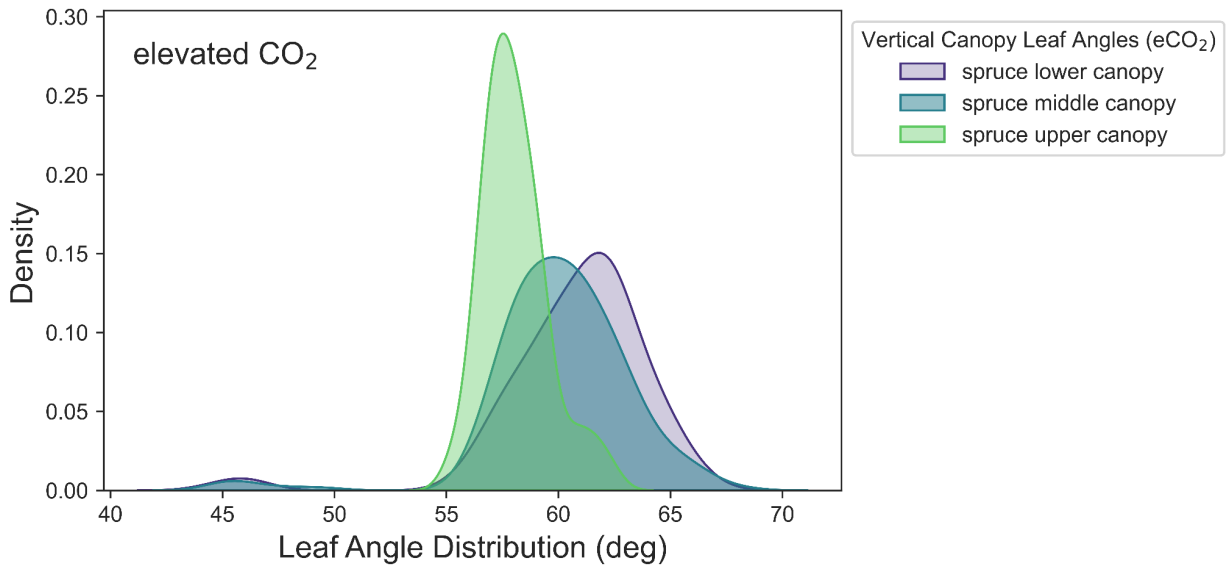

Figure B.15. Spruce upper canopy leaf angles (μ = 58°, range = 55° to 63°) under elevated CO_2 conditions were, on average, more symmetrically distributed than

middle and lower canopy leaves. Middle (μ = 60°, range = 45° to 68°) and lower (μ = 60°, range = 45° to 67°) canopies had more vertical distributions on average.

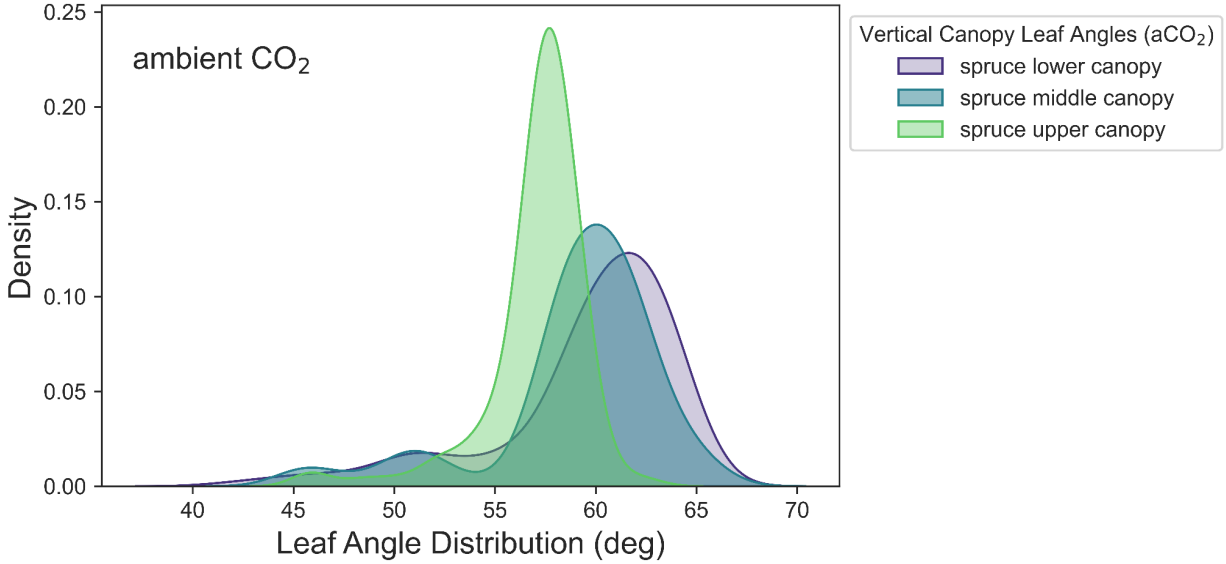

Figure B.16. Spruce upper canopy leaf angles (μ = 57°, range = 46° to 62°), middle (μ = 59°, range = 45° to 66° and lower canopies (μ = 56°, range = 42° to 66°) under ambient CO_2 conditions had, on average, symmetrically distributed leaf inclination angles.

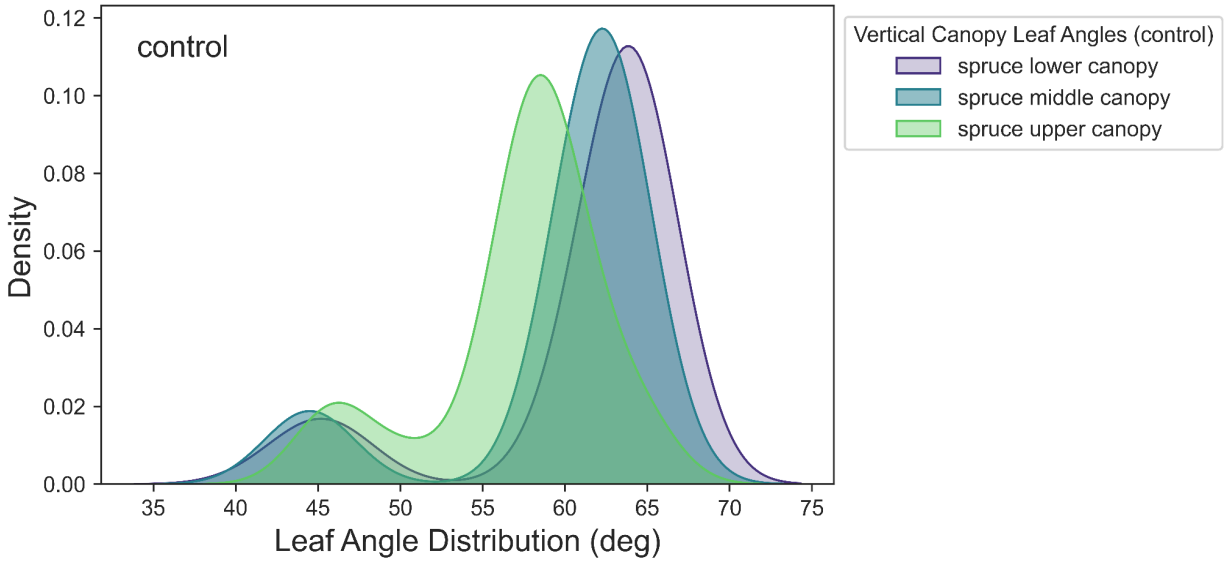

Figure B.17. Control plot spruce upper canopy leaf inclination angles demonstrated more symmetrical trends (μ = 57°, range = 45° to 65°). Middle (μ = 59°, range = 43° to 66°) and lower canopy (μ = 61°, range = 42° to 66°) were more vertical on average.

Table B.3. Mann-Kendall tests evaluating trends between leaf inclination angle and time for the spruce and larch species.

Species	Treatment	Independent Metric	Dependent Metric	p	coefficient
upper spruce	Elevated CO_2	Time	Average Leaf Inclination Angle	0.68	0.00
upper larch	Elevated CO_2	Time	Average Leaf Inclination Angle	0.16	-0.04
upper spruce	Control	Time	Average Leaf Inclination Angle	0.65	-0.10
upper larch	Control	Time	Average Leaf Inclination Angle	0.44	-0.05
upper spruce	Ambient CO_2	Time	Average Leaf Inclination Angle	0.24	-0.01
upper larch	Ambient CO_2	Time	Average Leaf Inclination Angle	0.32	-0.02
middle spruce	Elevated CO_2	Time	Average Leaf Inclination Angle	0.37	-0.01
middle larch	Elevated CO_2	Time	Average Leaf Inclination Angle	0.22	-0.01
middle spruce	Control	Time	Average Leaf Inclination Angle	0.06	-0.03
middle larch	Control	Time	Average Leaf Inclination Angle	0.50	-0.02

middle spruce	Ambient CO_2	Time	Average Leaf Inclination Angle	0.22	-0.01
middle larch	Ambient CO_2	Time	Average Leaf Inclination Angle	0.87	0.00
lower spruce	Elevated CO_2	Time	Average Leaf Inclination Angle	0.08	-0.01
lower larch	Elevated CO_2	Time	Average Leaf Inclination Angle	0.77	0.00
lower spruce	Control	Time	Average Leaf Inclination Angle	0.50	0.00
lower larch	Control	Time	Average Leaf Inclination Angle	0.50	0.00
lower spruce	Ambient CO_2	Time	Average Leaf Inclination Angle	< 0.05	-0.01
lower larch	Ambient CO_2	Time	Average Leaf Inclination Angle	0.19	0.00

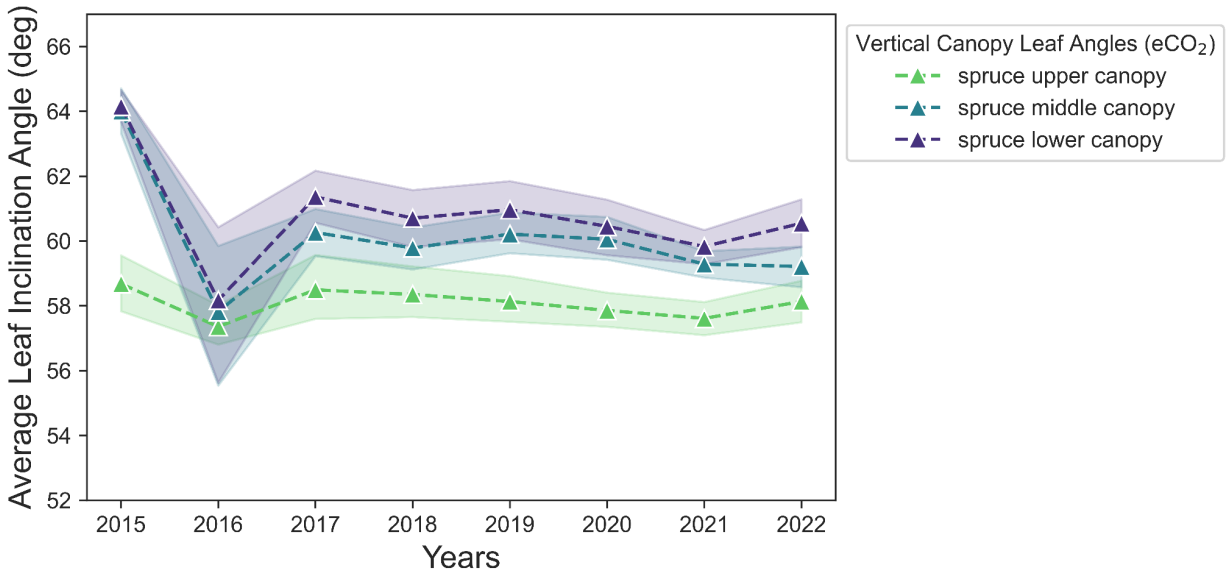

Figure B.18. Spruce leaf inclination angles over time under elevated CO_2 did not exhibit significant trends in any one direction.

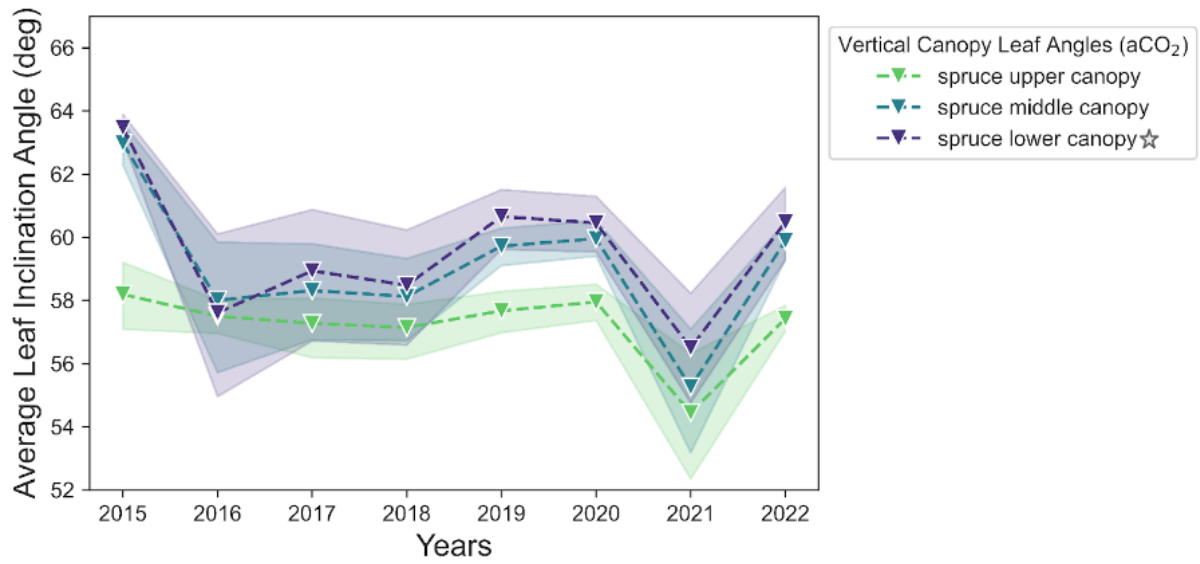

Figure B.19. Spruce leaf inclination angles in upper and middle canopies over time under ambient CO_2 did not exhibit significant trends in any one direction. Spruce

lower leaf angles showed a statistically significant downward trend ($p < 0.05$, m = -0.01). Stars indicate significance.

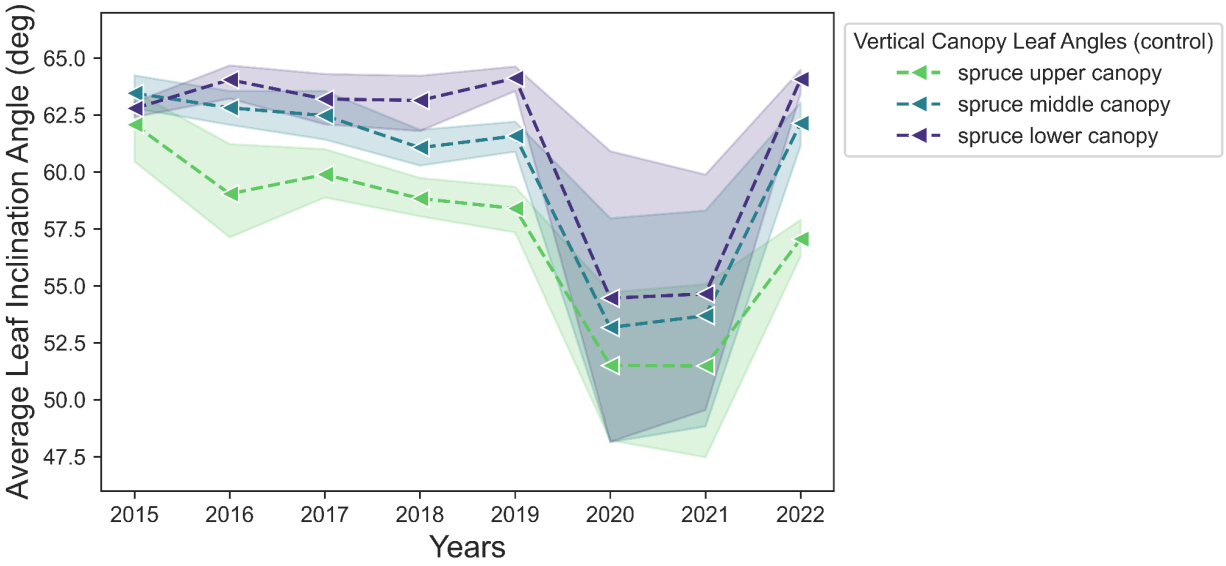

Figure B.20. Spruce leaf inclination angles over time under control conditions did not exhibit significant trends in any one direction.

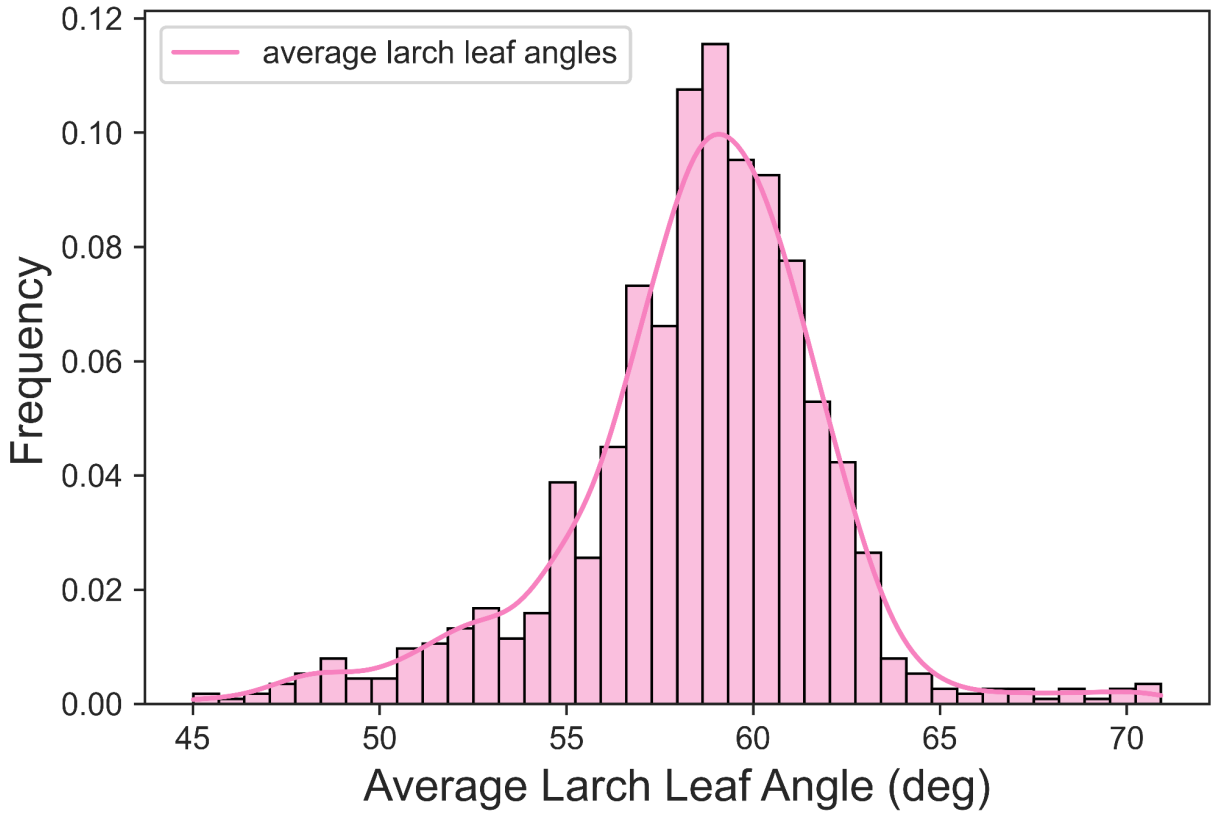

Figure B.21. Histogram with the average leaf inclination angle distribution for all eastern larch trees across the experimental site. N = 432, μ = 58°, the range was 45° to 71°. Cumulatively, spruce trees tended to represent either spherical or vertical leaf angle distribution patterns.

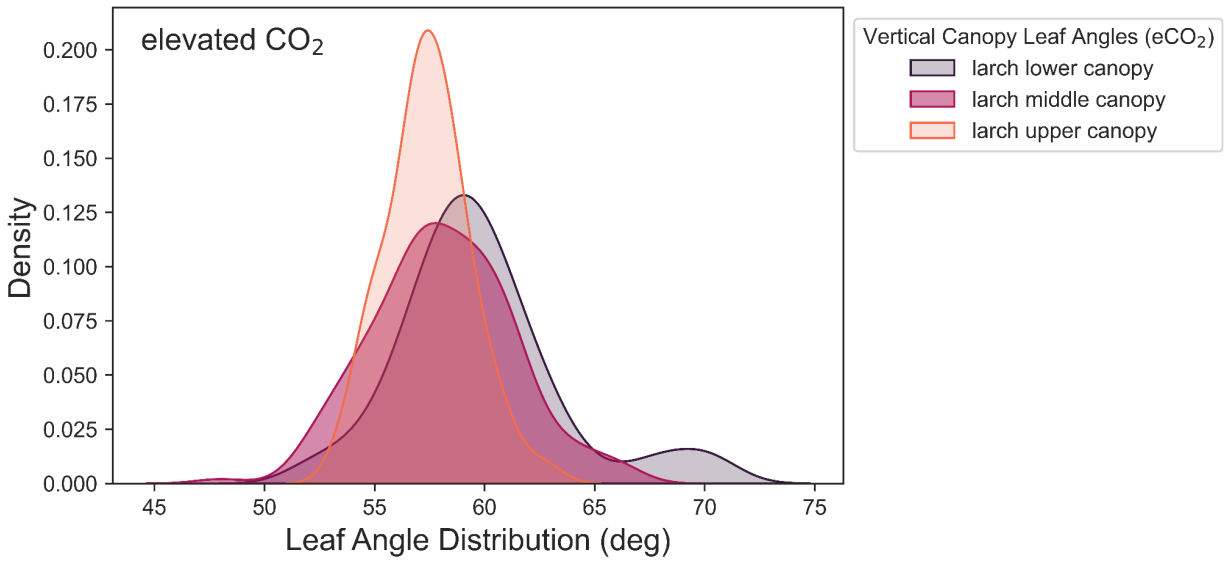

Figure B.22. Larch upper (μ = 57°, range = 54° to 63°), middle (μ = 58°, range = 48° to 66°), and lower (μ = 58°, range = 52° to 71°) canopy leaf angles under elevated CO_2 conditions were, on average, symmetrically distributed.

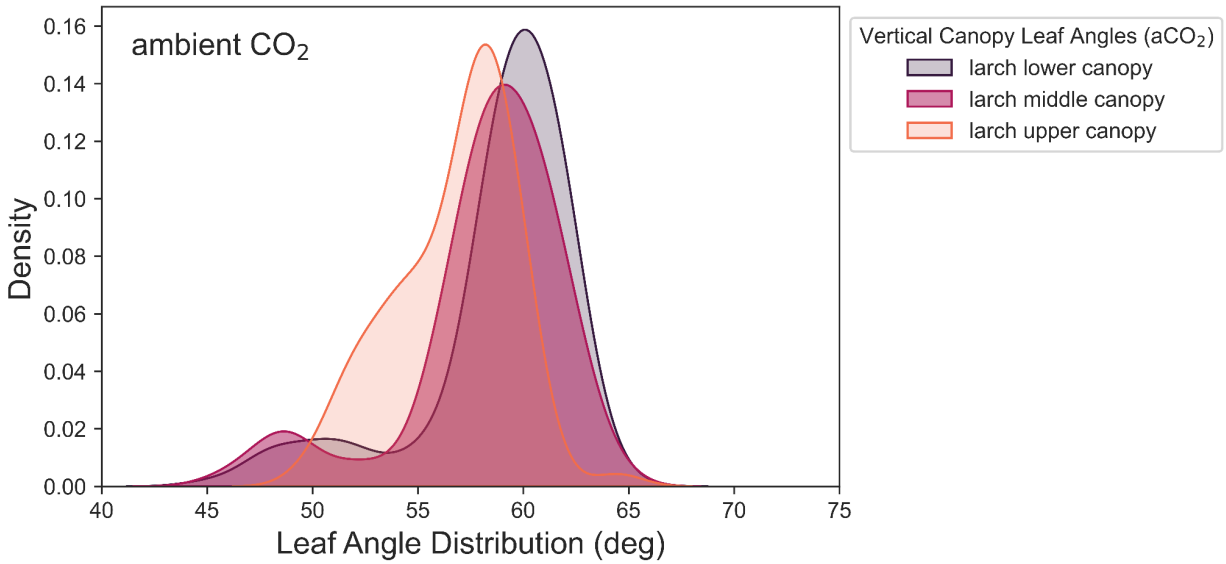

Figure B.23. Larch upper (μ = 57°, range = 50° to 65°), middle (μ = 58°, range = 45° to 65°), and lower (μ = 59°, range = 45° to 65°) canopy leaf angles under ambient CO_2 conditions were, on average, symmetrically distributed.

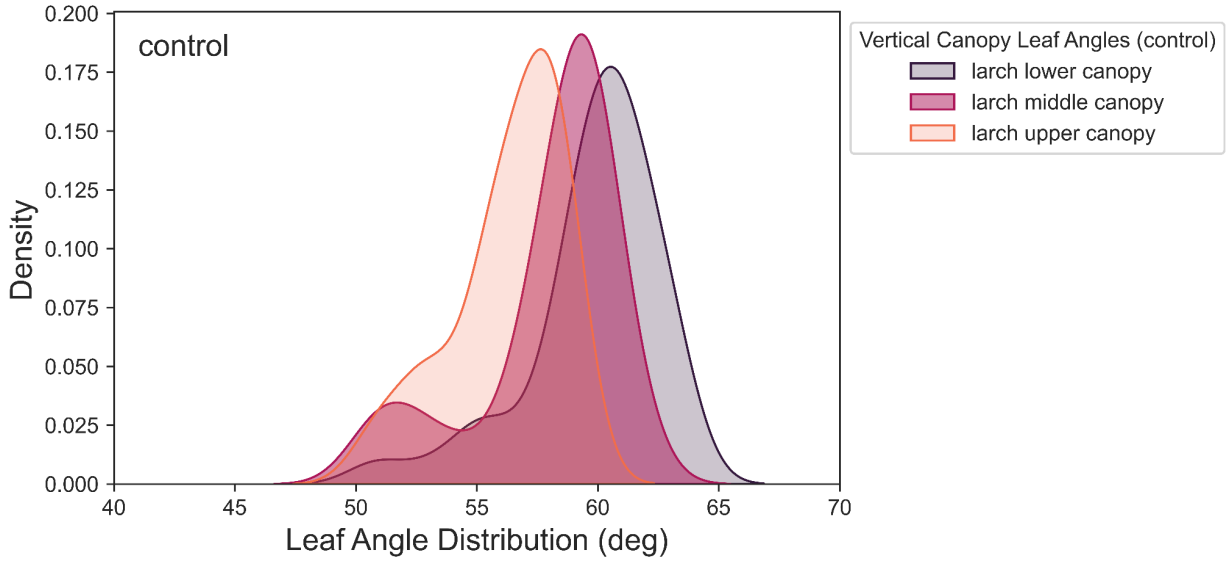

Figure B.24. Larch upper canopy (μ = 56°, range = 51° to 59°]) and middle canopy (μ = 58°, range = 50° to 62°) average inclination angles had a more spherical distribution than lower canopy (μ = 60°, range = 51° to 63°) larch inclination angles under control conditions.

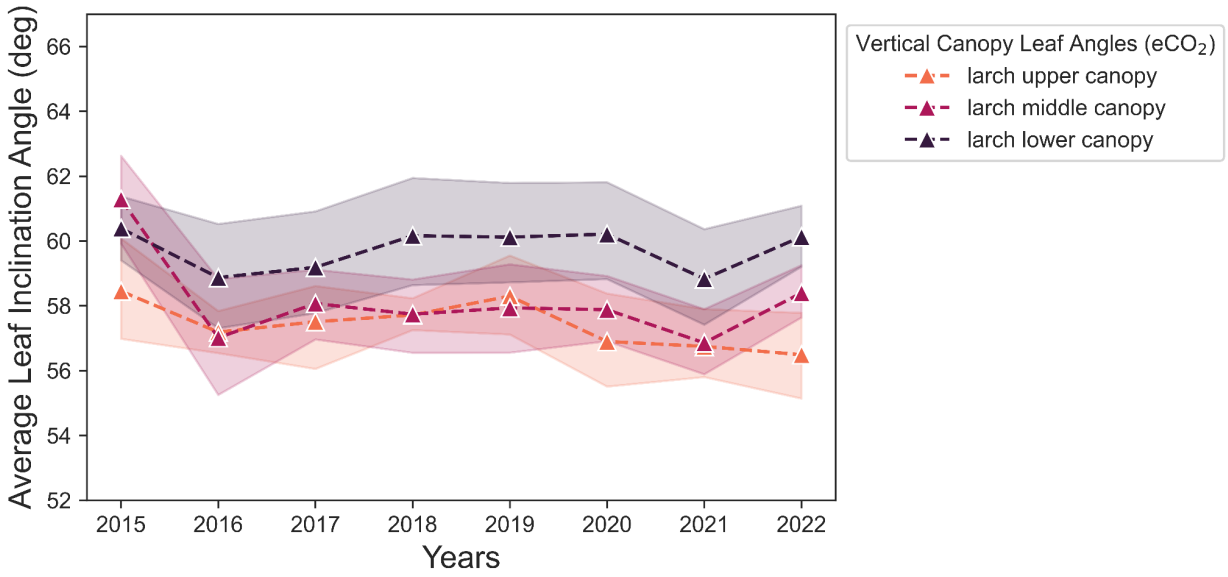

Figure B.25. Larch average leaf inclination angles under elevated CO_2 and warming did not have significant trends in any one direction.

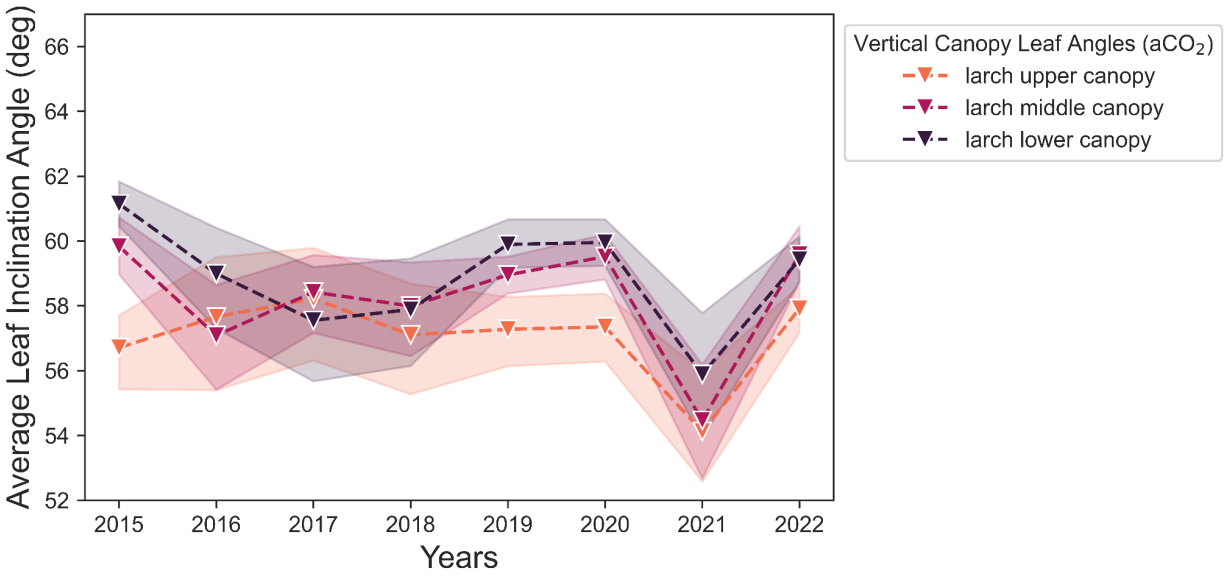

Figure B.26. Larch average leaf inclination angles under ambient CO_2 and warming did not have significant trends in any one direction. We saw an anomalous downward trend in leaf angles in 2021.

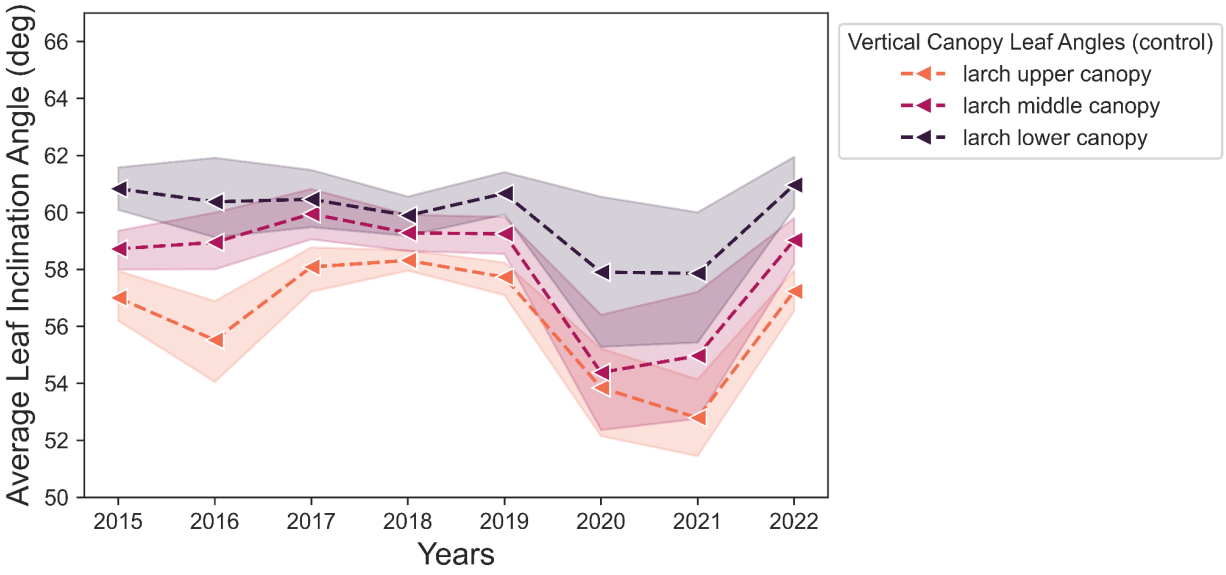

Figure B.27. Larch average leaf inclination angles under control conditions did not have significant trends in one direction. We saw downward trends in leaf angles in 2020 & 2021.